Intensivierung von flüssig-flüssig Extraktionskolonnen mit Mikrogelen

Intensification of Liquid-Liquid Extraction Columns by Microgels

Von der Fakultät für Maschinenwesen
der Rheinisch-Westfälischen Technischen Hochschule Aachen
zur Erlangung des akademischen Grades
einer Doktorin der Ingenieurwissenschaften genehmigte Dissertation

vorgelegt von

Miriam Anna Barbara Faulde

Berichter:
Univ.-Prof. Dr.-Ing. Andreas Jupke
Univ.-Prof. Dr. rer. nat. Dominik Wöll

Tag der mündlichen Prüfung: 21.01.2022

Vorwort

Die vorliegende Dissertation entstand in der Zeit von April 2015 bis Mai 2020 während meiner Tätigkeit als wissenschaftliche Mitarbeiterin am Lehrstuhl für Fluidverfahrenstechnik innerhalb der Aachener Verfahrenstechnik (AVT) an der RWTH Aachen. Die Arbeit wurde im Rahmen des Sonderforschungsbereichs 985 "Funktionelle Mikrogele und Mikrogelsysteme" durchgeführt.

Mein besonderer Dank gilt Prof. Andreas Jupke, für die Überlassung des interessanten Themas sowie das Vertrauen und die Möglichkeit, dieses sehr selbstständig zu bearbeiten. In meiner Zeit am Lehrstuhl haben mich sein Enthusiasmus, seine Neugierde sowie seine ambitionierte Mentalität stets angespornt und nachhaltig inspiriert. Prof. Dominik Wöll möchte ich für die Übernahme des Koreferats sowie für die Zusammenarbeit im Rahmen des SFB danken. Der regelmäßige Austausch und die anregenden Diskussionen in dieser Zeit haben mich stets motiviert und meinen fachlichen Blickwinkel erweitert. Mein Dank gilt außerdem Prof. Eike Stumpf für die Übernahme des Prüfungsvorsitzes.

Meine Arbeit an dem Thema wurde besonders durch die zahlreichen Kooperationen innerhalb und außerhalb des Sonderforschungsbereiches bereichert. Danken möchte ich besonders meinem Projektpartner Eric Siemes (IPC) für die vielen guten Diskussionen, seine Geduld und seine (im wahrsten Sinne des Wortes) "Experimentierfreudigkeit". Außerdem gilt mein Dank Michael Kather (DWI) und Agnieska Ksiazkiewicz (DWI), die mich stetig mit Mikrogelen versorgt haben. Die schönsten und gleichmäßigsten Mikrogel-besetzten Tropfen im Prototyp wären ohne die Expertise und den Pragmatismus von Hanna Wolff (AVT.CVT) nicht möglich gewesen. Außerdem möchte ich Steffen Bochenek (IPC) für die Vermessung der Kompressionsisothermen danken, die viel Licht ins Dunkel gebracht haben. Großer Dank gilt auch Sabrina Mallmann (DWI) die mich mit elektronenmikroskopischen-Aufnahmen der Mikrogele unterstützt hat. Die Mikrogele wahrhaftig an der Grenzfläche zu sehen, war sicherlich eine

Sternstunde meiner Promotion. Außerdem danke ich den Studierenden, insbesondere Berinike, Franziska, Julian, Moritz, Jesco, und Simon, die mit ihren Abschlussarbeiten oder als wissenschaftliche Hilfskraft zum Gelingen dieser Arbeit beigetragen haben. Ganz besonders möchte ich dabei Josia danken, dass er mich jahrelang zuverlässig unterstützt hat und sich von Fehlschlägen und unerwarteten Schwierigkeiten nie hat entmutigen lassen.

Neben der fachlichen Unterstützung war der kollegiale Zusammenhalt und die Atmosphäre am Lehrstuhl und in der AVT etwas, das ich sehr positive in Erinnerung behalten werde. Mit ihrer Frohnatur und hilfsbereiten Art hat mich Gabi damals als Erste am Lehrstuhl empfangen und in meiner gesamten Zeit viele bürokratische Hürden kleiner gemacht. Als Kollegen der ersten Stunde haben Andreas, Tim, Manuel und Armin meinen Start am Lehrstuhl mit Besuchen bei Lindt in der Mittagspause oder in der Pontstraße nach Feierabend versüßt. Meinen späteren Bürokollegen Daniel, Jan und Max danke ich für die immer wieder aufbauenden und lustigen Stunden in B103. Insbesondere Max hatte immer ein offenes Ohr und mit seinem sarkastischem Fatalismus viele schwierige Situationen entschärft. Teresa danke ich für die direkte Verbundenheit und anhaltende Freundschaft. Die Zusammenarbeit mit Moritz im letzten Jahr war ein echtes Vergnügen und von seiner skeptisch-enthusiastische Art wird das Thema Mikrogele in Zukunft sicher profitieren. Aus der Extraktionsgruppe möchte ich insbesondere Christian und Stephan danken, für die immer wieder schnelle und unkomplizierte Hilfe im Labor.

Zu guter Letzt gilt mein herzlichster Dank meiner Familie, meinen Eltern, die mich schon früh unterstützt haben meinem technisch- naturwissenschaftlichen Interesse nachzugehen. Ihre verlässliche vertrauensvolle Unterstützung auf meinem bisherigen Lebensweg war eine wichtige Voraussetzung für das Gelingen meiner Promotion. Ganz besonders danken möchte ich Simon, der mir zur Seite stand, meinen Wahnsinn immer wieder ertragen und relativiert hat, und dessen Beistand eine wichtige Stütze für mich war und ist.

The chase...is better than the catch

Hans Peter Geerdes - deutscher Musikpionier

Contents

Abstract

For extraction columns the drop size and drop size distribution are crucial for process performance. Small drops promote mass transfer by large interfacial area while larger drops withstand higher counter current flow rates. The tendency of the drop to coalesce requires constant energy input to break the drops. Hence, the interplay between coalescence and breakage regulates the drop size and often leads to broad size distribution.

A new approach to tackle this drop size dilemma is the application of microgels. The crosslinked polymers can stabilize and destabilize liquid systems on demand by a very sensitive temperature trigger. With the combination of interfacial activity and switchability, microgels enable new options for processes with defined monodisperse drop size.

For the successful introduction of microgels to extraction processes, the effect of the interfacial microgel layer on the processes relevant phenomena needs to be understood. Thus, the impact of microgels on fluid dynamics, mass transfer and coalescence is investigated in this work. To identify advantageous microgel properties four different microgels are utilized, differing in size and crosslinking. Furthermore, the propagation of effects is evaluated across scales from liquid-liquid interface to technical lab scale, with focus on single drops as smallest self contained unit of the process.

The results from single drop experiments indicate that the predominant effect of microgels is the reduction of interfacial mobility. The effect of the microgels on the drops´ fluid dynamics increases with increasing spreading and interpenetration of the microgels at the interface. This also affects the other investigated phenomena. A reduced mass transfer was observed at single drops, while no additional mass transfer resistance of the microgel layer itself was measured for small molecules at a flat interface. Thus the reduced interfacial mobility must cause a reduced decay of the concentration gradient inside the drop. Regarding coalescence the probability for two colliding drops is significantly reduced by microgels below their switching temperature. This could also be accounted to reduced interfacial mobility since it affects the film drainage and thus required contact time for coalescence. Moreover, phase separation by temperature shift was successfully demonstrated in a continuous operating prototype in technical lab scale.

Further, performance evaluation by process simulations with monodisperse microgel covered drops show a capacity increase to higher loads at equal separation performance. And at low loads monodisperse drops increase the separation performance and enable operation close to entrainment limit.

This work demonstrates the applicability of microgels in extraction columns and also identifies the interfacial spreading and mobility as crucial properties for this scope of application.

Zusammenfassung

Für Extraktionskolonnen sind die Tropfengröße und ihre Verteilung Schlüsselparameter. Kleine Tropfen verbessern den Stofftransport durch die große Grenzfläche, während große Tropfen im Gegenstrom bei hohen Flussraten aufsteigen. Die Tendenz dieser Systeme zu koaleszieren erfordert kontinuierlichen Energieeintrag. Das Zusammenspiel aus Koaleszenz und Bruch bestimmt die Tropfengröße und führt zu einer breiten Verteilung.

Einen neuen Ansatz dieses Tropfengrößen-Dilemma anzugehen bieten Mikrogele. Die quervernetzten Polymere können disperse Systeme gezielt stabilisieren und destabilisieren. Mit der Kombination aus grenzflächenaktiven und schaltbaren Eigenschaften ermöglichen Mikrogele neue Optionen für Prozesse mit definierter Tropfengröße.

Die erfolgreiche Anwendung von Mikrogelen in Extraktionsprozessen erfordert das Verständnis der Effekte der Mikrogel Schicht an der Grenzfläche auf die prozessrelevanten Phänomene. Daher wird in dieser Arbeit der Einfluss der Mikrogele auf Fluid Dynamik, Stofftransport und Koaleszenz untersucht. Um vorteilhafte Merkmale für den Prozess zu bestimmen wurden vier verschieden Mikrogele mit unterschiedlichem Quervernetzteranteil und Größe eingesetzt. Die Fortpflanzung von Effekten über Skalen hinweg, von flüssig-flüssig Grenzfläche bis zum Technikumsmaßstab, wird betrachtet, wobei der Fokus auf den Einzeltropfen, als kleinste in sich abgeschlossene Prozesseinheit, liegt.

Die Einzeltropfenexperimente zeigen, dass die Mikrogele vor allem die Grenzflächenmobilität reduzieren. Die Auswirkung auf die Fluid Dynamik der Tropfen nimmt mit zunehmendem Spreiten an der Grenzfläche zu und wirkt sich auch auf die anderen untersuchten Phänomene aus. Am Einzeltropfen wird der Stofftransport reduziert, während an der ebenen Grenzfläche kein zusätzlicher Stofftransportwiderstand für kleine Moleküle festgestellt wurde. Daher muss die reduzierte Grenzflächenmobilität die Durchmischung im Tropfeninneren und somit den Abbau des Konzentrationsgradienten vermindern. Die Koaleszenzwahrscheinlichkeit zweier Tropfen wird durch Mikrogele unterhalb ihrer Schalttemperatur deutlich herabgesetzt. Hier beeinflusst die Grenzflächenmobilität die Filmdrainage und somit die Koaleszenzzeit. Außerdem, wurde die schaltbare Phasentrennung erfolgreich in einem kontinuierlichen Prototyp im Technikumsmaßstab gezeigt.

Außerdem zeigen Prozess-Simulationen mit Mikrogel besetzten monodispersen Tropfen, dass die Kapazität zu höheren Belastungen, bei gleichbleibender Trennleistung, gesteigert werden kann. Anderseits kann bei kleinen Belastungen die Trennleistung, durch kleine Tropfen und Betrieb nahe der Flutgrenze, gesteigert werden.

Diese Arbeit zeigt die Einsatzmöglichkeit von Mikrogelen in Extraktionskolonnen und identifiziert das Spreiten und die Grenzflächenmobilität als kritische Eigenschaften für dieses Anwendungsfeld.

List of Abbreviations

Abbreviation	Full Meaning
AFM	atomic force microscopy
DLS	dynamic light scattering
DSA	drop shape analysis
DVT	drop volume tensiometer
EFCE	European Federation of Chemical Engineers
IPC	Institut für physikalische Chemie
MG	microgel
PNIPAM	poly(n-isopropylacrylamide)
SEM	scanning electron microscopy
SFB	Sonderforschungsbereich
VPTT	volume phase transition temperature

List of Symbols

Symbol	Meaning	Unit
A	area	m^2
a	pulsation amplitude	mm
a_{15}	transition parameter	-
a_{16}	transition parameter	-
b	interaction parameter	-
b_2	fitting parameter	-
c	concentration	$g\,L^{-1}$
C_D	drag coefficient	-
d	diameter	m
d_{um}	transition parameter	-
D	Diffusion coefficient	$m^2\,s^{-1}$
f	pulsation frequency	s^{-1}
FF	form factor	-
g	gravitational acceleration	$m\,s^{-2}$
h	height	m
k	distribution coefficient	-
k_B	Boltzman constant	$m^2\,kg\,s^{-2}\,K^{-1}$
K_{OG}	overall mass transfer coefficient	-
L	characteristic dimension	m
M_W	molecular weight	$g\,mol^{-1}$
n	amount of substance	mol
r	radius	m
R	mass transfer enhancement factor	-
R^2	coefficient of determination	$\%$
s	surface sphericity	-
t	time	s
T	temperature	K, ℃
U_P	direction of movement	-
V	Volume	m^3
x	concentration aquous phase	$kg\,kg^{-1}$
y	concentration organic phase	$kg\,kg^{-1}$
Z	compressibility factor	-

Greek Symbols

Symbol	Meaning	Unit
α	mass transfer enhancement factor	-
β	mass transfer coefficient	$\mathrm{m\,s^{-1}}$
δ	film thickness	m
ϵ	Young's modulus	Pa
η	surface packing fraction, viscosity	-, mPa s
γ	interfacial tension	$\mathrm{mN\,m^{-1}}$
Γ	surface coverage	$\mathrm{g\,m^{-2}}$
λ	interaction parameter	-
ν	velocity	$\mathrm{m\,s^{-1}}$
ϕ	particel sphericity	-
Π	surface pressure	$\mathrm{mN\,m^{-1}}$
ρ	density	$\mathrm{kg\,m^{-3}}$
θ	contact angle	°

Subscripts

Symbol	Meaning
ax	axial
b	bulk
c	continuous
cmc	critical micell concentration
col	column
d	disperse
D	drag
eff	effectively contributing
exp	experimental
i	interface
MG	microgel
P	particle
∞	terminal

Dimensionless Quantities

Symbol	Name	Equation
Ar	Archimedes	$Ar = \frac{\rho_c \Delta\rho g d^3}{\eta_c^2}$
Fo	Fourier	$Fo = \frac{4Dt}{d^2}$
Mo	Morton	$Mo = \frac{g\eta_c \Delta\rho}{\rho_c^2 \gamma^3}$
Re	Reynolds	$Re = \frac{\rho_c v_{sed} d_V}{\eta_c}$
Sc	Schmidt	$Sc = \frac{\nu}{D} = \frac{\eta}{\rho D}$
Sh	Sherwood	$Sh = \frac{\beta L}{D}$
Pe	Peclet	$Pe = \frac{vd}{D} (= Re \cdot Sc)$
We	Weber	$We = \frac{v_{sed}^2 d_d \rho_c}{\gamma}$

1. Introduction

The controlled, selective manipulation of system properties to overcome limiting drawbacks is a process engineers dream. In the holistic process view, promising improvements and measures for one challenge often lead to difficulties elsewhere in the process. One example is the drop size in disperse systems; to provide a large interfacial area for mass transfer a small drop size is desirable, on the other hand for the subsequent phase separation large drops are preferable. Smart materials, like microgels, can remedy this dilemma as their switchability allows for selective tuning of the system properties.

1.1. Microgels

Microgels are smart, crosslinked polymers which attract researchers attention due to their unique properties and the resulting high application potential. As the name “micro-gels” implies, the size of the spherical polymers is typically less than $1\,\mu m$ in diameter and they are soft and deformable [1]. This softness originates from the structure of the crosslinked polymer network which is strongly lyophilic and thus soaked with solvent. When the microgel particles are highly swollen with solvent the polymer network accounts for only $10\,\%$ volume share. This structural feature distinguishes microgels from colloidal solid particles [1, 2].

An additional unique feature is the microgels´ responsiveness to external trigger by drastic structural change. The best known trigger is temperature responsiveness. When exposed to temperatures above the volume phase transition temperature (VPTT) the extend of swelling decreases and the polymer network contracts, as sketched in figure 1.1. Due to the significant

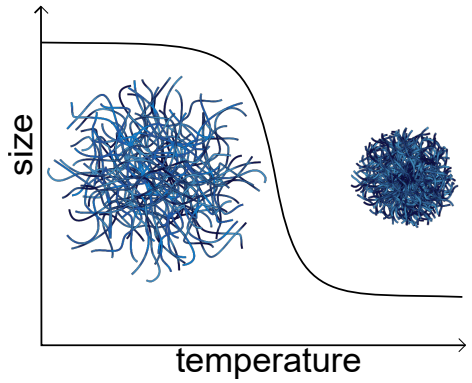

Figure 1.1.: Temperature sensitivity of the microgel size

change in size, which is also referred to as collapse. The temperature response is very sensitive and does not solely affect the size but also other properties of the microgels.

The most prominent microgel is PNIPAM (poly-(n-iso-propylacrylamid)), which was first introduced by Pelton and Chibante [3]. The physical properties of the microgels mainly depend on their size and the amount of crosslinker [1, 4]. Furthermore, additional functionalities can be introduced by addition of co-monomers during synthesis; for example, the incorporation of acidic or basic groups implies an additional pH sensitivity [5, 6, 7]. Thus, microgels can be tailored for different applications. However, to define the exact requirements of the tailored microgel, structure-property relations and their effects on different process scales have to be understood previously. Therefore, PNIPAM microgels of different size and crosslinking degree are utilized in this study.

The drastic changes combined with high sensitivity make microgels switchable smart materials and has inspired many ideas for application [4, 8, 9, 10], for example drug delivery systems [11] or switchable membranes [12, 13]. The application scope broadens even more combining the switchability with other porperties, e.g. their interfacial activity which allows for the formulation of switchable emulsions [1, 14, 15, 16, 17].

1.2. Process Concept

Liquid-liquid extraction processes are utilized for different applications. For all of them holds true that the performance highly depends on the drop size distribution. Two characteristics are important, the width of the distribution and the actual size of the drops. The drop size originates from the disperser at the bottom of the column, but it changes due to coalescence and breakage of the drops. Small drops offer the advantage of a large volume specific surface, but their low buoyancy and thus their movement in countercurrent flow limits their applicability. In contrast, large drops have a smaller surface area but can withstand the countercurrent in a wider operating range. Furthermore, a wide size distribution means a wide residence time distribution. The small drops at the lower end of the distribution move slowly due to the small lifting force while their large volume specific area ensures that the drop quickly approaches equilibrium. Large drops, at the upper limit of the distribution, provide less area and thus lower concentration while they rise quicker.

These contradicting conditions for the different drop sizes lead to a flat concentration profile along the apparatus. Small drops have a long residence time but do not significantly contribute to separation as their concentration is close to equilibrium. While large drops, with high mass transport driving force, quickly flow through the apparatus and do not reach equilibrium.

A common tackle is the redispersion of the drops between the stages, to homogenize the concentration in the drops and also rearrange the drops sizes which is shifted towards larger diameters by coalescence. Thus, most extraction columns require energy input to counteract coalescence and regulate the drop size distribution, e.g. by pulsation for sieve tray columns or rotation for Kühni columns [18, 19].

A new approach, not only addressing the symptoms of a wide distribution, but specifically prevent coalescence is the application of microgels at the drop surface. The surface active microgels cover the drop and stabilize it in the active part of the column. This protection against coalescence enables a uniform, monodisperse, drop size. This uniform drop size also

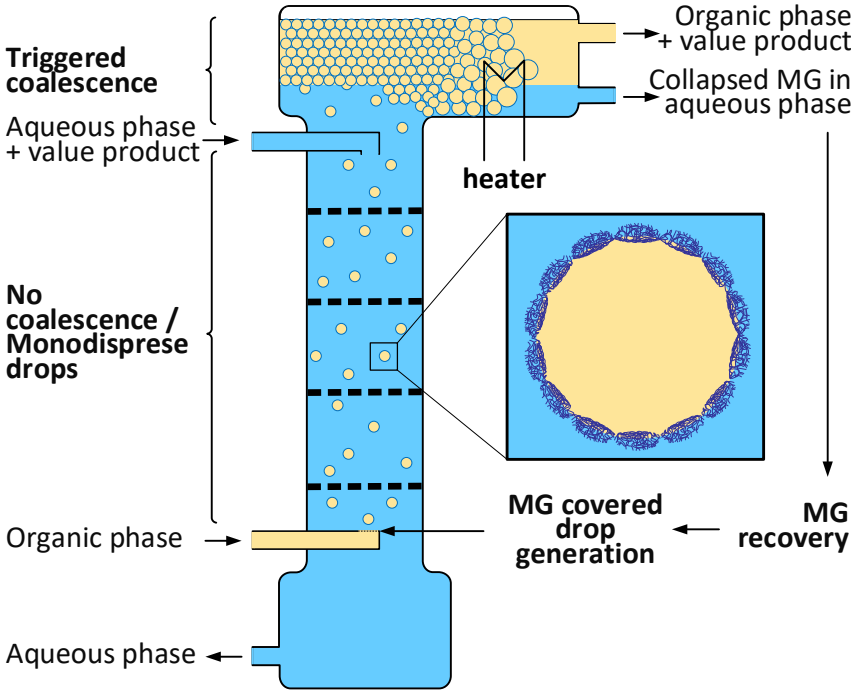

Figure 1.2.: Concept for the intensification of liquid-liquid extraction processes by the utilization of microgels

means uniform interfacial area and residence time, which steepens the concentration profile and thus the separation performance. At the top of the column, coalescence is required to separate the phases for the subsequent process steps. Here the microgels can be switched by temperature shift, above the VPTT, to cancel the stabilizing effect. An other beneficial feature of the microgels is the possibility to separate and concentrate them by a filtration step.[20] The filtration allows for easy recycling of the microgels, an important economic aspect.

Thus, this thesis aims to test the feasibility and to evaluate the intensification potential of the proposed concept. For a persuasive statement on the applicability the impact of the microgels on the process relevant phenomena needs to be understood, the research approach is presented in more detail in section 1.3.

1.3. Research Approach

To understand the impact of microscale polymer particles on technical scale processes, the propagation of effects across different scales must be regarded as sketched in figure 1.3. This is also reflected by the sequence in this thesis which is illustrated in figure 1.4.

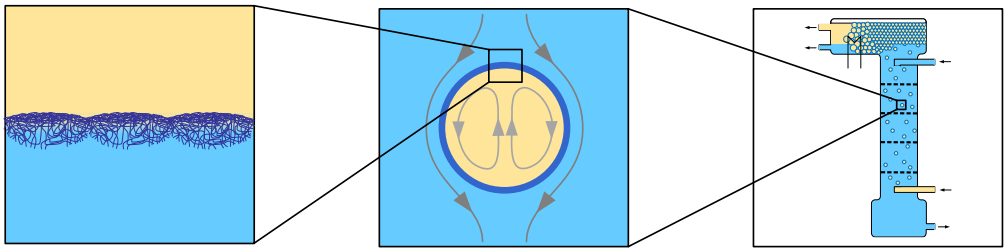

Figure 1.3.: Scales of the research approach to study propagation of effects of microgels from interfacial layer, via single drops to unit operation scale

The behavior and the properties of the interfacial microgel layer are fundamental for this approach and in focus of the first chapter. The adsorption of the microgels to the interface, qualitative visual appearance of the adsorption layer and the reduced interfacial tension as measurable effect of microgels adsorbed to the interface are presented and discussed in chapter 2.

Continuing along the propagation route of effects and structure-property relations, the impact of microgels on process relevant phenomena needs to be understood. Considering extraction as separation process mass transfer is the key phenomenon, considering the disperse character of the system fluid dynamic behavior of drops and coalescence are also key phenomena. Thus the effect of microgels on these crucial process phenomena are regarded in this thesis in chapters 3, 4 and 5. Thereby, single drops serve as smallest entity representing process conditions in all three chapters.

Since the introduction of microgels adds complexity to an already highly interconnected system the process relevant phenomena are investigated separately. However, the phenomena do not only affect each other but they are all affected by the interfacial conditions, predominantly the interfacial mo-

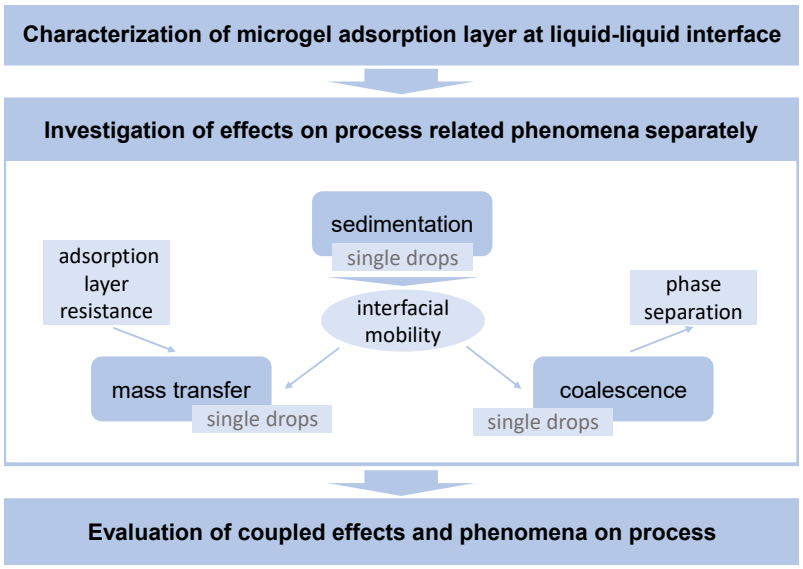

Figure 1.4.: Investigation approach steps and sequence in this work

bility or the permeability of the interface for momentum transfer, respectively. These conditions can be studied very well by the sedimentation behavior of single drops considering their velocity and their shape, which is in focus of chapter 3.

Moreover, chapter 4 deals with the effect of microgels on mass transfer in extraction processes. Two aspects are regarded in this chapter, a potential additional mass transfer resistance from the interfacial microgel layer and the coupled effects of interfacial layer and drop fluid dynamics by single drop mass transfer experiments.

Finally, coalescence is dealt with in chapter 5. For the process two forms of coalescence are distinguished, this is also reflected in this chapter: Coalescence in the active part of the column between rising drops is investigated by single drop coalescence experiments. While, coalescence at the top of the column for phase separation is regarded in a modified settler set up.

The experimental investigations in the three chapters are accompanied by model approaches for analysis and quantification of the effects.

Finally, these findings are utilized for the evaluation of the intensification potential by theoretical case study on apparatus scale in chapter 6. Therefore, an exisiting extraction column model, based on drop population balances, is utilized. The findings from the previous chapters are accounted for

by modified sub models and fitted parameters. The intensification potential in comparison to conventional extraction processes is analyzed considering separation efficiency, as well as operational flexibility.

1.4. Investigated Systems

To allow transfer of findings across the investigations of the different chapters, the same set of microgels and solvents systems has been utilized and is characterized in the following.

1.4.1. Utilized Microgels

In this work the focus is on the application of the microgels, therefore PNIPAM (poly-(n-iso-propylacrylamid)) microgels are used as well studied and configurable system. For the investigations four different PNIPAM microgels were synthesized with different radii and crosslinker content, since these predominantly control the microgels interfacial spreading and related properties (see section 2.2.3). As crosslinker BIS (n,n'-methylenebis(acrylamide)) is utilized, the chemical structure of the NIPAM monomer and the BIS crosslinker is depicted in figure 1.5. The degree of crosslinking is defined by the utilized amount of BIS crosslinker during synthesis and varies from $2.5\,\mathrm{mol}\,\%$ to $20\,\mathrm{mol}\,\%$.

The detailed composition of the reaction mixtures are listed in table A.1 in the appendix. The hydrodynamic radius is determined by dynamic light scat-

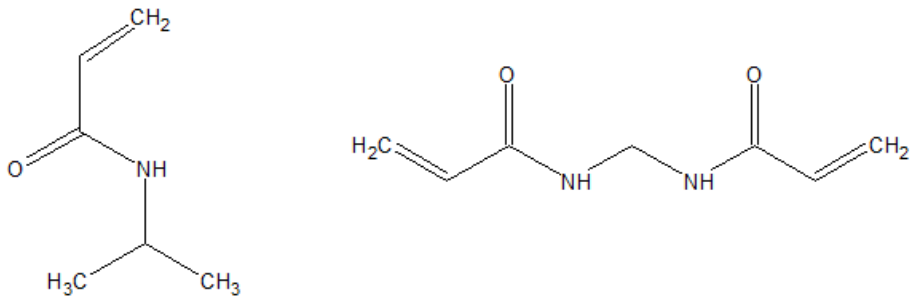

Figure 1.5.: Chemical structure of the NIPAM monomer (left) and the BIS crosslinker (right)

Table 1.1.: Characteristic properties of the utilized PNIPAM microgels

name -	crosslinker (BIS) content [mol %]	hydrodynamic radius (bulk,25 °C) [nm]
MG1	2.5	320
MG2	5	287
MG3	20	310
MG4	5	170

tering (DLS). The characteristics of the utilized microgels are summarized in Table 1.1.

All utilized microgels were synthesized by aqueous, free radical precipitation polymerization [21] and purified by dialysis with a cellulose tube or by ultracentrifugation and dispersion in Milli-Q® water. The syntheses were performed at 'DWI Leibniz-Institut für Interaktive Materialien e.V.' (DWI) and 'Institut für physicalische Chemie' (IPC) at RWTH Aachen University.

1.4.2. Solvent Systems

For the evaluation of the effect of microgels on extraction processes and the involved phenomena their behavior at the liquid-liquid interface is an important aspect. Therefore, three solvents with different properties are utilized. The key criteria for their selection is their interfacial tension with water. The interfacial tension with water of the utilized solvents n-decane, toluene and n-butyl acetate are listed in table 1.2. n-Decane is selected as very apolar solvent; hence, it has a very high interfacial tension with water, therefore it is commonly used in literature [16, 22, 23]. Toluene and n-butyl acetate are selected as they are recommended by the 'European Federation of Chemical Engineers' (EFCE) as standard test systems representing high and medium range interfacial tensions, respectively [24]. Systems with lower interfacial tension are not utilized as they are more polar and consequently the solubility of water increases. For example, in octanol ($\gamma = 8.5\,\mathrm{mN\,m^{-1}}$ at 25 °C) the solubility is significant and the octanol is incorporated in the

microgels leading to substantial differences in the behavior of these system e.g. the loss of the temperature responsiveness [25].
Toluene and n-butyl acetate are purchased from Merck (Darmstadt, Germany) in EMSURE® quality, n-decane is purchesed from Carl Roth with purity $\geq 99\,\%$.

Table 1.2.: Interfacial tension of different solvents with water at 25 °C ($\star$ values interpolated between 20 and 30 °C)

solvent	interfacial tension $[\mathrm{mN\,m^{-1}}]$	
n-decan	51.98	[26]
toluene	35.3$\star$	[24]
n-butyl acetate	13.97$\star$	[24]

1

2. Microgels at liquid-liquid Interfaces

Parts of this chapter have been published as:
Fluid Dynamics of Microgel-Covered Drops Reveal Impact on Interfacial Conditions, Polymers, 2018
Miriam Faulde, Eric Siemes, Dominik Wöll, Andreas Jupke
DOI: 10.3390/polym10080809

2.1. Introduction

For disperse systems the interface is of great importance; therefore, this chapter addresses the interface as a place of special conditions and how it is affected by microgels, to provide the basis for the investigations on microgel covered drops in this work. For comparison and classification of the impact of microgels, other surface active species such as rigid particles and surfactants are also considered. However, the effects on interfacial properties arising from structural differences between the utilized microgels are in focus. The microgels' morphology at the interface is visualized by cryo-SEM and interfacial tension measurements are used to characterize the differences between the microgels. Finally, a model approach for *in-situ* determination the microgel coverage of drops by their interfacial tension is presented and the difficulties of transfer in application are discussed.

2.2. Fundamentals

In colloidal and disperse systems the interface is a bustling place and the term 'interface' is elusive. From a mechanical and mathematical point the interface is a two-dimensional, thin separation plane between two immiscible phases [27]. Gibbs was the first scientist, who demonstrated thermodynamically, that concentrations at the interface differ from the bulk phase [28]. Therefore, the interface is a place of special conditions. These conditions are further affected by the presence of surface-active species. Their effect on interfacial properties such as the interfacial tension will be discussed in this chapter; especially, considering microgels which have structural and functional similarities to other well studies groups of surface-active species, such as surfactants, particles and macromolecules, whereby the molecules itself have a distinct orientation and consequently the interface is often considered as a three dimensional volume.[27] However, for the investigations in this work the interface is regarded as two dimensional area.

2.2.1. Interfacial Tension

Similar to the term 'interface' the interfacial tension can be derived from two perspectives, the mechanical and the molecular/ thermodynamic approach. The thermodynamic definition refers to a tension state at the interface due to different interaction forces for molecules at the interface compared to the molecules in condensed bulk phase, as shown by the arrows in figure 2.1. This meaning of tension results in the definition of the interfacial tension that work is required to bring a molecule from the condensed bulk to the interface. Since the molecules at the interface do not have a compensating counterpart the resulting vector is directed towards the bulk, generating a traction rectangular to the surface. Subsequently, work is required to enlarge the interface, which is shown in equation 2.1.

$$w = \int_0^A \gamma \, dA = \gamma A \tag{2.1}$$

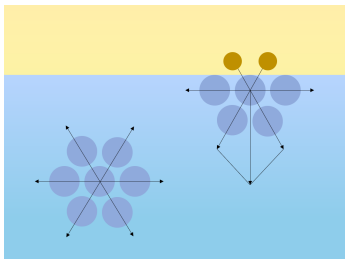

Figure 2.1.: Vectorial definition of the interfacial tension of two immiscable condensed phases (adopted from [27])

Due to the required work to enlarge the interface, bi-phasic systems are driven by minimization of interfacial area. This causes a variety of phenomena, some can be utilized to quantify the interfacial tension [27][29].

2.2.2. Effects of Surface Active Species

The endeavor of the system to minimize the system energy causes adsorption. The energy, and consequently the interfacial tension, is reduced by different mechanisms for the different species of surface active components, these are not directly transferable to microgels but help to understand and classify the effect of microgels.

Surfactants for example, minimize the energy of the system as they are amphipilic molecules and at the interface the hydrophilic and hydrophobic part are in contact with their favored phase, respectively [29]. In case of solid particles, the particle replaces contact area between the two liquid phases by the contact area between the liquid phase and the particle A_{P1} and A_{P2}, respectively [30]. As shown in figure 2.2(a) the area depends on the contact angle θ and the particle size, for spherical particles given by the radius r.

The energy E of attachment to or detachment from a liquid-liquid interface also depends on the interfacial tension γ of the solvent system and is described in equation 2.2.[30] The sign in the bracket term refers to the phase which receives the particle; negativ sign for removal to the aqueous

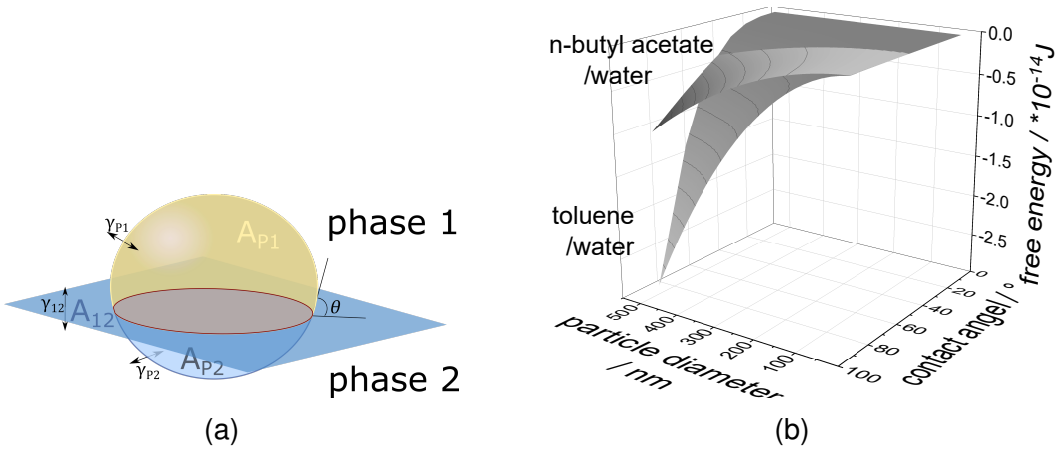

Figure 2.2.: Particle at interface between two fluid phases, (a) shows geometric measures (adopted from [31]), (b) shows the free energy of particle adsorption depending on the particle size and contact angle for two different solvent systems with different interfacial tension (toluene/water $\gamma = 35.3 mNm^{-1}$ and n-butyl acetate/water $\gamma = 13.97 mNm^{-1}$)) according to equation 2.2

phase and positive sign for removal to the air or organic phase.

$$E = \pi r^2 \gamma \left(1 \pm cos\theta\right)^2 \tag{2.2}$$

Gravitational forces are neglected for particle radius $< 10\,\mu m$ as the particle weight scales with r^3 while gravity scales with r. This relation is accounted for by the Bond number $Bo = gr^2 \Delta\rho / \gamma_{12}$, which also included the density difference between the averaged particle density and the surrounding media. For low Bond numbers gravitational forces can safely neglected.[31]

For the two standard test systems toluene/water and n-butyl acetate/water (see secion 1.4.2) the resulting energy depending on the particle size and contact angle is depicted in figure 2.2(b).

This example demonstrates the impact of the particle size and the contact angle θ which contributes by square to equation 2.2. Due to the high energy, the adsorption of larger particles is regarded as irreversible [31, 30].
Drawing direct inferences from the well understood rigid particles to microgels is challenging, due to their soft and fuzzy character. Nevertheless, the principles help to understand and highlight differences between the species

and will be presented in the following section.

2.2.3. Microgels at Interfaces

The behavior of microgels at interfaces has spellbound many research groups over the last decade. In bulk, the phase behavior and the rheological properties of microgels are similar to those of soft colloids [32], however, as they are approached to an interface their behavior is very different. Although, their dimensions are in the range of micro- or nanoparticles, their soft and fuzzy morphology makes them fundamentally different [33]. This swollen character also makes their characterization at the interface challenging. Although their typical size range is in the field of application of conventional microscopes, their observation with these methods is not applicable due to their swollen nature, which leads to a very low refractive index difference between the microgel and the aqueous phase [17]. Therefore, for the visualization of microgels at the interfaces cryo-SEM (scanning electron microscopy) [17, 16, 34, 35] and deposition and observation with AFM [36, 37] are most commonly used to study the conformation and morphology of microgels at interfaces. Also, contact angles as for rigid particles could not be determined for microgels due to the diffuse surface of the gels; attempts have been made to determine protrusion height for the deformed microgels at the interface by FreSCa cryo-SEM (freeze fracture shadow-casting cryo-scanning electron microscopy) [38]. As all these methods harden the systems, they are not applicable for studying dynamic processes. Here, fluorescent microscopy as a *not invasive* technique provides valuable insights to the system dynamics [39, 40]. Besides the direct visualization, the presence of microgels at the interface affects the interfacial properties which can be determined by other methods.

Interfacial Morphology and Properties

The extraordinary morphology of the microgels adds extra degrees of freedom and therefore complexity to the system [41]. Their softness also

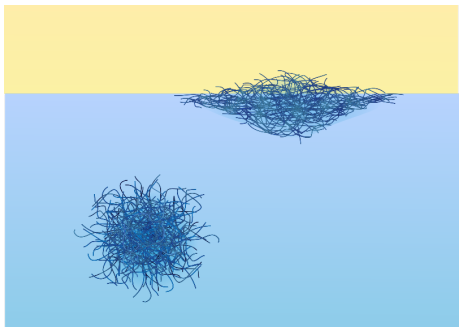

Figure 2.3.: Sketched microgel shape in bulk and deformation at the interface

dominates their interfacial properties [42]. This softness allows for different conformations at the interface. As mentioned in chapter 2.2.1 the interfacial area reduction is the thermodynamic driving force for the adsorption of colloids [31] and it is well known that the interfacial tension exerts strong forces to colloids at the interface [42]. Therefore, the deformation is commonly attributed to the strive of the microgels to maximize their contact area with the interface counteracted by their elasticity. This is expressed by $\Delta r = \frac{\Delta\gamma}{\epsilon}$ [43], where r is the microgel radius, γ the interfacial tension and ϵ the Young´s modulus accounting for the elasticity. The visual observation of microgels at the interface reveals their deformation. At the interface the microgels do no longer preserve their spherical shape, the soft polymers are compressed normal to the interface and stretched in lateral direction. Thereby, the microgel morphology by means of crosslinker content and distribution is decisively responsible for the deformation. The inhomogeneous crosslinking profile in radial direction leads to the anisotropic shape of the microgels that is often referred to as *fried egg* or *sombrero* structure [36, 41, 32, 34]. Figure 2.3 illustrates the shape difference of microgels in bulk and at the interface.

The extent of inhomogeneity of the morphology and consequently the deformation depends on the size and crosslinker content of the microgel [34, 1]. The resulting differences in deformation depending on the microgel morphology are depicted in figure 2.4. Microgels with a high crosslinker content spread less at the interface. Moreover, the crosslinking in smaller microgels is more homogeneous leading to less deformation (figure 2.4 left).[34] On the other hand, larger and less crosslinked microgels spread

more at the interface, respectively (figure 2.4 right). Destribats et al. report the ratio of the microgel diameter in solution to the center-to-center distance of the microgels at the interface as an indicator for the deformation. They measured the center-to-center distances from cryo-SEM images and report an increase of the diameter ratio from 1.16 to 1.72 for microgels with 242 and 726 nm in bulk diameter and 2.5 mol % crosslinking. For microgels with 5 mol % crosslinker the ratio increases from 1.09 to 1.49 with increasing microgel bulk diameter from 281 nm to 650 nm.[34] These observations are in good agreement with the data from other authors [38, 35].

As the crosslinking defines the mesh size of the microgel [32, 44], the deformation at the interface also affects the mesh size. Typical mesh sizes of microgels are in the range of 1 nm to 10 nm [43, 45]. Kyrey et al.[44] showed for microgels at solid interfaces with different crosslinking densities of 0.5 mol % and 5 mol % crosslinker an increase in mesh size by factor 1.63 and 1.30 respectively.

Besides the morphology of single microgels at the interface, the arrangement of multiple microgels is also studied widely [37, 16, 41, 34, 32, 46]. Similar to the spreading of single microgels, their interaction is affected by the crosslinker content [32, 46]. At high crosslinker contents microgels at the interface can be distinguished as individual particles, while at low crosslinker content the deformation reaches the point where no single particles can be detected. In this state, the flexibility of the dangling chains in the less crosslinked corona of the deformed microgel allow the overlapping microgel coronas to merge and form a film.[41] The effect on the center to center distance of the microgels is inconclusive. While Deshmukh et al.[41] report that the distance between the adsorbed microgels is not affected by the crosslinker content for equal sized microgels, Scotti et al.[32] found the crosslinker content predominantly affecting the microgels distances at the interface.

At low interfacial concentrations, clustering of microgels is observed at the interface but not in bulk solution [47, 41]. The clustering is irreversible.

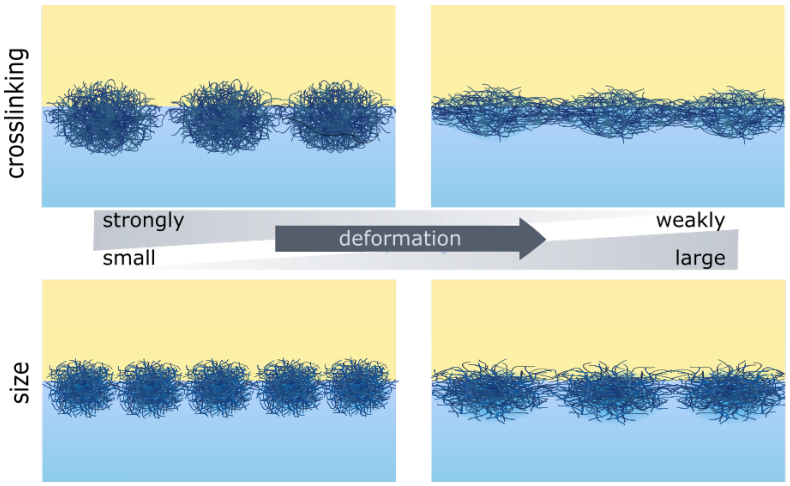

Figure 2.4.: Microgel deformation at the interface for different crosslinking and sizes

Long range capillary interactions leads to the clustering, once the microgels are close to each other, the dangling polymer chains interact [41]. The interaction between adsorbed microgels is dominated by their stretched fuzzy coronas [36]. At higher interfacial concentration the microgels form hexagonal packing [37, 34, 41].

The softness of the microgels affects not only their morphology at the interface but consequently also the properties of the interfacial microgel layer. Especially, rheological properties have been in the focus of research over the last years [32, 36, 37, 41]. The rheological properties are commonly investigated by compression isotherms obtained from Langmuir-trough experiments. These experiments provide insights on the interactions between the microgels at the interface. The interaction is mainly dominated by the overlapping coronas of the microgels [36]. Thereby, the additional degrees of freedom arising from embedding and deformation obstruct the estimation of the microgels interaction potential at the interface [41]. The deformability of the microgels enables larger interfacial loading [38].

Adsorption

For adsorption to an interface two aspects are important, the kinetics and the attainable interfacial load. Regarding adsorption as a dynamic process,

it can be described by multiple steps. Considering a drop or a liquid-liquid interface generated into a continuous bulk phase containing any surface active agent, the process is determined by three major steps [48, 27]:

- transport from bulk to the interface
- adoption to the interface
- conformation change at the interface

The adsorption process of microgels can be separated in two regimes depending on the interfacial coverage. At low interfacial loads, thus at short times and low bulk concentrations, the diffusion of microgels from bulk to the interface governs the process [43, 42]. Li et al. [42] showed this by the good agreement of the diffusion-controlled Ward-Tardoi model and their experimental data for concentrations below $2 \cdot 10^{-7}\,\mathrm{g\,L^{-1}}$ for time scales up to $1600\,\mathrm{s}$ [42]. In the second regime at high interfacial loads, obtained at long times and high bulk concentrations, respectively, the microgels already adsorbed to the interface create a barrier for the arriving microgels to adsorb, which results in an exponential relaxation of the interfacial coverage at long times [43]. Furthermore, experiments utilizing microgels with a polystyrene core demonstrated a kinetic limitation by the interfacial spreading [42]. In contrast, a study from Minato et al. [39] on larger PNIPAM hydrogels indicates that the deformation at the interface is so fast, that the crosslinker content, and thus the softness, has no detectable impact on the kinetics [39].

Regarding the attainable interfacial load, the first important aspect is that microgels form monolayers [17, 42, 22, 49] and the adsorption of microgels to the interface is irreversible [47, 7, 43]. Due to their size, the energy barrier for desorption is very high (compare section 2.2.1). Therefore, the attainable interfacial load is not directly dependent of the bulk concentration as it is not a matter of equilibrium [47]. This is in sharp contrast to other surface active species, e.g. surfactants, their equilibrium state is characterized by equal adsorption and desorption rate [50]. Therefore, the commonly used adsorption isotherms like the Langmuir or Frumkin isotherm are not applicable to discribe the adsorption behavior of microgels.

The dynamic adsorption process of microgels is regarded in various studies and it is commonly evaluated by the resulting change in interfacial tension [42, 51, 43]. To relate the interfacial coverage and the interfacial tension requires an equation of state. The surface pressure $\Pi = \gamma_0 - \gamma$ is a measure for the adsorption and particle interaction at the interface. There are many models to describe the surface pressure in a colloidal system. The ideal gas approach does not account for any interaction and should not be used, hence the simplest model is a 2D hard disks. The approach is extended to 2D soft disks by Groot and Stoyanov[52]. This approach introduces a new characteristic length scale d_{eff} accounting for the micro structure and polymer composition.

In their study they showed good agreement for the surface pressure depending on the surface coverage between the model and experimental data. They obtained a d_{eff} of $1.25\,\mathrm{nm}$ which is in range of typical microgel mesh sizes (compare section 2.2.3).[52]

2.3. Material and Methods

To determine properties and characterize the interfacial layer of the utilized microgels, different techniques are employed. Cryo-SEM images are taken of the microgels at the interface and analyzed regarding the microgel arrangement at the interface. Furthermore, the interfacial tension is measured by different methods, the drop volume tensiometry (DVT50, Krüss, Germany) and drop shape analysis (DSA, Krüss, Germany). With regard to the application of microgels as stabilizers of solvent drops surrounded by the aqueous microgel containing phase, the focus is on this dispersion case. For the investigation the microgels and the solvent systems introduced in section 1.4 are utilized.

2.3.1. Cryo-SEM Measurement

The appearance of the interfacial microgel layer was observed by cryo-SEM (cryo-scanning electron microscope) at DWI. The measurements are con-

ducted utilizing a Hitachi S4800 FeSEM set-up. Prior to the measurement, an micro-emulsion is prepared, in order to derive interfaces in an observable scale. Per microgel type a 20 mL sample is produced containing 6 mL n-butyl acetate and 14 mL aqueous microgel solution with a microgel concentration of 1 mg/ml. The micro-emulsion is generated utilizing an Ultra-Torrax®(T18 from IKA Germany) stirring with 14.000 min for 30 s. A sample of 10 µL is placed in the sample holder and frozen in liquid nitrogen. The sample is transferred to the microscope. Conditions in the microscope are kept to −140 °C and $4 \cdot 10^{-5}$ mbar. In the preparation chamber, the sample is fractured with a scalpel-blade. Then the sample is sublimated twice for 90 s rising the temperature to −80 °C. After decreasing the temperature again, the probe is sputtered with an Ag-Pd layer and transferred to the observation chamber.

The obtained pictures are evaluated using the image analysis software 'ImageJ'. The scale bar from the microscopy image is used to set the scale. The microgels center to center distance is determined by line measurements, the microgels center is determined by visual judgment. At least 188 line measurements are taken to determine the average microgel center to center distance. The measurement points are shown in figure A.1 in the appendix.

2.3.2. Interfacial Tension Measurement

Two methods that have been applied in this work the drop volume tensiometry (DVT) and the drop shape analyses (DSA), their physical principles are described in appendix A.4. The measurements with drop volume and drop shape methods ar conducted using a DVT50 and a DSA10, respectively, both from Krüss (Germany).

The microgel solution of different concentration is prepared by weight using bidestilled water and the microgel stock solution. For all interfacial tension measurement the aqueous phase and the solvent are mutually saturated to avoid inaccuracies due to mass transfer. The densities of the microgel solutions are determined prior to the experiment (DSA48 from Anton Paar, Austria). The organic phase is placed in the reservoir for the drop phase, while the microgel solution is placed as continuous phase in

the measurement tube or chamber, respectively.

Both instruments allow to measure the interfacial tension for different surface ages. In case of the DVT50, the surface age is set by adjusting the flow rates of the drop phase. For each flow rate the first three drops are discarded and the data collection starts with the fourth drop. At least three drops are measured per flow rate and the resulting interfacial tension is averaged. If the deviation is above $0.2\,\mathrm{mN\,m^{-1}}$ additional drops are generated and measured. The maximum number of drops per flow rate was set to 5.

For the measurement in the DSA10 the drop is formed once and the interfacial tension is determined from a contour fit to the drop shape. The contour fit is executed in user specific time intervals. To observe the short term adsorption the interval was set to $0.5\,\mathrm{s}$, for the long term observation it was set to $5\,\mathrm{s}$.

Details on the two measurement methods and their data evaluation can be found in the appendix A.4.

2.4. Experimental Results

The effects of the microgels on the interfacial properties are presented in this chapter. First the microgels morphology at the interface is discussed by observations from cryo-SEM images. Moreover, the effect of the microgels on the interfacial tension in the utilized systems is regarded. Finally, with regard to the determination of the microgel coverage of drops, attempts to relate the interfacial tension to the surface coverage are presented.

2.4.1. Cryo-SEM Observation

Figure 2.5 shows images from the cryo-SEM observation of small drops covered with microgels. The weakest cross-linked microgels MG1, shown in figure 2.5(a), appear almost as a smooth film. However, the individual microgels are still recognizable. In contrast, the morphology of the medium cross-linked microgels MG2 in figure 2.5(b) appears to be more bumpy at the interface. For MG3 and MG4 no analyzable images are obtained,

since the microgels are unstable under exposure to the electron beam and degenerate immediately.

Regarding the images obtained with higher magnification in figure 2.6(a) and (c), this observation is reinforced. The weaker crosslinked microgels MG1 have an average center to center distance at the interface of $1.25 \pm 0.26\,\mu m$ which is about twice their hydrodynamic diameter in bulk solution (see table 1.1). In figure 2.6(a) the arrangement of the microgels at the interface is not uniform. Nevertheless, there are areas with an almost ideal hexagonal packing (green and yellow hexagons in figure 2.6(a)) as it is commonly reported [37, 41, 34]. In this area the average distance is $1.32 \pm 0.09\,\mu m$, the lower deviation confirms the impression of an ideal packing. There are also areas where the microgels seem to cluster in straight lines, in this areas hexagonal packing is slanted in the direction of the cluster (blue hexagon in figure 2.6(a)). The areas with isolated microgels are not evaluated, as the evaporation of the ice layer might have been incomplete in the area covering the underlying microgels.

The medium crosslinked microgels MG2 are more uniformly unevenly packed at the interface. The average distance measured by 188 lines is $0.80 \pm 0.16\,\mu m$. For areas with mostly hexagonal packing (compare figure 2.6(c) green, yellow and blue hexagon) the average distance is $0.73 \pm 0.09\,\mu m$, and the deviation is reduced from $19.54\,\%$ to $12.7\,\%$ compared to the overall average distance. The ratio of the diameter at the interface and in bulk is 1.4.

(a) MG1 $2.5\,mol\,\%$ (b) MG2 $5\,mol\,\%$

Figure 2.5.: Cryo-SEM images of microgel-covered n-butyl acetate drops with different degree of cross-linking

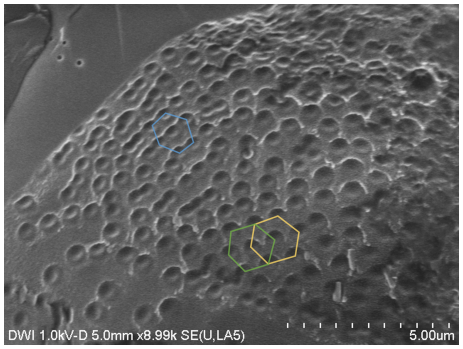

(a) MG1 2.5 mol %

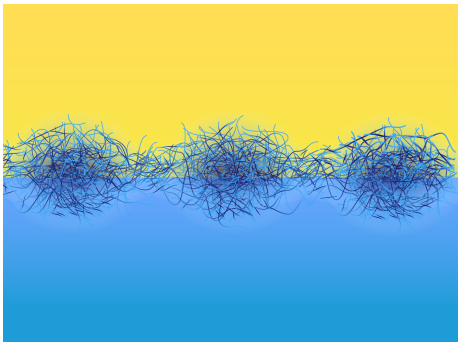

(b) MG1 2.5 mol %

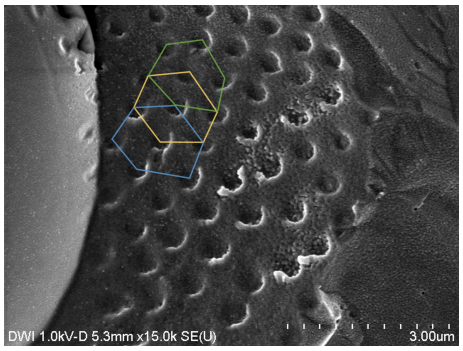

(c) MG2 5 mol %

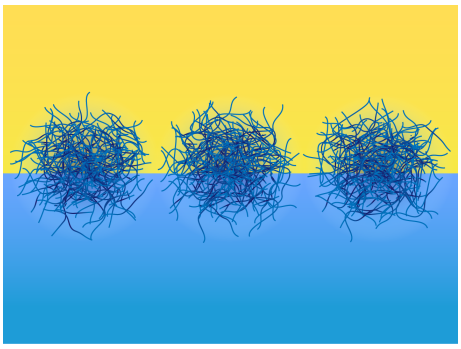

(d) MG2 5 mol %

Figure 2.6.: Cryo-SEM images (a),(c) (with different magnification) and illustration (b),(d) of microgels at the interface with different cross-linking

Scotti et al. report a ratio of 1.9 for microgels with 5 mol % crosslinker [32]. The differences might originate from the microgels size and their measurement, as they transfer the microgels from the interface to a solid substrate and measure the distances by AFM. While the measurement in this work is less accurate due to distortion from the three dimensional sample. However, the trend of increasing deformation and spreading with decreasing crosslinker content matches the findings from Destribats et al.[34].

Concluding, the larger diameter ratio of MG1 compared to MG2 suggests that these less crosslinked microgels are more stretched at the interface. This is in good agreement with findings from other studies [42, 32]. However, the independence of the center to center distance from the crosslinker content at constant microgel size as reported by Destribats et al. cannot be confirmed for the utilized microgels, which diameters deviate by 20 %.

2.4.2. Effect of Microgels on Interfacial Tension

When microgels adsorb to liquid-liquid interfaces they reduce the interfacial tension as described in sections 2.2.1 and 2.2.3. In this work the interfacial tension is used to characterize the microgel system. Therefore, the time resolved interfacial tension reduction is regarded considering the impact of the microgel morphology as well as the solvent system. Finally, the interfacial tension could be used as an indicator for the interfacial coverage. Therefore, the adsorption process is modeled using the results from interfacial tension and surface pressure measurements performed within the collaborate research center SFB985 at 'Institut für Physikalische Chemie'(IPC), RWTH Aachen University.

Impact of Microgel Type and Concentration

With the setup described in section 2.3.2 the interfacial tension was measured as result of the time resolved microgel adsorption. As described in literature and above in section 2.2.3 the early adsorption is diffusion limited and thus concentration dependent. For the utilized microgels this is shown in figure 2.7. Since the focus is on the effect on the interfacial tension, the relative change of interfacial tension is displayed which is defined as $\gamma^+ = \frac{\gamma_0 - \gamma(t)}{\gamma_0 - \gamma_{end}}$. For this observation the microgel concentration is varied from $0.01\,\mathrm{g\,L^{-1}}$ to $0.5\,\mathrm{g\,L^{-1}}$ which leads to very different time scales for the adsorption process. As a well observable comparison, the time required to reduce γ^+ to 0.6 is regarded for MG2 (magenta) in figure 2.7. At low concentration ($0.01\,\mathrm{g\,L^{-1}}$) more than $2000\,\mathrm{s}$ are required for the reduction γ^+ to 0.6. Whereas, at high concentration (of $0.5\,\mathrm{g\,L^{-1}}$) the adsorption of the same amount of microgels, and thus the same reduction in interfacial tension, requires only $8\,\mathrm{s}$.

Furthermore, the microgel morphology also affects the adsorption kinetics. Comparing microgels with similar bulk diameter, MG1 and MG2, the less crosslinked MG1 (green) reduces the interfacial tension more quickly than the more crosslinked MG2. This effect decreases with increasing concentration. For high concentration the time required for $60\,\%$ of total reduction in interfacial tension ($\gamma^+ = 0.4$), differs in total by $7\,\mathrm{s}$ between the microgels,

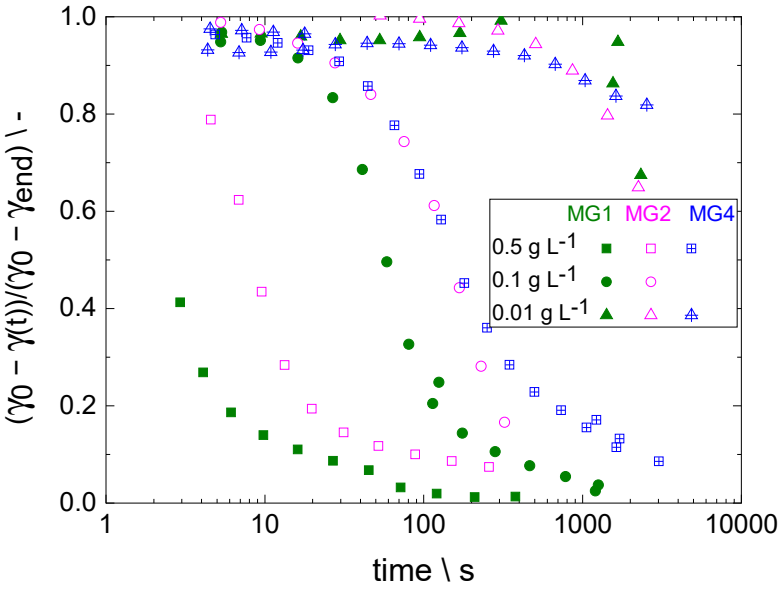

Figure 2.7.: Time resolved development of the interfacial tension for different crosslinked microgels (MG1 and MG2) and different sized microgels (MG2 and MG4) for different concentrations, measured by DVT method

which is 70 % in relative. At medium concentration the required time differs by 60 s, which equals 53 %.

At low concentration no difference between the microgels is observed. This could be explained by the different time scales of the processes involved in the adsorption process. As the microgels are similar in size, their diffusion coefficient differ only slightly. Thus the spreading of the microgels would cause differences in the interfacial coverage at short time scales of early adsorption and responsible for the large relative differences. Less crosslinked microgels would requiere a higher quantity at the interface to obtain the same coverage as softer microgels and thus at equal size and diffusion subsequently more time.

With progressing adsorption and thus interfacial loading the deformability with regard to compression becomes more relevant. The compression isotherms for the utilized microgels were experimentally derived at the IPC, the data is shown in the appendix A.2.

Combining the findings from figure 2.7 and the compression isotherms in figure A.2 it can be concluded that the more deformable microgels reduce the interfacial tension at lower interfacial loads (mass per area) and that the

compression of the microgels at the interface at higher loads leads to the differences observed. For the smaller microgel with medium crosslinking (MG4) the reduction of the interfacial tension is significantly slower as can be seen in figure 2.7 (blue). Due to smaller size the required amount of microgels to cover the interface is higher surpassing the faster diffusion.

To test the time scales of two different regimes the time depended change is regarded in more detail. Diffusion limited adsorption to an interface can be described very well using the equation from Ward and Tordai [27]. The equation relates the adsorption proportional to the square root of time. It provides the interfacial load Γ based on the diffusion coefficient D, the bulk concentration c_0 and time t. For microgels desorption can be neglected due to their large size and the associated high desorption energy. This simplifies the Ward and Tordai equation to [42]:

$$\Gamma_t = 2\sqrt{\frac{D}{\pi}} c_0 \sqrt{t} \tag{2.3}$$

Therefore, assuming a linear relation between surface coverage and interfacial tension a diffusion limitation can be detected by plotting the interfacial tension over the square root of time as shown in figure 2.8 for the weakly and medium crosslinked microgels MG1(olive) and MG2(magenta).

The degree of certainty (R^2) is above $96\,\%$ for all fits. The great certainty of the linear fit indicates a diffusion limitation at early stages. The time scale range for the medium and low concentration are in good agreement with literature, Li et al. report linear behavior upto $80\ s^{1/2}$ for concentrations of $10^{-4}\,\mathrm{g\,L^{-1}}$ ($d_{MG} = 500$ nm with $3.2\,\mathrm{mol}\,\%$)[42]. Still, this method only gives a qualitative impression, since it assumes a linear relation between interfacial tension and interfacial coverage, which might be appropriate but higher interfacial coverage require more detailed insights [51, 43] and will be discussed in section 2.5.

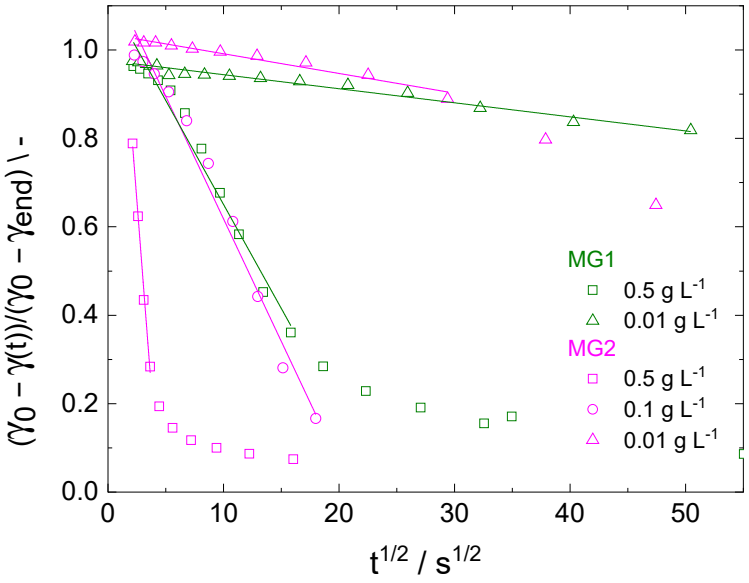

Figure 2.8.: Normalized interfacial tension as function of $\sqrt{t}$ and linear fits for different concentration of MG1 and MG2

In order to ensure that the observed behavior is truly attributable to the microgels adsorption kinetics and not an artifact of the measurement method comparative measurements are performed. In drop volume tensiometry measurements, the drop is generated with different volume flow rates. Hence, the drop grows with increasing drop age. To exclude this effect measurements are performed using the pendent drop method. Here, the drop is generated completely at the start of the measurement and interfacial tension is obtained via drop shape analysis. The details of both methods are explained in more detail in the appendix (see A.4). The results in figure 2.9 show a difference between the two methods. In case of the DVT method the course of the change in interfacial tension is delayed compared to the DSA method. This can be attributed to the drop growth during the measurement and thus the increasing drop surface over time. It should also be mentioned that the measurements of the DSA method starts after the drop is generated and thus the measurement contains a short lag time at the beginning. However, the trend, especially at higher loads, is in good agreement.

With regard to the application in disperse systems the transferability of the results to different solvent systems is regarded. Therefore, interfacial tension

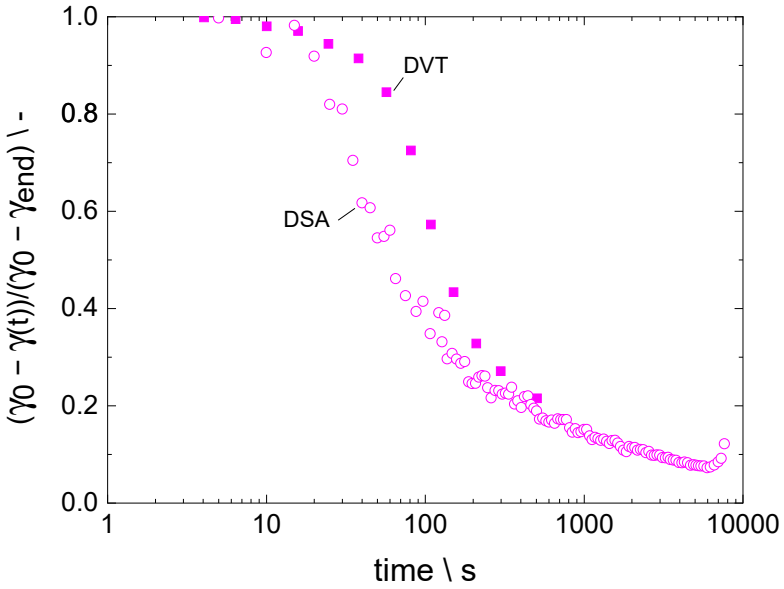

Figure 2.9.: Comparison of normalized interfacial tension measured with drop volume tensiometry (DVT) and drop shape analysis (DSA) for toluene drops in aqueous solution containing MG2 with $0.1\,\mathrm{g\,L^{-1}}$

measurements are conducted using different organic solvents with different polarity and interfacial tensions. For better comparison, the obtained interfacial tensions are again normalized and shown as γ^+ in figure 2.10. The time resolved change in interfacial tension for the utilized microgels using different solvents are in excellent agreement. Thus, the adsorption process is not affected by the solvents polarity neither at high nor at low concentrations. An effect of the solvent on the adsorption dynamics as reported in literature is not observed [53]. Mendoza et al.[53] attribute th effect to long range solvent mediated interactions, in the regarded systems these interactions are either too small to observe or surpassed by the direct microgel interaction. However, this leads to the conclusion, that the findings mentioned above are predominantly microgel specific and thus transferable to other solvents systems.

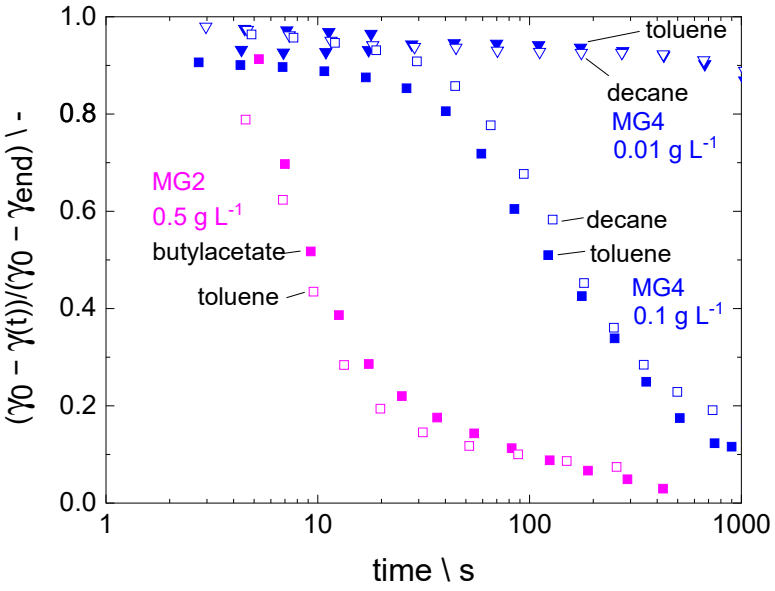

Figure 2.10.: Normalized interfacial tension for MG2 and MG4 with different organic solvents: n-butyl acetate, toluene, and n-decane, measured by DVT method

2.5. Model Approach

For the estimation of the interfacial coverage of the drops used for the single drop experiments the interfacial tension is an accessible measure. However, the correlation between the interfacial tension and the interfacial coverage and cannot directly be derived from the interfacial tension measurements. Nevertheless, the interfacial tension measurements derive valuable insights and can be used to check the proposed relation and assumptions.

In literature two model approaches are presented. Zhang and Pelton [51] proposse a simple Langmuir kinetic model assuming a linear relation between interfacial tension and coverage, while Deshmuck [43] uses a Soft Disc approach from Groot [52] for the equation of state.

2.5.1. Model Setup

For the comparison to the experimental data a model is setup in Matlab®. The adsorption process is described by two steps, the diffusion from bulk to the interface and the adsorption (see section 2.2.3). Therefore, the

model depicts the microgel concentration at the drop surface and in the surrounding aqueous microgel solution. The model is resolved in radial direction and over time. The simulated radius of the continuous phase is $1000\,\mu m$ and is divided into 1000 compartments with constant width along the radius. This configuration was tested to be sufficient to model the developing concentration profile, so that the condition of constant bulk concentration is fulfilled at the outer radius. The adsorption to the interface is modeled using a probability approach, the more microgels are already adsorbed to the interface the less likely the arriving microgel arives at a free side as the adsorbed microgels create a barrier [41].

$$\Gamma_t = \Gamma_{t-1} + (1 - \frac{\Gamma_{t-1}}{\Gamma_{max}}) m_{MG,t,1} \tag{2.4}$$

Therefore, the surface coverage Γ depends on the previous coverage and the surface coverage fraction, respectively, and the microgels available in the first compartment at the interface $m_{MG,1}$. The maximum coverage Γ_{max} is estimated from Langmuir trough experiments, since the exact value is hard to extract from the experiments it is also fitted. The amount of microgels available in the first compartment is determined by diffusion from the bulk. The microgels diffusion coefficient is taken from DLS measurements. The time steps size is adopted to the gradient of the concentration profile to be below $\Delta y = 0.005$ the minimum time step size is fixed at $10^{-8}\,s$.

Since the microgels are soft particles with complex interfacial behavior, the linear relation for the interfacial tension and coverage can only be assumed for low interfacial coverage (see section 2.2.3). The results from Zhang and Pelton show good results for early adsorption and thus low interfacial coverage, but they do not reflect the flattening course for long time scales as it can also be seen for the utilized microgels in figures 2.7 and 2.10. This implies a more complex relation. Deshmuck et al. used the soft disc approach from Groot [52] as an equation of state to relate the coverage and

the surface pressure Π.[52, 43]

$$\Pi = \frac{4k_BT}{\pi d_{eff}^2}\left(\frac{b\eta Z(\eta)}{\lambda} - b_2\eta^2\right) \tag{2.5}$$

The equation uses the Boltzmann constant k_B, temperature T. The parameter d_{eff} reflects the size of the correlated domains within the microgel which is physically interpreted as the distance between crosslinks and can be used for fitting. The parameters b and λ denote repulsive interactions, for the microgel system the values for both parameters can be set to unity [43]. Attractive short range interactions are denoted by the parameter b_2, Deschmuck report extremely small values in the range of 10^{-4}, thus this parameter can be neglected. The soft character of the discs is accounted for by the compressibility factor Z:

$$Z = \frac{1 + \eta^2/8}{(1-\eta)^2} - \frac{0.043\eta^4}{(1-\eta)^3} \tag{2.6}$$

The coverage of the interface is reflected by the surface packing fraction η, which is defined in this work by the adsorbed mass per area $\eta = \frac{\Gamma}{\Gamma_{max}}$. The surface pressure depending on the mass per area is taken from the Langmuir trough experimental data from IPC (see appendix A.3). The fitted equation of state is shown in figure 2.11.

The fitted d_{eff} is $1.15\,\mathrm{nm}$ and thus in the range of microgel mesh sizes between $1,10\,\mathrm{nm}$ reported in literature [43, 44, 32]. The obtained fit is in good agreement for low mass per area, but does not reflect the behavior for higher loads. Therefore, a logistic function is chosen for alternatively fitting, which is a sigmoidal function typically describing saturation processes.

$$y = \frac{A_1 - A_2}{1 + (\frac{x}{x_0})^p} + A_2 \tag{2.7}$$

The parameters A_1 and A_2 determine the initial and final value of the

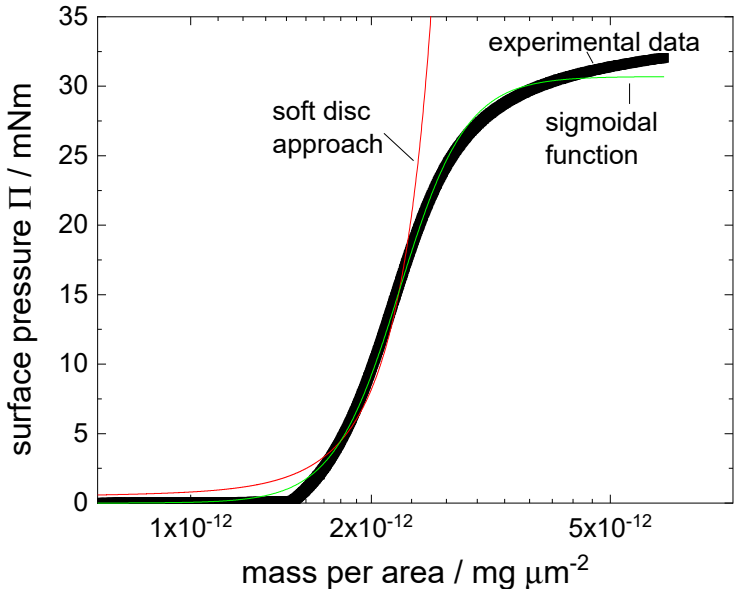

Figure 2.11.: Relation between interfacial microgel loading and surface pressure for MG2, experimental data from Langmuir trough experiments and fitting of soft disc (equation 2.5) and sigmoidal approach (equation 2.7)

surface pressure; hence, A_1 is set zero. The fraction $\frac{x}{x_0}$ can be regarded similar to the surface packing fraction η in equation 2.5, since x_0 represents the center of the saturation process it is defined as $50\,\%$ coverage, thus $\frac{\Gamma_{max}}{2}$. The exponent p determines the slope of the saturation and is fitted to the experimental data to 7.83. The fit has a certainty of $R^2 = 0.96$ and is shown in figure 2.11.

2.5.2. Results

The interfacial tension obtained over time from simulation and experiments is shown for MG2 and a bulk concentration of $0.25\,\mathrm{g\,L^{-1}}$ in figure 2.12(a). The parameter d_{eff} from equation 2.5 is varied based on the inertial guess from the fitting to the Langmuir trough experiments between $1\,\mathrm{nm}$ to $1.3\,\mathrm{nm}$. For early adsorption and thus the evolution of the interfacial tension for small time scales the simulation has good accordance to the experimental data and the findings on the diffusion limited adsorption from section 2.4.2. However, the flatting course for longer time scales and thus higher interfacial loads is not reflected. Regarding the interfacial coverage over time in figure

2.12(a), the interface saturates with microgels over time. At the end, when the interface is highly covered the saturation increases less rapidly, due to the probability approach from equation 2.4. This does not propagate to the evaluation of the interfacial tension due to the lag of accuracy for higher surface coverage of the equation of state proposed by Deshmuck [43].

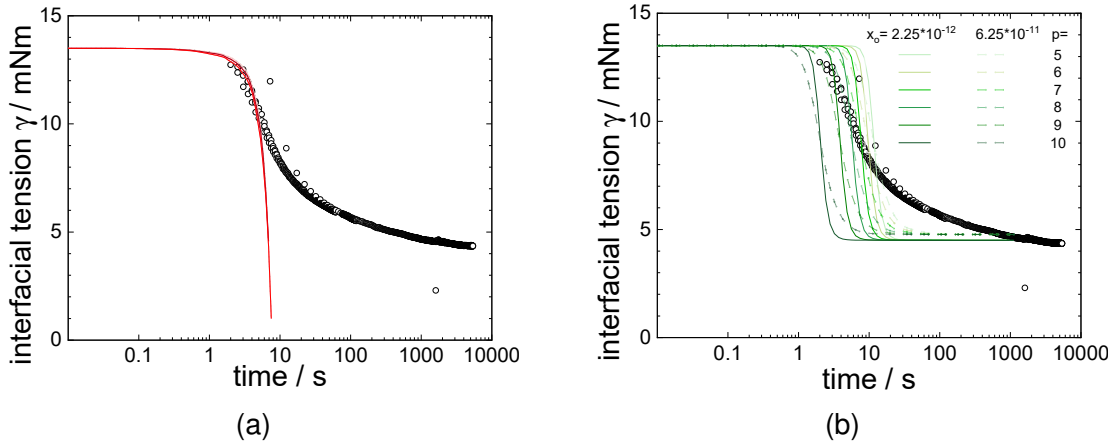

Figure 2.12.: Time dependent interfacial tension, experimental data from pendent drop measurement for MG2 ($0.25\,\mathrm{g\,L^{-1}}$) and simulation results obtained using the soft disc approach in 2.5 for d_{eff} between $1\,\mathrm{sec}$ to $10\,\mathrm{sec}$ in (a) and the sigmoidal function in equation 2.7 with fitting parameters x_0 ($\mathrm{mg\,\mu m^{-2}}$) and p (-) in (b)

To display the behavior for high interfacial loads more correctly, the fitted sigmoidal function is also tested. The resulting time resolved evolution of the interfacial tension is shown in figure 2.12(b). This approach displays the early development also well and moreover a threshold value for the interfacial tension. Nevertheless, the flattening course is not reflected although the fit with the Langmuir trough data is of good certainty. Therefore, the flattening course at longer times scales indicates most likely that the adsorption of microgels at high interfacial coverage is more complex than the probability approach accounts for. In case of proteins and other polymers a reconfiguration of the interfacial layer is reported [54]. Furthermore, the particles elasticity becomes more significant with increasing surface coverage [46]. Although, the adsorption of microgels at interfaces is generally regarded as irreversible, Deshmukh et al. [43] propose partly desorption of the microgels uncrosslinked periphery as energetically favorable at high

interfacial loading. Investigating these phenomena requires more detailed insights on the microgels interaction at a microscopic or molecular scale, a promising approach are molecular dynamic simulations as presented by Bushuev et al. [46] for mechanical microgel compression at the interface. Hence, in this work the evaluation fo the coverage of drops with microgels via interfacial tension cannot be used in a quantitative manner.

2.6. Conclusion

The results presented in this chapter show the complexity of microgels behavior at the interface. The findings from the cryo-SEM images, confirm the impact of the crosslinker on the interfacial morphology for the utilized microgels. This is also reflected by the adsorption behavior and the less crosslinked MG1 reduces the interfacial tension more efficiently than the other microgels. Furthermore, no impact of the solvent system was observed which allows a transfer of the results between the utilized solvent systems. The relation between the interfacial coverage and the interfacial tension is found to be very complex. Thus the interfacial tension cannot be utilized to quantify the coverage of drops with microgels. Nevertheless, the findings in this chapter show the relation between the microgel structure and the interfacial behavior and thus they provide the basis for the investigation of the impact of the microgels on extraction relevant phenomena in the following chapters.

2

3. Fluid Dynamics of Microgel covered Drops

Parts of this chapter have been published as:
Fluid Dynamics of Microgel-Covered Drops Reveal Impact on Interfacial Conditions, Polymers, 2018
Miriam Faulde, Eric Siemes, Dominik Wöll, Andreas Jupke
DOI: 10.3390/polym10080809

3.1. Introduction

The fluid dynamics of drops, with the sedimentation velocity as simple measure, are a versatile tool to characterize and describe dipserse systems. On the one hand, the sedimentation velocity of single drops is used in process simulation as part of the description for extraction processes. On the other hand, the sedimentation velocity is very sensitive to the physical properties of a system, especially at the interface. Hence, it can be utilized as an easily accessible measure to shed light on the impact of surface active species like microgels on the interfacial conditions.

Therefore, the impact of microgels on the sedimentation velocity is investigated by single drop experiments. The results are compared with theoretical models to help to quantify effects and draw conclusions about the underlying phenomena and conclusions on propagation of microgel structure-property relation causing effects on single drop scale. Furthermore, the comparison to a surfactant and investigation on drop shape reinforce the complexity of effects on interfacial properties, exceeding the simple reduction of interfacial tension.

3.2. Fundamentals

3.2.1. Sedimentation Behavior of Drops

Regarding a single drop rising in a quiescent surrounding liquid due to the density difference, the velocity of the drops depends on its diameter as shown in figure 3.1. A specialty of disperse liquid systems is the mobility of the fluid interface, leading to a behavior different to solid spheres.[55] For solid particles and rigid interfaces there is an adhesion condition at the interface and the velocity is zero (see figure 3.1 on the right green). On the other hand, if the interface is mobile and thus permeable to momentum transfer, the shear stress at the interface leads to movement of the interface, and the velocity is non-zero. This induces a circulativ flow pattern inside the drop (see figure 3.1 on the right in blue).[56, 19] The reduced relative velocity between the interface and the continuous phase leads to reduced friction and the sedimentation velocity of the drop is higher compared to a rigid sphere.[57]

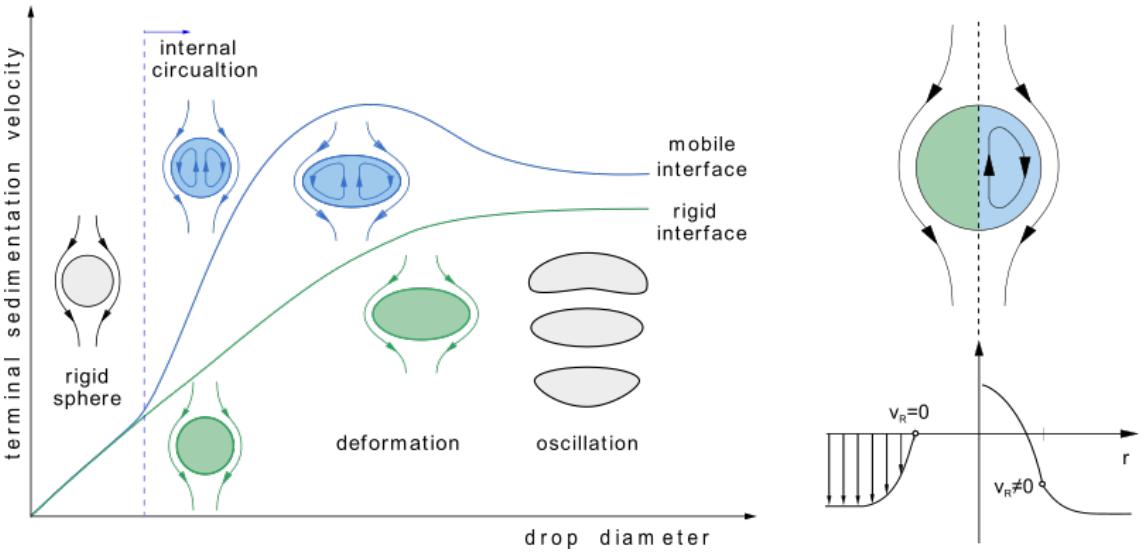

Figure 3.1.: Terminal velocity and drop shape as function of the drop diameter for mobile and rigid interfaces (adopted from [19]) and corresponding velocity profiles (adopted from [58]).

According to Henschke [19] for drops in technical systems four regimes can be distinguished corresponding to their diameter and drop shape. [19]

- Drops with an immobile interface
- Drops with a mobile interface
- Oscilllating drops
- Deformed drops

The sedimentation of small drops equals rigid spheres, because trace impurities accumulate at the interface. The drop is spherical and has an immobile interface due to the impurities.[19] As the drop diameter increases the impact of trace impurities diminishes and interfacial mobility increases. Circulation inside the drop occur and the sedimentation velocity increases. With increasing velocity the pressure at the interface in direction of movement increases and for larger drops the drop pressure, pursued by the interfacial tension, is not sufficient to preserve the spherical shape of the drop, hence the drop begins to oscillate.[19, 59] For these drops, the velocity does not increase with increasing drop diameter. For larger drops the drops shape becomes umbrella like and the drop is ‘wabbeling‘ in direction of sedimentation.[19]

The behavior explained above describes pure standard solvent systems, if surface active species are present they form an adsorption layer at the interface affecting many physical properties of the system and thus changing the behavior drastically.[60, 61] The adsorption layer reduces the interfacial tension which acts as a shape conserving force counter the deformation of the drops. Thus the reduction of interfacial tension leads to deformation of drops for smaller diameters and lower velocities, respectively.[62] Most importantly, the adoption layer reduces the interfacial mobility. This can be described depending on the interfacial coverage by the stagnant cap angle. In case of a not fully covered interface, the shear stress at the interface moves the molecules to the downstream side of the drops forming a stagnant cap. The coverage can be expressed by the stagnant cap angle as shown in figure 3.2. It can be also seen that the internal circulation is reduced with increasing coverage and for fully covered drops with a stagnant cap angle of $0°$ the interface is immobile.[62]

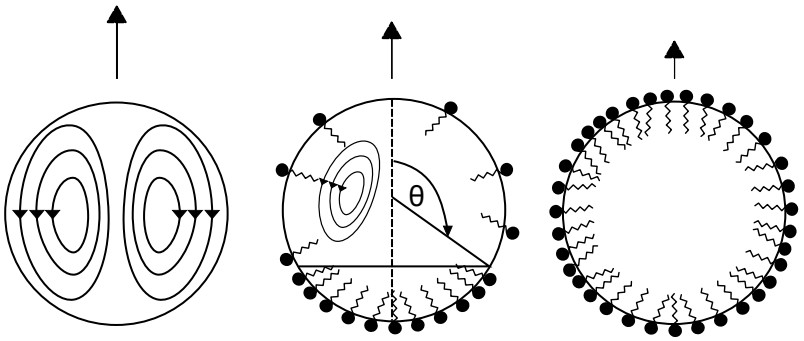

Figure 3.2.: Schematic sketch of the stagnant cap (adopted from [62]).

This theory gives reason to suppose that a surfactant concentration in the range of the critical micell concentrations, which indicates maximum interfacial load, is required to cause rigid sphere like behavior. However, many experimental studies found sedimentation velocities in surfactant systems implying rigid conditions at the interface at concentrations far below the critical micell concentration. Wegener and Paschedag [63] report a divergence in the range of $10^4\,\mathrm{mmol\,L^{-1}}$ for the anionic surfactant SDS in the toluene/ water system. Comparing different surfactants and solvent systems Paul [62] concludes that the sensitivity of the system to surfactants increases with decreasing viscosity ratio, as a lower viscosity ratio implies more pronounced effect of the interfacial mobility on the sedimentation velocity. Furthermore, he concludes that the adsorption behavior of the surfactant plays an important role.[62]

3.2.2. Models for Sedimentation of Drops

The physical basis of all models is a force balance on a sedimenting object as shown in figure 3.3. The following forces act on the volume of the object: Weight force F_W, buoyancy force F_M, drag force F_D, and inertial force F_I. The direction of movement depends, whether the weight force or the lifting buoyancy force is larger. An object with lower density ρ_d than the density of the surrounding fluid ρ_c rises.[55]

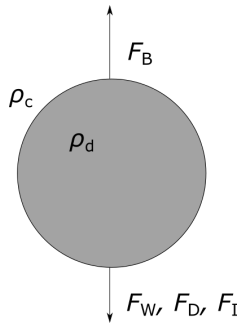

Figure 3.3.: Force balance on a sedimenting drop.

Weight force $F_{\mathrm{W}} = V_d \rho_d g$
Buoyancy force $F_{\mathrm{M}} = V_d \rho_c g$
Drag force $F_{\mathrm{D}} = C_W \frac{\rho_c}{2} v_{Sed}^2 A_p$
Inertial force $F_{\mathrm{I}} = V_d \rho_d \frac{\mathrm{d}v_{Sed}}{\mathrm{d}t}$

Drops reach their terminal velocity very quickly, e.g. 3 mm toluene drops reach their stationary velocity in aqueous phase in approximately 1 s [64]. Therefore, only the terminal state of the sedimentation velocity is regarded in this work. Hence, the inertial force can be canceled from the force balance since $\frac{\mathrm{d}v_{Sed}}{\mathrm{d}t} = 0$ and thus $F_I = 0$. This simplifies the determination of the sedimentation velocity from the force balance, shown in 3.1. [65]

$$\begin{aligned} F_{\mathrm{B}} &= F_{\mathrm{W}} + F_{\mathrm{D}} \\ V_d \rho_c g &= V_{\mathrm{d}} \rho_{\mathrm{d}} g + C_D \frac{\rho_c}{2} v_{\mathrm{sed}}^2 A_p \\ v_{\mathrm{sed}} &= \sqrt{\frac{2g}{C_D} \frac{V_{\mathrm{d}}}{A_p} \frac{(\rho_{\mathrm{c}} - \rho_{\mathrm{d}})}{\rho_{\mathrm{c}}}} \end{aligned} \tag{3.1}$$

Besides the densities (ρ_c and ρ_d) of the system the calculation requires the volume V_d and the projected area in direction of movement of the object A_p, and the drag coefficient C_D. Vice versa the drag coefficient can be

calculated for known sedimentation velocity.

$$C_D = \frac{2g}{v_{\mathrm{sed}}^2} \frac{V_{\mathrm{d}}}{A_p} \frac{(\rho_{\mathrm{c}} - \rho_{\mathrm{d}})}{\rho_{\mathrm{c}}} \tag{3.2}$$

Drag Coefficients for Solid Spheres and Spherical Drops

For the prediction of the sedimentation velocity of solid spheres drag coefficient correlations are commonly used. The drag coefficient is determined as a function of the Reynolds number.

$$Re = \frac{\rho_{\mathrm{c}} v_{\mathrm{sed}} d_{\mathrm{V}}}{\eta_{\mathrm{c}}} \tag{3.3}$$

For a continuous phase with constant density ρ_{c} and dynamic viscosity η_{c} the Reynolds number only varies by the product of sedimentation velocity and diameter. Thereby, the diameter d_{V} refers to a volume equivalent sphere.

For creeping flows with very small Reynolds numbers ($Re \ll 1$) the drag coefficient C_D can be described by Stokes approach:

$$C_D = \frac{24}{Re} \tag{3.4}$$

The correlation is extended to a significantly wider scope of flow regimes by different authors, e.g. Brauer and Mewes[66]. A selection of these correlations and their range of application are listed in table 3.1.

As mentioned above, in contamination free liquid-liquid systems spherical drops have a mobile interface [55]. For the determination of the drag in these systems not only the Reynolds number, but also the viscosity and density of the phases must be considered to account for the fluid character of the system [57]. Experimental studies indicate that the impact of the density ratio is very small and can be neglected [71]. For the viscosity ratio ($\eta^* = \eta_{\mathrm{d}}/\eta_{\mathrm{c}}$) two limiting cases exist. In case of very high viscosity ratios ($\eta^* \to \infty$) the drop behaves similar to a ridgid sphere. For very small

Table 3.1.: Selected C_D correlations for rigid spheres

Author	Correlation	Valid range
Stokes (1850) [55]	$C_D = \frac{24}{Re}$	$Re << 1$
Clift and Gauvin(1971)	$C_D = \frac{24}{Re}(1 + 0.15Re^{0.687}) + \frac{0.42}{1+4.25\cdot10^4 Re^{-1.16}}$	$Re < 3 \cdot 10^5$
Brauer and Mewes(1972)	$C_D = \frac{24}{Re} + \frac{4}{Re^{0.5}} + 0.4$	$0 \leq Re \leq 10^4$
Brauer(1973)	$C_D = \frac{24}{Re} + \frac{3.73}{Re^{0.5}} + \frac{4.83\cdot10^{-3} Re^{0.5}}{1+3\cdot10^{-6} Re^{1.5}}$	$Re < 3 \cdot 10^5$
Martin(1980)	$C_D = \frac{1}{3}(\sqrt{\frac{72}{Re} + 1})^2$	$Re < 3 \cdot 10^5$
Henschke et al.(2000)	$C_D = \frac{432}{Ar} + \frac{20}{Ar^{1/3}} + \frac{0.51Ar^{1/3}}{140+Ar^{1/3}}$	$Re < 3 \cdot 10^5$

viscosity ratios ($\eta^* \to 0$) its behavior is similar to a gas bubble. Selected drag correlations for spherical drops are listed in table 3.1.

Figure 3.4 compares the limiting cases and experimental data from Wegener et al. [58]. The drag decreases with increasing Reynolds number and increases rapidly for higher Reynolds numbers. The onset of the increase marks the onset of oscillation and deformation of the drops.[58] It can be characterized by the Weber number We, which proportionates deforming and shape conserving forces.

$$We = \frac{v_{\mathrm{sed}}^2 d_{\mathrm{d}} \rho_{\mathrm{c}}}{\gamma} \tag{3.5}$$

Different studies determined the onset of deformation for various solvent systems for a critical Weber number of $We_{\mathrm{crit}} = 4$ [72, 73, 74]. However, it should be noted that the Weber number considers the interfacial tension as only shape conserving force.

As mentioned in section 3.2.1 the presence of impurities and surface active species at the interface affects the sedimentation of drops drastically. Grace et al.[75] derived an empirical correlation to describe the sedimentation velocity of drops in contaminated systems, using the dimensionless

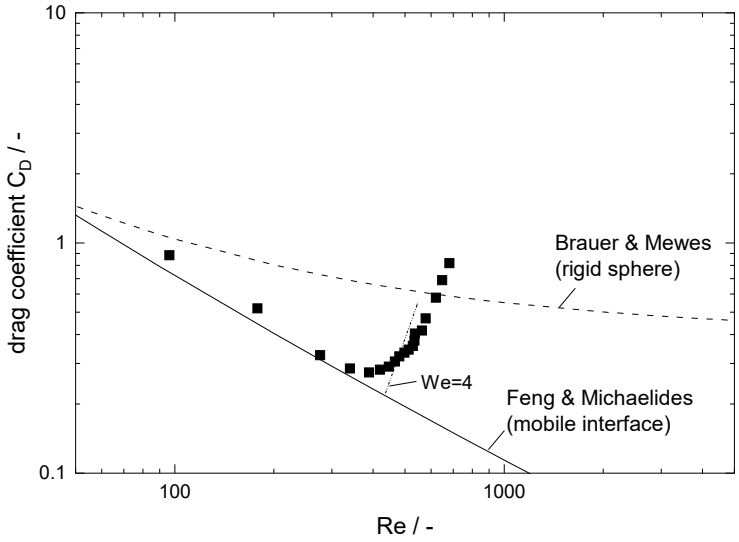

Figure 3.4.: Drag coefficient as function of the Reynolds number, comparison of correlations for the limiting cases and typical trend of experimental data (from Wegener et al. [58])

Table 3.2.: Selected empirical correlations for the drag coefficient of spherical drops.

Author	Correlation	Valid range
Rybczynski (1911)	$C_D = \frac{24}{Re}\frac{2/3+\eta^\star}{1+\eta^\star}$	$Re \ll 1$
Hamielic et al.(1963)	$C_D = \frac{3.05(783\eta^{\star 2}+2142\eta^\star+1080)}{(50+209\eta^\star)(4+3\eta^\star)Re^{0.74}}$	$4 < Re < 100$
Feng and Michaelides (2001)	$C_D = \begin{cases} \frac{2-\eta^\star}{2}C_D(Re,0) + \frac{4\eta^\star}{6+\eta^\star}C_D(Re,2) & 0 \le \eta^\star \le 2 \\ \frac{4}{\eta^\star+2}C_D(Re,2) + \frac{\eta^\star-2}{\eta^\star+2}C_D(Re,\infty) & 2 \le \eta^\star \le \infty \end{cases}$	
	$C_D(Re,0) = \frac{48}{Re}\left(1 + \frac{2.21}{\sqrt{Re}} - \frac{2.14}{Re}\right)$	
	$C_D(Re,2) = 17.0Re^{-2/3}$	$5 \le Re \le 1000$
	$C_D(Re,\infty) = \frac{24}{Re}(1 + \frac{1}{6}Re^{2/3})$	

Morten Mo and Eötvös Eo number:

$$v_{\mathrm{sed}} = \frac{\eta_{\mathrm{c}}}{\rho_{\mathrm{c}} d_{\mathrm{d}}} Mo^{-0.149}(J - 0.857) \tag{3.6}$$

using

$$J = \begin{cases} 0.94H^{0.757} & 2 < H \leq 59.3 \\ 3.42H^{0.441} & H > 59.3 \end{cases} \quad \text{with } H = \frac{4}{3} EoMo^{-0.149} \frac{\eta_{\mathrm{c}}}{0.9mPas} \tag{3.7}$$

Drag Coefficients for Deformed Drops and Rigid Objects

With increasing drop diameter and sedimentation velocity, respectively, the forces acting on the rising drop increase, as pointed out by equation 3.5. When the friction forces exceed the shape conserving force of the interfacial tension the drop deforms. According to Clift et al.[59] three different drop shapes should be considered:

- spherical drops: interfacial forces are dominant
- ellipsoid drops: flattened form, the drops can oscillate periodically or random
- umbrella shaped drops: strong deformation, no symmetry in direction of movement

As computers evolved, approaches to determine velocity and drop shape have increased complexity over time, from simple graphical approaches [75] to dynamic numerical simulation [56, 76]. These simulations show excellent agreement with experimental data but are very calculation-intensive. On the other hand graphical determination uses simple dimensionless quantities, the Eötvös number and the Morten number, which both solely require the physical properties of the system. These numbers are utilized to determine the sedimentation velocity and drop shape for an estimated Reynolds number.[75] Besides these two extremes, correlations are presented, e.g. by Harper[77] for the drag coefficient of deformed drops also considering the

Morten number: [77]

$$C_D = \frac{MoRe^4}{48} \tag{3.8}$$

with

$$Mo = \frac{g\eta_c\Delta\rho}{\rho_c^2\gamma^3} \tag{3.9}$$

In case of strongly deformed, oscillating drops Thorsen et al.[78] obtained good agreement with their equation.

$$v_{\mathrm{sed}} = \frac{6.8}{1.65 - \frac{\Delta\rho}{\rho_d}} \frac{\sqrt{\frac{\gamma}{3\rho_d+2\rho_c}}}{\sqrt{d_d}} \tag{3.10}$$

The equation reflects the decreasing sedimentation velocity with increasing drop diameter in this regime (see figure 3.1), by the dependency of the velocity to the square root of the diameter in denominator.

For the drag coefficient of non spherical objects with rigid surface an overview is given by Xu et al.[79]. Besides the Reynolds number these correlations consider different input parameters referring to the geometric shape of the regarded object.

- d_V the diameter of a volume equivalent sphere
- d_A the diameter of an area equivalent circle to the projected area of the regarded object in direction of movement
- D the diameter of the cylinder in which the object sediments
- the spehricity
  - s the surface sphericity
  - ϕ the particle sphericity

The surface sphericity s is defined by Tran-Cong et al.[80] as the ratio of the circumference of an area equivalent circle to the actually projected

circumference of the object in direction of movement U_{P}.

$$s = \frac{\pi d_{\mathrm{A}}}{U_{\mathrm{P}}} \tag{3.11}$$

The particle sphericity is defined by Haider and Levenspiel as the surface of a volume equivalent sphere and the surface of the regarded object.

$$\phi = \frac{O_{\text{sphere}}}{O_{\text{object}}} \tag{3.12}$$

An overview of the different correlations their input parameter and application range is given in table 3.3

Table 3.3.: Selected drag correlations for deformed solids from Xu et al.[79]

Author	Correlation	Valid range
Haider and Levenspiel(1989)	$C_D = \frac{24}{Re} + \frac{24}{Re}\exp\left(2.3288 - 6.4581\phi + 2.4486\phi^2\right) Re^{(0.0964+0.5565\phi)} + \frac{Re\cdot\exp\left(4.905-13.8944\phi+18.4222\phi^2-10{,}2599\phi^3\right)}{Re+\exp\left(1.4681+12.2584\phi-20.7322\phi^2+15.8855\phi^3\right)}$	isometric particles $Re < 26000$
Ganser(1993)	$\frac{C_D}{K_2} = \frac{24}{ReK_1K_2}\left(1 + 0.1118\left(ReK_1K_2\right)^{0.6567}\right) + \frac{0.4305}{1+\frac{3305}{ReK_1K_2}}$ $K_1 = \begin{cases} \left(\frac{1}{3} + \frac{2}{3}\phi^{-1/2}\right) - 2.25\frac{d_{\mathrm{V}}}{D} & \text{isometric} \\ \left(\frac{1}{3}\frac{d_{\mathrm{A}}}{d_{\mathrm{V}}} + \frac{2}{3}\phi^{-1/2}\right) - 2.25\frac{d_{\mathrm{V}}}{D} & \text{not isometric} \end{cases}$ $K_2 = 10^{1.8148(-log\phi)^{2.574}}$	$K_1K_2Re < 10^5$
Chien(1994)	$C_D = \frac{30}{Re} + \frac{67.289}{e^{5.030\phi}}$	$10^{-3} < Re < 10^4$ deviations upto 25 %
Tran-Cong et al.(2004)	$C_D = \frac{24}{Re}\frac{d_A}{d_V}\left[1 + \frac{0.15}{\sqrt{s}}\left(\frac{d_A}{d_V}Re\right)^{0.687}\right] + \frac{0.42\left(\frac{d_A}{d_V}\right)^2}{\sqrt{s}\left[1+4.25\cdot10^4\left(\frac{d_A}{d_V}Re\right)^{-1.16}\right]}$	$0.15 < Re < 1500$ $0.8 < \frac{d_{\mathrm{A}}}{d_{\mathrm{V}}}$ $0.4 < s < 1$

Sedimentation Model from Henschke

The correlations for the drag coefficient use the Reynolds number, which is a function of the drop diameter and the velocity. In practical applications not the drag coefficient is the target quantity, but the sedimentation velocity for a given drop diameter is quested. Since both values are included in the Reynolds number, an iterative approach is required for the solution using the drag coefficient correlations. The model proposed by Henschke overcomes this drawback by determining the drag coefficient as a function of the Archimedes number $Ar = \frac{\rho_c \Delta\rho g d^3}{\eta_c^2}$, which represents the dimensionless ratio between buoyancy force and drag force.[19]

The model describes the sedimentation velocity of drops in the four regimes presented in section 3.2.1 as function of the drop diameter. It can be applied to all sorts of free sedimenting objects, for spheres (for Reynolds numbers $Re < 3 \cdot 10^5$), bubbles and drops. The model is presented in detail by Henschke[19]. The most relevant parameters and their function are briefly described in the following. It consists of mainly two parts describing spherical drops with internal circulation and second, oscillating and umbrella shaped drops. The model contains three fitting parameter, their impact is illustrated in figure 3.5.

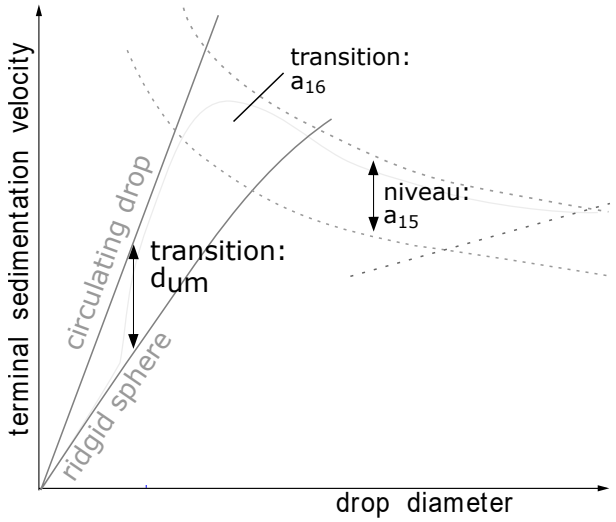

Figure 3.5.: Impact of the three fitting parameters used in the Henschke single drop sedimentation model (adopted from [19])

The parameter d_{um} refers to the transition from rigid sphere like behavior to the onset of internal circulation. This transition is very sensitive to impurities and occurring mass transfer. The presence of impurities and surface active species shifts the transition to larger diameters. Depending on the solvent system and its purity the transition occurs typically at diameters from 1.5 mm to 10 mm. The parameter a_{16} determines the sharpness of transition from a spherical drop to the oscillating regime. The oscillating regime is characterized by the parameter a_{15}.

3.3. Material and Methods

The impact of microgels at the drop surface on the fluid dynamic behavior is investigated, the sedimentation velocity is an accessible measure for this purpose. However, previously the procedure of the generation of microgel covered single drops is described.

3.3.1. Generation of Microgel Covered Single Drops

The drops are generated with a glass nozzle or stainless steel cannula. The disperse phase is dosed by a syringe pump (PSD2 Hamilton, Switzerland). The drop forms at the tip of the nozzle or cannula. The size of the drop is determined by the dosed volume and can be adjusted by the step number of the pump. At the end of the dosing process the drop detaches from the tip and rises. The detachment must be clean, so no satellite drops are formed and no disperse phase remains at the tip. This can be prevented by adjustment of the dosing speed and the nozzle diameter. The syringe pump is controlled via LabVIEW (National Instruments, USA). For the pure solvent system and the surfactant containing system the nozzle is placed directly in the cell. For the generation of microgel-covered drops an additional glass adapter is integrated. At the bottom the nozzle or cannula is placed, at the side the microgel solution is injected (see detail in figure 3.6). The volume of the adapter is 4.5 mL, before each drop fresh microgel solution with a defined

concentration is injected using a second syringe pump (PSD2 Hamilton, Switzerland). The drop is formed analog to the procedure describe above. After the measurement the microgel solution is withdrawn by the pump and conveyed to a tank, before the adapter is filled with fresh microgel solution for the next drop. This procedure ensures equal conditions for the subsequent measured drops. Tests with the pure system and the adapter show that the adapter itself does not affect the measurement.

The drop generator is designed to allow a defined coverage of the drops. As the microgel solution within the drop generator is replaced for each drop to avoid dilution effects, the amount of microgels available for adsorption on the drop surface (n_{MG}) can be calculated from the microgel concentration in the drop generator (c_{MG}) and the volume of the path of the rising drop within the drop generator (V_{path}):

$$n_{MG} = c_{MG} \cdot V_{path} \quad \text{with} \quad V_{path} = \pi \frac{d_{drop}^2}{4} \cdot h_{path} \tag{3.13}$$

The number concentration of the microgels is determined by the formula introduced by Destribats et al. [34]. Since the drop is generated at a nozzle tip above the bottom of the generator, the height of the path is less than the height of the drop generator.

Alternatively, it was also tested to adjust the drops coverage by variation of the residence time of the drop in the microgel solution in the generator. This did not lead to drops with different coverage. Their behavior only varied when different microgel concentrations were utilized. Thus, the concentration is determining for the coverage and the procedure described above is utilized.

3.3.2. Single Drop Sedimentation Velocity Experiments

For the measurements of the sedimentation velocity a cylindrical, double walled DN80 cell made of glass is utilized as shown in figure 3.6. The cell is filled with 2.5 L of the continuous phase. In this work the aqueous phase is always the continuous phase. To exclude mass transfer effects, both phases are mutually saturated. Since the microgels are temperature responsive,

the temperature is adjusted by the double wall of the cell and a thermostat (Julabo GmbH, Germany).

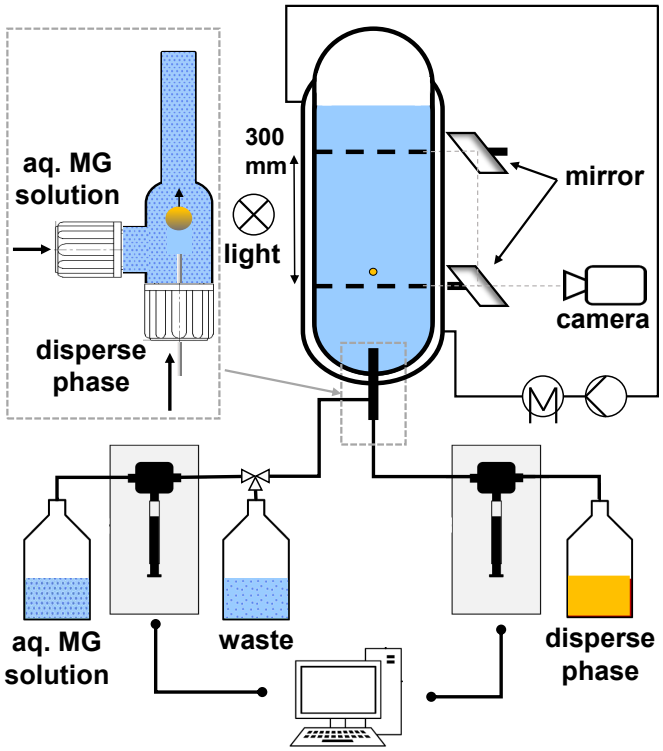

Figure 3.6.: Experimental set up of the single drop cell for sedimentation velocity measurements, with additional device for generation of microgel covered drops

The sedimentation velocity of the drop is determined by the time required for the drop to pass the measurement length of 300 mm. The sedimenting drop is recorded by video camera (HDC-SD600, Panasonic) with a frame rate of $25\,s^{-1}$. On the glass cell marks are placed with 300 mm distance. The first mark is located 150 mm from the bottom of the cell and drop generation, respectively, to ensure the drop reaches its terminal velocity before it enters the measurement. The camera is mounted on a tripod at the height of the first mark. To avoid measurement errors due to optical distortion of the measurement length by the camera angle, the passing of the second mark is observed trough a mirror. The recorded videos are evaluated using the software VirtualDub (Avery Lee, GNU General Public License). Based on the frame rate the time required by the drop to pass the measurement distance can be determined very accurately. For the performed measurements at least 5 identical drops are measured and averaged.

3.3.3. Drop Shape

Besides the drop velocity the drop shape is also of interest. Hence, the drop shape is also evaluated by image analysis using two different methods. The commonly used aspect ratio of width/height and a more detailed form factor is used. Both methods use image analysis by a Matlab® script. The script converts the image to black and white image by a brightness threshold (figure 3.7 a) and b)).

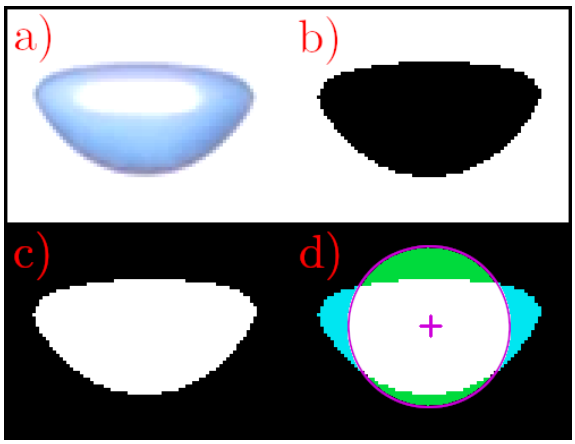

Figure 3.7.: Image analysis procedure for the determination of the form factor. a-d show the different conversion steps performed by the matlab srcipt, starting with the original image in a, d indicates the calculated areas utilized for determination of the form factor.

After the image is inverted (3.7 c)) the drops height and width are determined in pixels and can be used to calculate the aspect ratio. For the form factor the drop area is also determined from the picture in pixels and the areas centroid is calculated. Then an area equivalent circle is drown from the centroid (see figure 3.7 d)). The areas outside the intersection of drop and circle can be divided in sections that are within the drop but outside the circle (green) and sections that are within the circle but outside the drop (blue). The form factor FF is then defined as the ratio of the sum of the

areas of these sections to the overall area of the drop.

$$FF = \frac{\sum A_{blue} + \sum A_{green}}{A_{drop}} \tag{3.14}$$

3.3.4. Investigation Approach

For the investigation and classification of the impact of microgels on the drops fluid dynamics different parameters are varied. The approach is shown schematically in figure 3.8. The microgels' structure and resulting different interfacial morphology, as described in chapter 2, is taken into account by testing different microgels. The microgels differ in their crosslinker content from 2.5 mol % to 20 mol % and size from 170 nm to 320 nm in radius, the details for the four utilized microgels are listed in table 1.1.

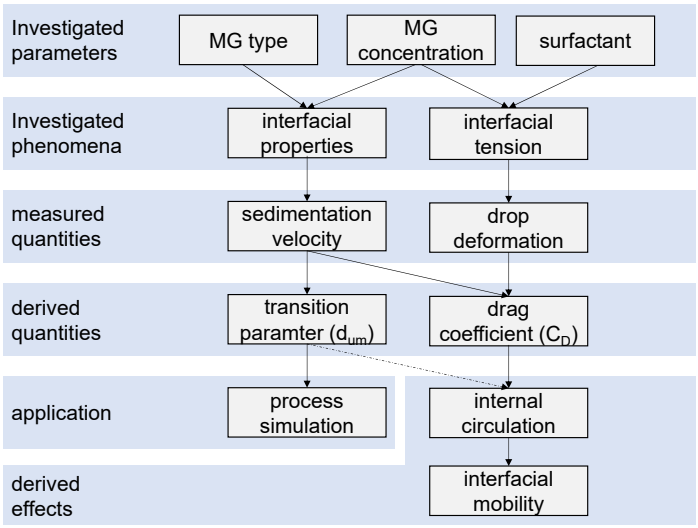

Figure 3.8.: Experimental approach for the investigation of the impact of microgels on fluid dynamics of drops

Furthermore, different microgel concentrations are tested to investigate the impact of different interfacial coverage fractions. Surfactants are also regarded as a reference system for other surface active agents, since they lower the interfacial tension and thus affect the fluid dynamics of the drops. As mentioned in the beginning, the sedimentation velocity of drops is an easily accessible measure and can be described by the model approach

introduced in section 3.2.2, which is also utilized in simulation of extraction processes [19]. The approach reflects the sedimentation velocity very well, but it is no accurate indicator for the interfacial mobility as it does not take into account the drop deformation and therefore the contribution of the shape to the drag. Therefore, the drop deformation and the resulting drag is regarded separately to draw conclusions on the internal circulation and consequently on the interfacial mobility.

3.4. Results

The sedimentation velocity of drops is measured using the set-up described in section 3.3.2. To allow conclusions on the impact of the microgels on the fluid dynamics and especially the interfacial mobility, only measurements without mass transfer are conducted. The experiments are conducted using toluene and n-butyl acetate as disperse phase, due to the sensitivity of the toluene/ water system the effect of the microgels compared to the pure system is very strong and the effects of parameters like microgel concentration or type vanish. Therefore, the experimental results for n-butyl acetate are presented in the following, as the system allows to distinguish these effects. First, the measured sedimentation velocities are discussed and subsequent the deformation of the drops is regarded to separate the effect of drop shape on the velocity.

3.4.1. Sedimentation Velocity of Microgel-covered Drops

For reference, the sedimentation velocities of the pure water/n-butyl acetate system are measured (black squares in Figure 3.9). The obtained velocities are in good agreement with data reported in literature [19, 76, 56]. The trend of sedimentation velocity with increasing drop diameter shows a steep increase between drops of $1.68\,\mathrm{mm}$ to $3.22\,\mathrm{mm}$ from $52.22\,\mathrm{mm\,s^{-1}}$ to $126.26\,\mathrm{mm\,s^{-1}}$, respectively. For drop diameters between $3.22\,\mathrm{mm}$ to $4.06\,\mathrm{mm}$, the velocity has a maximum and is almost constant. For diameters larger than $4.06\,\mathrm{mm}$, the velocity decreases with increasing diameter and deformation of these drops

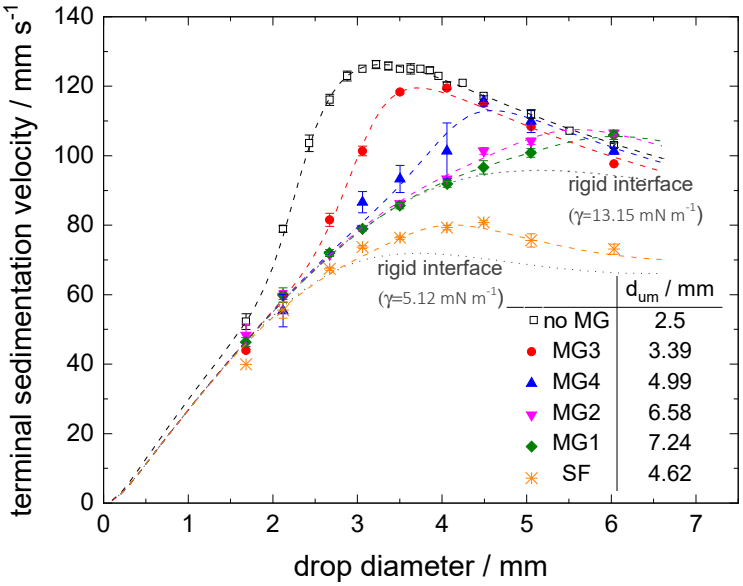

Figure 3.9.: Impact of different microgels and surfactant CTAB (SF) on the sedimentation velocity of single drops, limiting cases of the pure system (no MG) with mobile interface, and rigid interface shown. The lines indicate the fitted Henschke approach, the fitted values for d_{um} parameter are summerzied in the inserted table

is observed in the experiment. The deformation increases with increasing drop diameters. For drops larger than approximately 4 mm in diameter, oscillating movement is observed. The deformation is discussed in more detail in section 3.4.2. This trend in sedimentation velocity for increasing drop diameters is identifying for systems with mobile interfaces. For the investigated system, the circulating regime, which is characterized by acceleration due to the onset of internal circulation, starts between drop diameters of 2 mm and 3 mm, which is also reflected by the transition parameter d_{um} of the Henschke model obtained from fitting.

The impact of the microgels is shown in figure 3.9 for identical microgel concentration in the drop generator of $0.05\,\mathrm{g\,L^{-1}}$ for all four microgels. For small drops with diameter 1.6 mm the velocity is only marginally effected, but with increasing drop diameter the difference increases significantly to the pure system and among the different microgels. For MG1 and MG2 (figure 3.9 green diamonds and magenta triangles, respectively) the velocity increases with increasing drop diameter is less pronounced than for the

other microgels.

Furthermore, for these two microgels no maximum in velocity is observed. Their course is in good agreement with the prediction for a rigid sphere. However, two things have to be noted: First for drops of 5 mm and larger the sedimentation velocity of the drops is slightly faster than the limiting case of a rigid sphere. And second, the displayed limiting case of a rigid sphere in figure 3.9 is obtained for interfacial tension of the pure system, but the microgels lower the interfacial tension, the limiting case of a rigid interface for the reduced interfacial tension is also shown.

Both observations are related to the deformation of the drops. The microgel covered drops deform less, thus the drag is reduced compared to the displayed limiting cases. This indicates that the interfacial conditions of microgel covered drops are more complex and can not solely be described by a change in interfacial tension, this will be discussed in more detail in section 3.4.2.

The course of the sedimentation velocity of MG3 and MG4 (figure 3.9 red circles and blue triangles, respectively) is similar to the pure system but shifted to larger diameters. These two microgels have a maximum velocity although the absolute velocities are smaller compared to the pure system.

Comparing the velocities of the pure system and the different microgel covered drops for a drop diameter of 3 mm, MG1 and MG2 reduce the sedimentation velocity the most, the reduction by MG4 is less, and MG3 reduced the velocity the least. Hence, the order of impact relates with the ability of the microgels to spread at the interface. The more the microgels tend to spread at the interface, the more the velocity is reduced. Since the velocity is an indication of the interfacial mobility, it can be further concluded that the less cross linked microgels reduce the interfacial mobility more, thus impeding the formation of internal circulation leading to a slower velocity. On the other hand, the more cross linked or smaller microgels, which spread less at the interface reduce the interfacial mobility less, leading to faster velocities.

Relating these findings to the observations from chapter 2 and the results from Destribats et al. [34] it can be assumed that the interpenetration of the

microgels in the adsorption layer, which has also be described as microgel film by Destribats et al. [34], reduce the interfacial mobility very efficiently leading to an actual immobile behavior as the position of microgels in the network is fixed. On the other hand, the more cross linked or smaller microgels deform less and do not interpenetrate as much. Therefore, it can be assumed that the position and orientation of single microgels in the layer is not fixed and their movement in the interface could explain the partly mobile behavior of the drop interface.

Effect of Microgel Concentration

An other important aspect is, that the results discussed above are obtained for identical microgel concentrations, which does not guarantee identical interfacial coverage. As shown in section 2.4.2 the spreading also reduces the required amount of microgel required for complete coverage of the interface; hence, equal concentration does not ensure equal coverage. The effects of different concentration are shown exemplary for MG4 for drop sizes between $2.12\,\mathrm{mm}$ to $5.05\,\mathrm{mm}$ in figure 3.10. For better classification of the results the limiting cases of a mobile interface from the pure system and the rigid interface obtained from the Henschke model for $d_{um} \to \infty$ are also shown.

For small drop diameters like $2.12\,\mathrm{mm}$ the velocity decreases continuously with increasing microgel concentration. The surface to volume ratio of these drops is much higher than for larger drops. Thus, they are especially sensitive to surface active species such as microgels. For larger drop diameters the trend is different. For $3.06\,\mathrm{mm}$ and $4.06\,\mathrm{mm}$ drops the velocity is not affected by the presence of microgels at low microgel concentrations in the drop generator. For these cases the obtained velocities match the pure system velocities of a mobile interface. When increasing the concentration to $0.047\,\mathrm{mg/ml}$, an abrupt reduction in velocity is observed. Therefore, it is assumed that drops are fully covered when leaving the drop generator with concentrations above $0.047\,\mathrm{mg/mL}$.

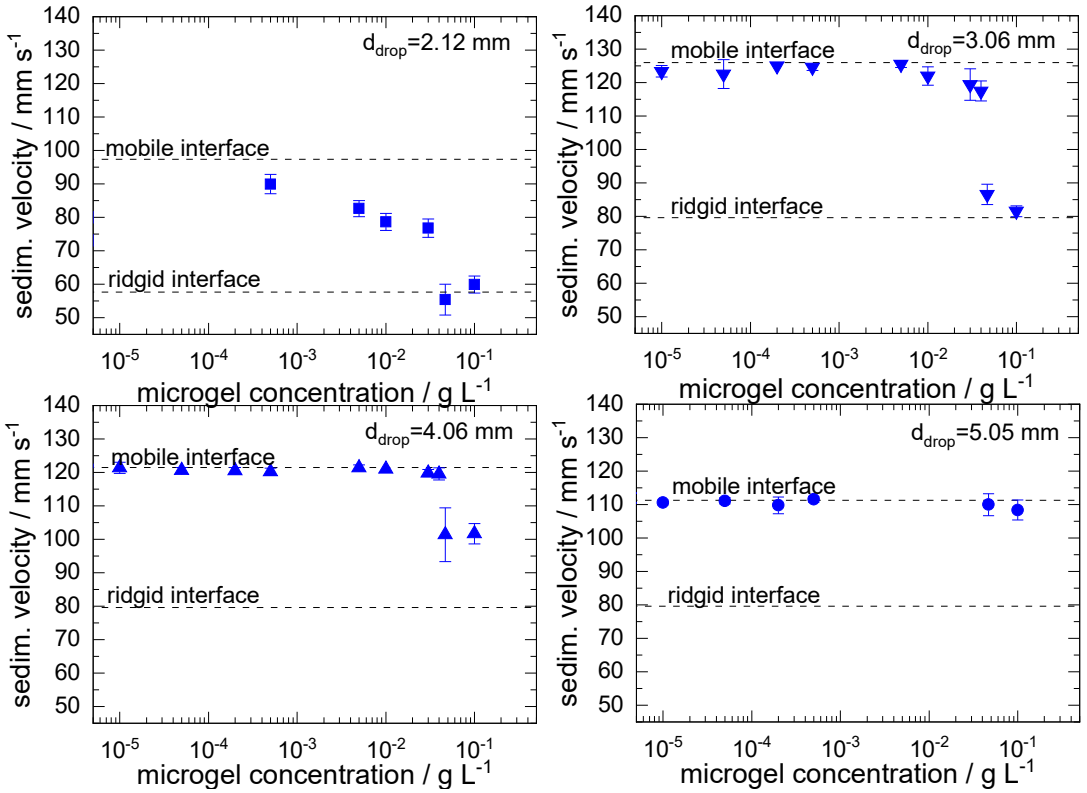

Figure 3.10.: Impact of microgel concentration on terminal sedimentation velocity for MG4

To rationalize this result, the coverage of the drop is estimated using the calculation presented in section 3.3.2. Assuming that all microgels within the path of the drop within the drop generator adsorb to the drop surface and estimating the area covered by a single microgel as the circular area of its bulk diameter, the resulting area covered by the microgels is approx. 100 times larger than the surface of the drop. Thus, the concentration of microgels in the path is by far sufficient to cover the full drop at a concentration of $0.047\,\mathrm{mg/mL}$.

Moreover, it can bee seen that for concentrations higher $0.047\,\mathrm{mg/mL}$ the extent of reduction decreases with increasing drop diameter, especially for the $5.05\,\mathrm{mm}$ drop the velocity is not affected by the concentration and implicit a mobile behavior of the interface. However, the microgel covered drops deform less and therefore the drag is reduced leading to increased velocity compared to the rigid sphere from the Henschke model, this effect is discussed in section 3.4.2. Consequently, the observation of the sedimen-

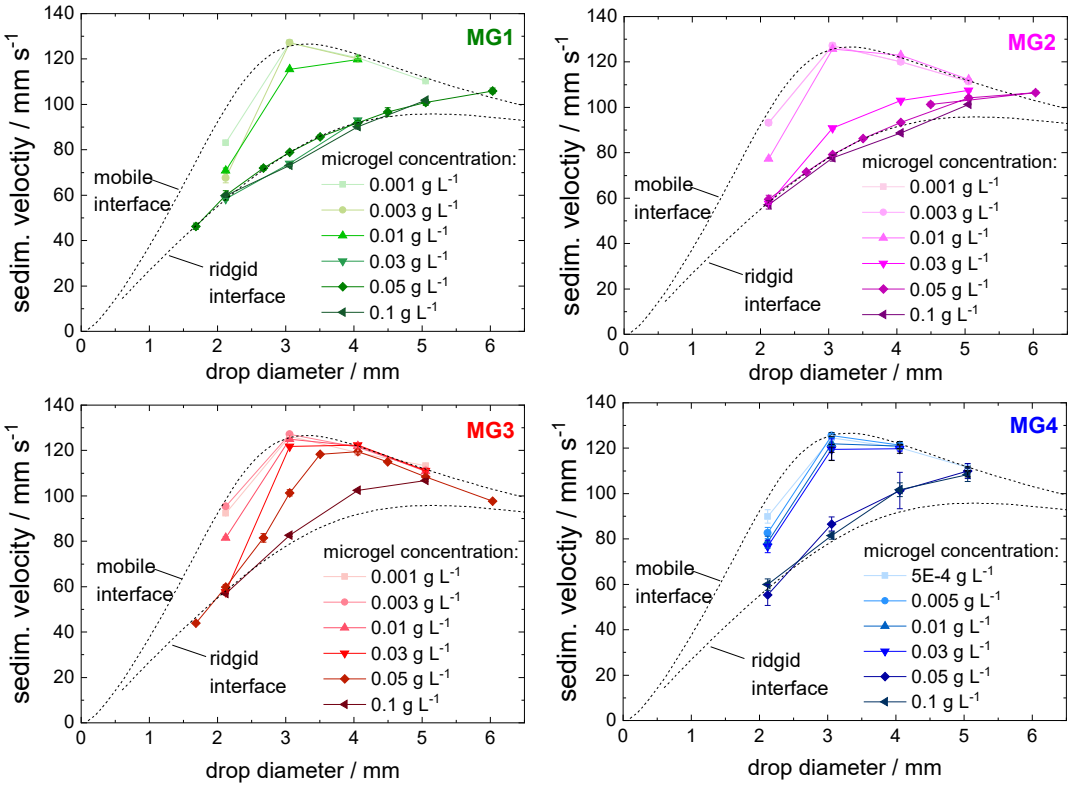

Figure 3.11.: Comparison of the effect of microgel concentration on the sedimentation velocity for different microgels

tation velocity is not sufficient to draw conclusions on interfacial mobility; nevertheless, these observation show that there is a critical concentration required for the complete coverage affecting the sedimentation velocity.

Since the microgels differ significantly in their interfacial properties, especially the deformation and spreading at the interface, the critical concentration range is microgel specific. in figure 3.11 the sedimentation velocities of the different microgels are shown for concentrations ranging from $0.001\,\mathrm{g\,L^{-1}}$ to $0.1\,\mathrm{g\,L^{-1}}$. For all microgels a dependency of the velocity on the concentration can be observed. The velocities obtained for very low concentrations are in the range of the pure system and decrease with increasing concentration. The weaker crosslinked microgels MG1 and MG2 decrease the velocity significantly for concentrations of $0.01\,\mathrm{g\,L^{-1}}$, while velocity of the the drops covered with MG3 and MG4 at these concentration indicates mobile interfacial behavior.

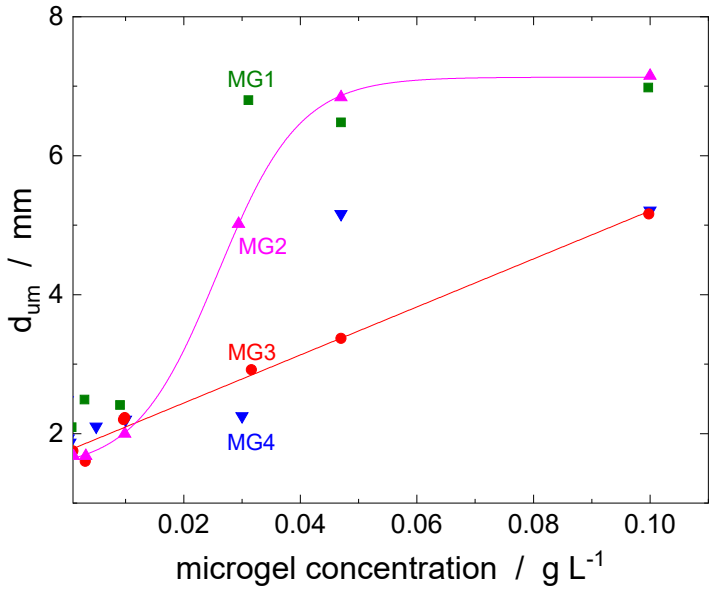

Figure 3.12.: Effect of microgel concentration on Henschke parameter d_{um} for different microgels, parameters a_{15} = 2.34 and a_{16} = 3.75 constant. Fitting for MG2 with sigmoidal function and linear fit for MG3.

Application of the Henschke Model

To rate the effect of concentration among the microgels, the Henschke model is employed and the parameters fitted to the experimental data points. The parameters a_{15} and a_{16} are not systematically affected by the microgels and vary only by 2.9 % and 8.3 %, respectively, while d_{um} varies by 47.1 % among the pure system and the different microgels. Therefore, only the parameter d_{um} is fitted and the other parameters are fixed to the values from the reference system.

Considering the physical function of the parameters, d_{um} is most relevant as is describes the transition to mobile behavior of the interface and formation of internal circulation. Figure 3.12 shows the fitted values of the transition parameter for different microgels and concentrations.

Analog to the observations from figure 3.11 for all microgels the transition diameter is in the range of the pure system for low concentrations and increases with increasing microgel concentration. However, the weakest crosslinked microgel the increase is the most pronounced to d_{um} =6.98 mm and occurs at the lowest concentration. Relating this result to the findings

from section 2.4.2 the conclusion from the start is substantiated, that the low crosslinked microgels impede the interfacial mobility and thus the velocity more efficiently due to their deformed morphology and the interpenetration of the adsorbed microgels causing a microgel film impermeable for momentum transfer. Whereas, the more cross linked microgels less deformed and interpenetrated morphology enables momentum transfer and thus the formation of internal circulation up to higher concentrations.

In the observed concentration range the related value of d_{um} is lower for the more cross linked and the smaller microgel, indicating a more mobile interface. However, as mentioned before the deformation of the drops needs to be considered too. For microgels MG1, MG2 and MG3 with increasing concentration a terminal value of the transition parameter is reached. For MG2 this relation can be described using a Boltzman fit for saturation processes, supporting the estimation of increasing surface coverage with increasing concentration. Furthermore, the findings from section 2.4.2 indicate that a certain coverage of the interface is required to cause recognizable changes in the physical properties of the interface. For MG2 the fit has a certainty $R^2 > 99\%$, for MG1 MG4 no distinct fit can be performed since the exact transition can not be determined from data points. For MG3 no terminal value of the transition parameter is reached in the investigated concentration range, and the data can be represented by a linear fit with a certainty of $R^2 > 98\%$.

The parameter set for MG2 and MG3 is used to describe the sedimentation velocity depending on the drop diameter and microgel concentration is shown in figure 3.13. The model matches the experimental data very well. The linear fit and the obtained surface plot for MG3 indicate that the complexity of the microgel interaction decrease with increasing crosslinker. The obtained parameters can be used to describe the sedimentation behavior in process simulation.

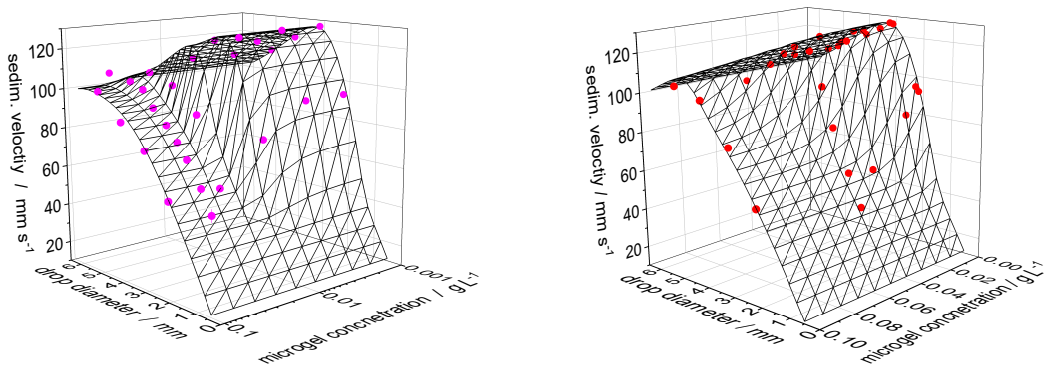

(a) MG2 5 mol %

(b) MG3 20 mol %

Figure 3.13.: Sedimentation velocity of drops for different concentrations of MG2 (a) and MG3 (b). Comparing experimental data and Henschke model with modified d_{um} as function of the microgel concentration from figure 3.12.

3.4.2. Deformation of Microgel-Covered Drops

The findings of the sedimentation behavior and the observations during the experiments showed that microgels effect the drop shape by introducing a resilience of the interface towards deformation. The sedimentation velocity is an assembly two contributors, the drop internal flow regime, which is affected by the interfacial mobility, and the drop shape, which is determined by the resistance of the interface towards the deformation. Thus, the drop deformation is regarded separately in this part to understand the microgel impact and to distinguish between interfacial mobility and shape conservation.

The extend of drop deformation for the pure system and microgel covered drops is shown in figure 3.14 as aspect ratio of drops for different diameters. The deformation of the pure system (black squares) is most pronounced. Even the smallest drops of 2.12 mm have an aspect ratio of 1.13, the aspect ratio increases continuously up to 2.35 for 4 mm drops. For larger drops the mean aspect ratio is reduced but the standard deviation increases significantly due to oscillation of the drops.

Also in the surfactant system the aspect ratio increases with increasing drop diameter as shown in 3.14. The course of the aspect ratio in the sur-

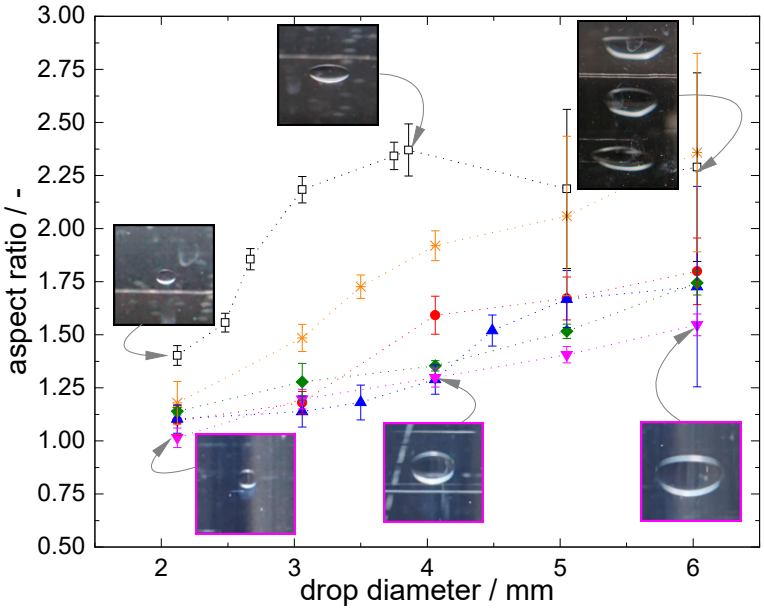

Figure 3.14.: Deformation of drops displayed as aspect ratio (width to height ratio)((□ pure system, ◆ MG1, ▼ MG2, ● MG3, ▲ MG4 and ⁎ surfactant (SF)). Microgel-covered drops generated with 0.047 mg/ml, surfactant data for $c_{SF} \gg cmc$, dotted lines solely as guide to the eyes

factant system is the steepest for the regarded systems ranging from 1.13 to 2.35 for drops between 2.12 and 6.06 mm. The drops of the surfactant system show a deformation at larger diameters, although the reduced interfacial tension would favor an earlier onset of the deformation. The delayed onset can be explained by viscoelastic forces acting in indirect proportion to the reduced interfacial tension as demonstrated by Paul et al. [84].

The microgel-covered drops show significantly lower deformation compared to the pure system and the surfactant system. With increasing drop diameter, the deformation increases slightly and becomes almost linear. In the observed range the maximum aspect ratio is between 1.51.8, for the largest drops of 6 mm for all microgels. There are no clear differences in this trend for the different microgels observable. Regarding the elastic properties of interfacial microgel layers, it is known that these are predominantly affected by the polymer type and the packing density of the layer. The cross-linking does not significantly affect the mechanical properties of the interfacial microgel layer [22]. This matches the absence of differences for the utilized microgels, since all utilized microgels are pure PNIPAM micro-

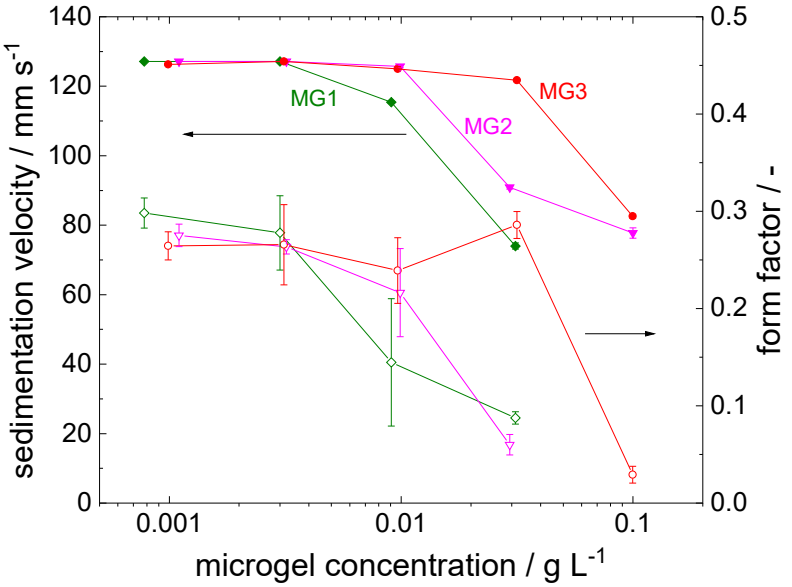

Figure 3.15.: Comparision between the sedimentation velocity (filled symbols) and the form factor (open symbols) for MG1, MG2 and MG3 depending on the microgel concentration in the drop generator for 3.06 mm drops.

gels, and their packing density at the interface is similar due to the equal conditions in the drop generator as observed for the microgels MG1 and MG2 (figure 2.5). The trend of the aspect ratios for the different systems confirms the observation from section 3.4.1.

Furthermore, the connection between the drop deformation and velocity must be considered, as the deformation occurs when the drag forces exceed the shape conserving forces. Thereby, the drag forces increase with increasing velocity of the drop. The velocity and the deformation for 3.06 mm drops are regarded for different microgel concentrations in figure 3.15. The deformation is referred to as form factor, describing the deviation of the drop profile normal to the direction of movement from a circle as described in section 3.3.3.

With increasing microgel coverage of the drops both the sedimentation velocity and the deformation decrease. Leaving the question, whether the decrease in velocity or a stabilizing effect of the microgel layer is responsible for the less pronounced deformation. To separate these effects the drag coefficients resulting from the experimental data are compared to drag correlations presented in section 3.2.1.

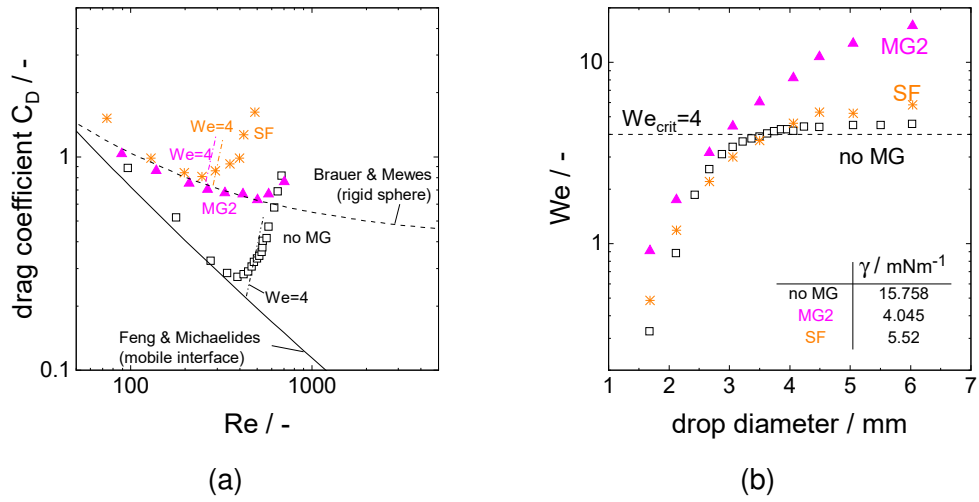

Figure 3.16.: Drag coefficient as function of the Reynolds number (a) and Weber number as function of the drop diameter (b) both for the pure system, MG2 ($0.05\,\mathrm{g\,mol^{-1}}$) and the surfactant (SF) CTAB (double c_{cmc})

Comparing the drag coefficient for the pure system, for MG2 with $0.05\,\mathrm{g\,L^{-1}}$, and the surfactant system with $c = 2c_{cmc}$ in figure 3.16(a). The drag coefficient is derived from the drop diameter and the velocity [56, 19]. In figure 3.16(a) the drag is displayed as a function of the Reynolds number. The trend of rigid spheres and that of mobile interfaces are determined by the empirical models from Brauer and Mewes [66], and Feng and Michaelides [71], respectively. The pure system drag coefficients match the correlation for a mobile interface from Feng and Michaelides[71] very well for Reynolds numbers up to 300. The drag coefficient increases as the droplet begins to deform for larger Reynolds numbers. The onset of deformation is commonly related to the Weber number (equation 3.5), which rates the frictional force of the drop to the stabilizing surface force. The deformation starts for $We \geq 4$ [85, 56]. For the pure system, this approach matches the findings very well.

For the surfactant-covered drops, the drag coefficient is larger than for the pure system and for the microgel-covered drops. For Reynolds numbers smaller 250, the decreasing trend of the drag coefficient is similar to the model of a rigid sphere. The increase in the drag coefficient at Reynolds number 260 is in good agreement with the critical Weber number. However, the drag increases less with increasing Reynolds number than for the pure

system.
For the microgel-covered drops, the drag coefficient is significantly larger than for the pure system and can be described by the trend of the rigid sphere model from Brauer and Mewes [66] for Reynolds numbers smaller 500. For larger Reynolds numbers, the drag coefficient increases, but this increase is less pronounced than for the pure system. The increase estimated by the critical Weber number is at Reynolds number 260. The prediction of the onset of deformation by the critical Weber number does not hold for the microgel-covered drops.

The development of the Weber number over drop diameter is shown in figure 3.16(b). The Weber number increases with increasing diameter and velocity. For the pure system the Weber number reaches a plateau after the value exceeds the critical value of $We = 4$. The trend for the surfactant system is comparable. A comparison of the diameter of the maximum velocity in figure 3.9 and the diameter of the critical Weber number in figure 3.16(b) shows only a small deviation for the pure and the surfactant system, respectively. However, the characteristics of the deformation of microgel-covered drop are not correctly displayed. The critical Weber number is reached for drops about $3\,\mathrm{mm}$, but there is no maximum in velocity observable in this drop diameter range (compare figure 3.9). This discrepancy can be explained by the definition of the Weber number (equation 3.5), where the shape preserving force is solely represented by the interfacial tension. The measured values for the interfacial tension are listed in figure 3.16(b), more detailed data of the dynamic interfacial tension can be found in chapter 2. Since the microgels reduce the interfacial tension the most, the obtained Weber numbers are larger, and the critical Weber number is reached for smaller diameters and slower velocities, respectively. Since the microgel layer at the interface does not solely reduce the interfacial tension but also affects the mechanical properties such as the viscoelasticity [22, 14], more detailed insights on these properties are required for the the adequate description of this behavior.

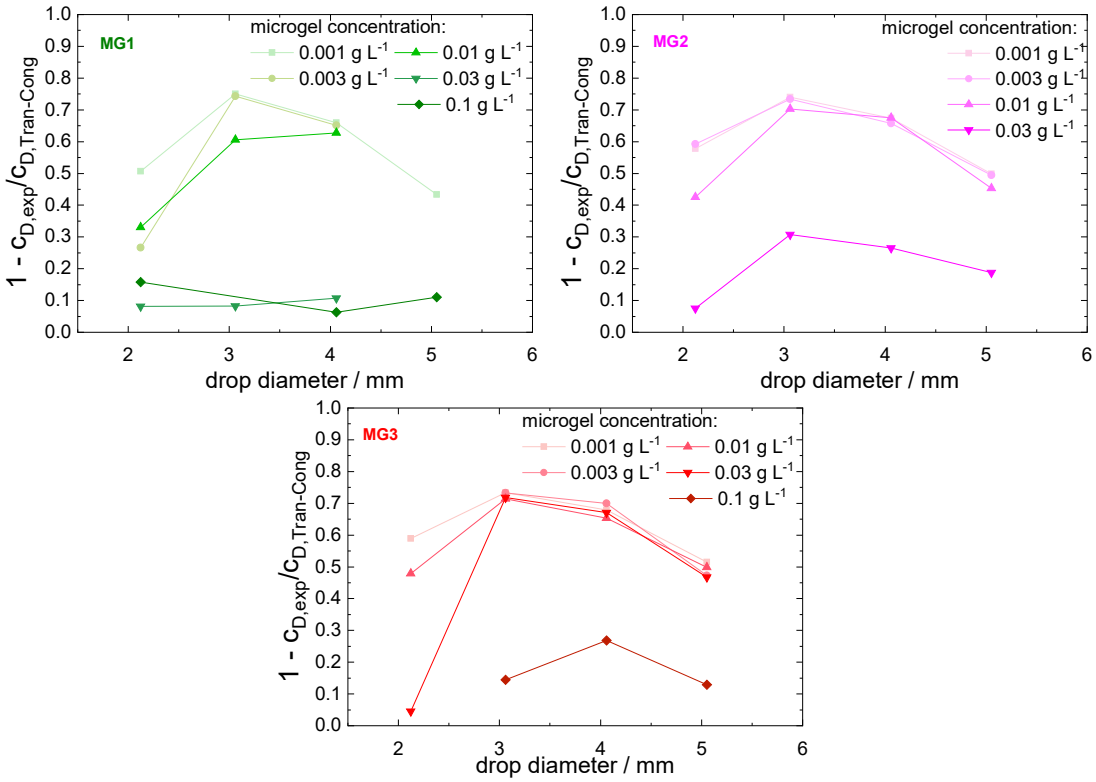

Figure 3.17.: Comparison of the drag coefficient from experimental data and for equally deformed rigid spheres obtained by correlation from Tran-Cong et al.[80] in table 3.3.

Regarding the consequences for the internal circulation and thus conclusions on the interfacial mobility as important factor for mass transfer and coalescence the effect of deformation on the drag needs to be excluded as it is not correctly reflected by the commonly used correlations. Therefore, the resulting drag from experimental data is compared to the drag of an equally deformed object with rigid surface obtained from the correlation of Tran-Cong et al.[80]. The deviation must be caused by the internal circulation. The deviation is indicted as $1 - \frac{C_{D,exp}}{C_{D,TranCong}}$ and displayed for MG1, MG2 and MG3 for concentrations ranging from $0.001\,\mathrm{g\,L^{-1}}$ to $0.1\,\mathrm{g\,L^{-1}}$ in figure 3.17.

For low concentrations significant deviation is shown for all microgels, with a maximum for $3\,\mathrm{mm}$ drops. The maximum matches the drop diameter of maximum velocity of the pure system, reflecting the formation of internal circulation. With increasing concentration the deviation decreases. Small drops of $2.12\,\mathrm{mm}$ are especially sensitive to the microgels, due to the larger surface area to volume ratio. For larger drops the extend of reduction cor-

relates with the microgels crosslinker content. Comparing the results at $0.03\,\mathrm{g\,L^{-1}}$ the deviation for MG1 is very small with 0.1, while $3\,\mathrm{mm}$ drops covered with MG2 at the same concentration show a deviation of 0.3, indicating the formation of weak internal circulation. While for MG3 the deviation is not affected for large drops at this concentration. For higher concentrations of $0.1\,\mathrm{g\,L^{-1}}$ the deviation and thus the internal circulation is also reduced for MG3.

This finding supports the relation from section 3.4.1 that the interpenetrated layer of the weaker crosslinked microgels reduces the interfacial mobility more effectively than the more crosslinked microgels. Furthermore, the comparison shows that the shift of the maximum in sedimentation velocity is also reflected for high concentrations of MG3. This indicates that the deviation in sedimentation velocity from rigid interface observed in figure 3.11 for $4\,\mathrm{mm}$ drops is not solely caused by the deformation, but is also caused by weak internal circulation. For larger diameter the difference in sedimentation velocity from rigid interface persist but the internal circulation decreases as shown by the decreasing deviation for $5\,\mathrm{mm}$ drops in figure 3.17. Hence, the differences in sedimentation velocity for larger diameters is caused by the more spherical drop shape.

3.5. Conclusion

In this chapter the impact of microgels on the fluid dynamics of single drops is studied in detail. Regarding the sedimentation velocity as an indication for interfacial mobility it is shown that microgels reduce the sedimentation velocity. The extend of the effect scales with the crosslinker content of the microgels. Furthermore, the maximum velocity shifts to larger drop diameters with increasing spreading of the microgels at the interface. A correlation for the sedimentation velocity as function of the drop size and the microgel concentration is presented for MG2 and MG3.

Furthermore, the microgels make the drops interface more resistant against deformation although they reduce the interfacial tension. This can

be explained by the mechanical properties of the microgel layer. Therefore, the common tools for the prediction and description of the fluid dynamics like dimensionless quantities, e.g. the Weber number for drop deformation, cannot be applied as they consider solely the interfacial tension as shape conserving force.

The reduced sedimentation velocity at simultaneous decreased deformation of the drops indicate the large impact of the interfacial microgel layer. To draw conclusions on the impact of the microgels on the internal circulation and thus the interfacial mobility which is also important regarding mass transfer and coalescence, the effect is regarded isolated from deformation by comparison of drag coefficients. The comparison supports the findings from the observations on the sedimentation velocity, the weaker crosslinked microgels suppress the internal circulation more effectively. This is attributed to the resistance of the interfacial microgel layer to momentum transfer, the resistance increases with increasing interpenetration and deformation of the microgels at the interface which correlates to decreasing cross-linker content.

The results and findings of this chapter can be applied to the investigation of mass transfer and coalescence with regard to interfacial mobility and the fitted parameter from the Henschke model will be used in process simulation for process performance evaluation.

3

4. Mass Transfer

Parts of this chapter have been published as:
Microgels for the Intensification of Liquid-Liquid Extraction Processes - Feasibility and Advantages, Chemical Engineering and Technology, 2020
Miriam Faulde, Josia Tonn, Andreas Jupke
DOI: 10.1002/ceat.201900407

4.1. Introduction

For the application of microgels in liquid-liquid extraction processes, the understanding and quantification of their effect on mass transfer is essential, since it directly affects the process efficiency. Single drops are regarded as the smallest self contained mass transfer unit in extraction processes. Although this approach reduces complexity, mass transfer remains very intricately; especially, as it is highly coupled to other phenomena. The presence of microgels further increases complexity, thereby two effects of the interfacial microgel layer on mass transfer are considered and investigated separately:

First, the potential mass transfer resistance added by the interfacial microgel layer as a physical barrier to mass transfer. The hypothesis arises from the radial expansion of the adsorption layer as a zone with conditions different from bulk. This effect is investigated in experiments at a flat interface, utilizing transfer agents of different molecular weight, and thus size, to investigate the permeability of the microgel covered interface.

Second, the potential reduced decay of the drop internal concentration gradient. The microgels affect the interfacial mobility as shown in section 3.4.1, which is very relevant for the mass transfer in disperse systems. A

mobile interface allows for internal mixing inside the drop reducing the radial concentration gradient and thus enhances mass transfer significantly, while in case of an immobile interface mass transport inside the drop is solely diffusive. These mixing effects are related to internal circulation (as discussed in chapter 3) or interfacial instabilities caused by concentration induced interfacial tension gradients. The latter are especially interesting in systems where the interfacial tension is affected by surface active substances such as microgels. Hence, mass transfer with and without microgels present at the interface is visualized qualitatively by the Schlieren technique at a flat interface.

Finally, mass transfer is integrally investigated at single drops and the results are compared to mathematical models for mass transfer in disperse drops to characterize and classify the microgels impact.

4.2. Fundamentals

Mass transfer is generally caused by a difference in chemical potential, which can result from a gradient in temperature or concentration. Thus the driving force for mass transfer is the concentration difference to equilibrium. For a biphasic system, where mass transfer occurs across the interface a typical concentration profile is depicted in figure 4.1. The depicted concentration profile is based on the idea that the interface is a one dimensional area with no intrinsic resistance and that at the interface equilibrium conditions prevail instantaneously. The equilibrium between the interfacial concentrations (y_i and x_i) can be described by the partition coefficient k as shown in equation 4.1.[18]

$$y_i = k \cdot x_i \tag{4.1}$$

The mass transfer to the interface in both faces can be described as mass flow $\dot{m}$ per area A_i by the concentration difference between the bulk and the interface (x_b, x_i and y_b, y_i respectively), the phase density ρ and the mass

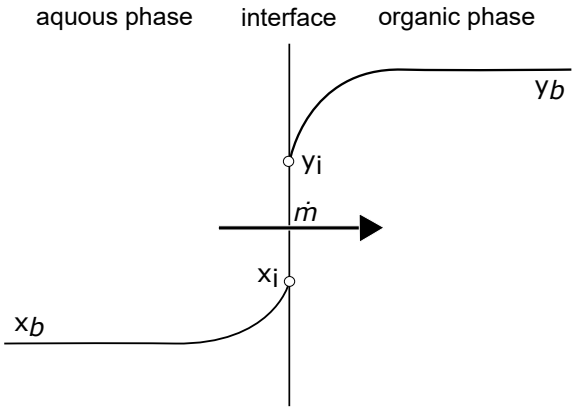

Figure 4.1.: Schematic concentration profile of a transfer component, for mass transfer from aqueous bulk (x_b) to organic bulk phase (y_b) across the interface assuming instantaneous equilibrium concentrations at the interface (x_i, y_i)

transfer coefficient β.

$$\frac{\dot{m}}{A_i} = \beta_c \rho_c (x_i - x_b) \qquad \frac{\dot{m}}{A_i} = \beta_d \rho_d (y_b - y_i) \tag{4.2}$$

Both equations are linked by the interfacial equilibrium in equation 4.1. Applying the continuum law an expression for the mass transfer across the interface is derived with an overall mass transfer coefficient K_{OG}.

$$\dot{m} = A_i K_{OG} (y_b - k x_b) \tag{4.3}$$

This overall mass transfer coefficient can be regarded as a serial resistance of the single mass transfer coefficients by assuming a linear equilibrium relation [86, 19].

$$\frac{1}{K_{OG}} = \frac{1}{\beta_d \rho_d} + \frac{k}{\beta_c \rho_c} \tag{4.4}$$

The individual mass transfer coefficients depend on the physical properties and the flow conditions. For experimental determination of mass transport kinetics a cell with two individually stirred phases has been introduced by Nitsch et al. [87], especially to investigate transport limitations for reactive systems, but it can also be used to characterize adsorption layers, which will be elaborated in sections 4.2.2 and 4.3.1. Since the mass transfer resistance highly depends on the flow conditions, the findings from flat inter-

faces cannot simply be transferred and applied to disperse systems.[19] The coupled fluid dynamics and mass transfer at single drops will be discussed in the following.

As mentioned previously, mass transfer highly depends on the physical properties and the flow conditions of the system. The complex interactions of these parameters and coupled effects makes the prediction of mass transfer, as it is required for apparatus design, very challenging.[58]

Considering a single drop as the smallest unit in a disperse system, equation 4.4 implies that the mass transfer resistance can be different in the two phases. Hence, three scenarios can be distinguished: [62, 57]

- external problem, predominant mass transfer resistance in continuous phase
- internal problem, predominant mass transfer resistance in dispersed phase
- conjugated problem , mass transfer resistance in both phases is of the same setup

For process relevant drop sizes and velocities ($d_d > 0.5mm$ and $v_d > 20mms^{-1}$) the Peclet number in the continuous phase typically reach values greater than 10^5; thus, the mass transfer in the continuous phase is dominated by advective transfer and independent of time.[19] Henschke [19] supports the thesis with CFD simulations of a n-butyl acetate drop with transport of acetone from disperse to continuous phase. In these simulation the transfer component is found only in the wake of the drop and the concentration boundary layer forming at the drop outside is very small. This is caused by the rapid transport of the transfer agent by the surrounding flow and the transfer component exits the drop downstream. Due to the rapid transport and the thin boundary layer, Henschke [19] expects the mass transfer resistance mainly on the inside of the drop.[19] Whereas, Piarah et al. [88] numerically investigated the same system and compared their results to the experimental data from Henschke and Pfennig [89]. They conclude that the resistance in the continuous phase needs to be considered and a

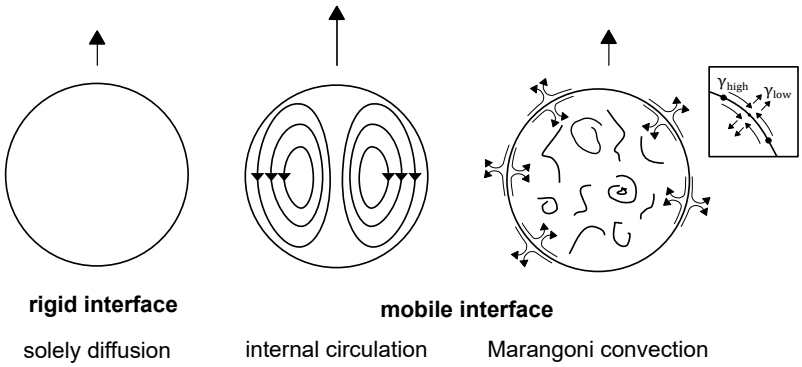

Figure 4.2.: Flow regimes of drops depending on interfacial conditions and resulting mixing inside the drop, the arrow depicts qualitatively the relative sedimentation velocity of the drop (based on [57])

conjugated problem is present. The contradict interpretations emphasizes the difficulty of simple classification and the complexity of description.

Focusing on the drop internal resistance, the mass transfer is significantly affected by the drop internal fluid dynamic conditions and vice versa. Three different regimes for the drop internal flow conditions are found in literature which are illustrated in figure 4.2, the velocity of the drop is indicated by the arrows on top of the drops. The different flow regimes are distinguished by the mobility of the interface. In case of a rigid interface the inside of the drop is quiescent and mass transfer is solely diffusive (figure 4.2). In case of a mobile interface the presence of laminar internal circulation, as described in sections 3.2.1 and figure 4.2 middle, leads to a mixing inside the drop, reducing the radial concentration gradient. The results of many experimental studies exceed the mass transfer predicted by simple diffusion and laminar circulation (models for the prediction are presented in detail in section 4.2.1). The enhancement of the mass transfer in drops is often related to turbulent flow patterns inside the drop (figure 4.2).[64, 19, 90, 89] At a mobile interface, beside the advective flow, concentration gradient induced instabilities at the interface can occur and affect mass transfer. These flows disrupt the circular internal flow pattern and lead to isotropic internal flows as depicted in figure 4.2 on the right.[57] The formation and appearance of these flows is described in the following and their effect on single drop mass transfer is discussed.

In ternary systems local concentration gradients of the transfer component at the interface cause a change in interfacial tension, if the interfacial tension is sensitive to the transfer component concentration.[19] [57] The compensation from regions of high interfacial tension to low interfacial tension induces Marangoni convection, a flow originating from the interface (figure 4.2 detail on the right). Two different forms of appearance of these flows are reported in literature: [19, 91, 92]

1. regular or stationary flow patterns, such as roll cells or oscillation
2. irregular or instationary flow patterns, which appear as eruptions or flickering

Besides the interfacial tension, the effect of the transfer agent on the density is also relevant. The appearance of instabilities is often coupled to density effects. If the concentration of the transfer component leads to a density increase towards the interface in the heavy phase or a density decrease towards the interface in the light phase instabilities occur. Thus, the appearance of instabilities also depends on the mass transfer direction. [93, 94] For the standard test systems toluene/water/acetone and n-butyl acetate/water/acetone only the mass transport of acetone from the aqueous to the organic phase is sensitive to instabilities.[19]

Wegener and Paschedag [63] investigated the mass transfer in the dispersed toluene(d)/water(c) system with acetone as transfer agent, they report a significant increase in mass transfer for the direction $c \rightarrow d$ compared to $d \rightarrow c$. Thus, they relate their observation to the direction of dispersion and not the phases densities. These instabilities and the resulting isotropic flow significantly increase mass transfer at single drops, as the mixing transports the transfer component away from the interface. Their appearance and impact of mass transfer has been studied intensively. However, the underlying phenomena are very complex and strongly coupled, and not fully understood yet [91, 19]. Contamination, such as surfactants, further increase the complexity of the system since they affect the physico chemical properties as well as interfacial properties. They absorb and lower the interfacial tension, they block the interface and impede mobility, to name

only some effects. [63, 95, 60]
Most significantly the contamination reduces the interfacial mobility, however, Wegener and Paschedag [63] observed in their experiments at high surfactant concentrations sedimentation velocities of rigid spheres, but still significantly enhanced mass transfer compared to a rigid sphere diffusion limited scenario. The authors conclude from the results that the interface must be partially mobile and can be divided in a stagnant cap and a relatively free mobile part.[63] Their experimental observation are in good agreement with experimental results from other groups [95, 61]. Furthermore, numerical results from Cuenot et al. [96] show that the drops drag and velocity equals a rigid sphere for stagnant cap angle of $65°$, while mass transfer is still enhanced and not at rigid sphere regime at this angle [96]. Moreover, surfactant induced Marangoni effects are discussed in literature as the surfactant lowers the interfacial tension and thus local differences in surfactant concentration could lead to Marangoni effects at the interface. [63, 60]

4.2.1. Single Drop Mass Transfer Models

Models can be used to describe and characterize mass transfer. Various models have been introduced in literature, reaching in their physical and mathematical complexity from empirical correlation to analytical models. Since mass transfer characteristics like the mass transfer coefficients are not directly accessible by experiments dimensionless quantities are commonly used to allow for a differentiated comparison. The most important dimensionless quantities are described in the following.

The Sherwood number Sh (equation 4.5) is a key quantity for the determination of the mass transfer coefficients, it relates the effective mass transfer in a system, with the characteristic dimension L, to diffusive mass transfer.[97]

$$Sh = \frac{\beta L}{D} \tag{4.5}$$

The Schmidt number relates momentum and mass diffusivity by accounting for the viscosity of the system.

$$Sc = \frac{\nu}{D} = \frac{\eta}{\rho D} \tag{4.6}$$

The Peclet number describes the contribution of advective and diffusive mass transport. It contains the velocity v, the drop diameter d and the diffusion coefficient. It is the product of Reynolds and Schmidt number.

$$Pe = \frac{vd}{D} (= Re \cdot Sc) \tag{4.7}$$

For the description of instationary transport phenomena the Fourier number also considers the time t.

$$Fo = \frac{4Dt}{d^2} \tag{4.8}$$

Another measure making the results more broadly applicable and comparable, is to rescale concentrations dimensionless by introducing the dimensionless quantity y^+. It describes the distance of a concentration to the corresponding equilibrium concentration and takes values between 0 and 1. If $y^+ = 0$, equilibrium is reached, whereas at $y^+ = 1$ the concentration has not changed with respect to its initial value. It is calculated according to equation 4.9, where y^* describes the equilibrium concentration for y_b and is calculated by equation 4.10 under the assumption that the bulk concentration in the other phase x_b remains constant. $\bar{y}_b(t)$ is the mean bulk concentration at time t and $y_{b,0}$ is the concentration in the disperse phase at time $t = 0$.

$$y^+ = \frac{y^* - \bar{y}_b(t)}{y^* - y_{b,0}} \tag{4.9}$$

$$y^* = k \cdot x_{b,0} \tag{4.10}$$

Newman [98] introduced a model for the calculation of instationary transport inside a spherical drop without internal circulation. Therefore, the contribution of advective flow inside the drop is zero (thus $Pe_d \to 0$) and the model is derived from the solution of Fick's 2. law, assuming a constant diffusion coefficient and that the interfacial concentration is spatially independent.

$$y^+ = \frac{6}{\pi^2} \sum_{n=1}^{\infty} \frac{1}{n^2} \exp\left(\frac{-4n^2\pi^2 t D_d}{d^2}\right) = \frac{6}{\pi^2} \sum_{n=1}^{\infty} \frac{1}{n^2} \exp\left(-n^2\pi^2 Fo_d\right) \tag{4.11}$$

The result of the serial expansion can be approximated by the following solutions.[19]

$$y^+ = \begin{cases} 1 - \frac{6}{\sqrt{\pi}}\sqrt{Fo_d} + 2.996Fo & \text{for } Fo_d < 0.1584 \\ \frac{6}{\pi^2} \exp\left(-\pi^2 Fo_d\right) & \text{for } Fo_d \geq 0.1584 \end{cases} \tag{4.12}$$

This model presents the limiting case of a immobile interface, where mass transfer inside the drop is solely diffusive. To account for circulation Kronig and Brink [99] present a solution based on the stream function from Hadamard [100] for laminar circulation at small Reynolds numbers. The parameters B_n and λ_n are listed by Heertjes et al. [101].

$$y^+ = 1 - \frac{3}{8} \sum_{n=1}^{\infty} B_n^2 exp\left(-64 \frac{\lambda_n D_d t}{d^2}\right) \tag{4.13}$$

Handlos and Baron [102] present a model that considers the mixing inside the drop as random turbulent like diffusion. They regard the internal velocity profile as spherical tori and also account for the drop velocity by utilizing a

modified Peclet number.

$$y^+ = 1 - exp\left(-\frac{\lambda_n v t}{128 d(1+\frac{\eta_d}{\eta_c})}\right) \tag{4.14}$$

The model was modified by Wegener and Paschedag [90] by introducing the factor α which reflects the difference to ideal mixing. For ideal mixing applies $\alpha = 1$, therefore $\alpha \leq 1$ can be adjusted to experimental data. Initially, the model was introduced to allow for the consideration of different initial concentration, as the extend of turbulence by Marangoni convection and thus mixing is related to the concentration gradient. In later studies they investigated the effect of anionic surfactants on mass transfer in the toluene(d)/water(c)/acetone($c \rightarrow d$) systeme and obtained good agreement with experimental for the modified model by adjusting α.[63]

$$y^+ = 1 - exp\left(-\alpha\frac{\lambda_n v t}{128 d(1+\frac{\eta_d}{\eta_c})}\right) \tag{4.15}$$

Calderbank and Korchinski [103] presented the idea of an effective diffusion coefficient by introducing the enhancement factor R, with $R = 2.25$. They use the modified diffusion coefficient $R \cdot D_d$ in the derivation of the stagnant interface case to obtain equation 4.16.

$$y^+ = 1 - \sqrt{1 - \exp\left(\frac{-4\pi^2 t R D_d}{d^2}\right)} \tag{4.16}$$

Henschke and Pfennig introduced an instability constant C_{IP} to account for turbulence inside the drop caused by interfacial phenomena as described in section 4.2. The model is based on idea of random turbulent like diffusion in the drop from Handlos and Baron [102] and introduces an effective diffusion coefficient, which is shown in equation 4.17. The effective diffusion coefficient can be used to determine an effective Fourier number Fo equation 4.8 to calculate the dimensionless concentration analogous to Newman's

approach and the approximate solution for the serial expansion in equation 4.12. The model also reflects the scenario of purely diffusive mass transfer for $C_{IP} \to \infty$, thus D_{eff} equals D_d. While for $C_{IP} \to 0$ the limiting case of infinitely fast turbulent mixing is reached. C_{IP} is specific to the solvent system and can be fitted to experimental data. The authors emphasize that this model does not include internal circulation, since turbulence disturbs circulating flows. [89, 19]

$$D_{eff} = D_d + \frac{v_\infty d}{C_{IP}(1 + \frac{\eta_d}{\eta_c})} \tag{4.17}$$

All models, except Newman, use an enhancement of regular diffusion, which agrees with previously recorded data, that shows regular diffusion models systematically underpredict the mass transfer rate. These models can also be utilized to estimate mass transfer in disperse systems for apparatus design.

4.2.2. Mass Transfer in Microgel Systems

The structural differences of microgels to other surface active agents are also reflected in their impact on mass transfer. Their open and porous structure combined with their switchability, inspired many research groups on applications of microgels as sponge-like programmable uptake and release systems.[4] These studies focus on the transport inside the microgel. Other applications locate the microgels at interfaces to introduce switchable permeability e.g. for membranes [12, 104] or capsules [15, 105].

The microgel is swollen by solvent and thus allows diffusion of small entities [4]. The mass transfer inside the gel is determined by its porous structure and is often characterized by the mesh size of the gel [4, 12, 15, 105, 45, 46, 9]. The size ratio between the microgels mesh size and the transfer agent is decisive for the permeability [4]. The mesh size is determined by the crosslinker content, for PNIPAm microgels typical mesh size are reported between 1 nm to 10 nm [2, 32, 46]. The permeability of

PNIPAM hydrogels is investigated by Fänger et al. for crosslinker contents of 2.5 and $5\,\mathrm{mol}\,\%$ and fluorescent labeled dextranes with molecular weight of $4, 70, 150\,\mathrm{kg\,mol^{-1}}$. The microgels showed only a neglectable uptake of the macromolecules, for dextranes of $70\,\mathrm{kg\,mol^{-1}}$ and larger, no uptake at all was observed. The authors demonstrated that the permeability can be increased by incorporation of PEG regions during synthesis, leading to separated phases in the gel and significantly increase permeability even at high crosslinker contents.[45] The diffusion of guest molecules in polyacrylamid gels was studied by Lehmann et al. [106] also using fluorescent dextrane tracers with molecular weights between $3\,\mathrm{kg\,mol^{-1}}$ to $70\,\mathrm{kg\,mol^{-1}}$. The obtained and normalized diffusion coefficients increase with increasing tracer size, thus reflecting the impact of the transfer agent size.[106]

Simulative studies by Kamerlin and Elvingson [107] point out the flexibility of the polymer network as important factor. The presence of impenetrable polymer chains reduce the diffusion coefficient within the network, the reduction was less pronounced for flexible network structure. The authors make the flexibility of the network also accountable for the permeability for molecules with molecular sizes above the mesh size of the gel. [107] The latter findings regard single, suspended microgels. As the microgels deform at the interface (2.2.3), a transfer of the described results to microgel covered interfaces should be made cautiously.

When adsorbed to an interface, the microgels remain permeable [46]. The permeability of microgel coated liquid interfaces was demonstrated qualitatively by Monteillet et al. [108]. They investigated extraction in ionic liquid water system stabilized by PNIPAM microgels. In their emulsion experiments, they used β-carotene and pyromethene, a fluorescent dye, as visible transfer agents to show the permeability of the microgel-covered drop interface.[108]

Moreover, microgel covered interfaces in emulsion can be used as templates for microgel capsules, thereby the microgels are often immobilized by interconnection or incorporation in a second layer e.g. a silica [15, 105, 109]. The permeability of these capsules can be tuned by the microgel

properties and switchabliliy [15, 105, 109]. Furthermore, the permeability and selectivity of immobilized microgel layers is investigated for membrane applications. In these pressure-driven processes the permeability of high molecular weight compounds, such as humic acid and different dextrans, is significantly reduced for swollen microgels [12, 104].
Concluding, the mass transfer through microgels is predominately affected by their structure. The tuning of polymer volume fraction and mesh size could allow the design of application tailored microgels in future [110].

4.3. Methods and Material

For the investigation of mass transport phenomena in biphasic systems with microgels at the interface three different experimental setups are utilized. The approach is shown schematically in figure 4.3. Analogous to the investigation on fluid dynamics in chapter 3 different microgels and microgel concentrations are tested. The investigations aim to identify the impact of the microgels on mass transfer. Two possible types of impact are considered: First, the potential additional mass transfer resistance of the adsorption layer, and second the decay of the radial concentration gradient inside the drop which is mainly affected by the interfacial conditions. To test the mass transfer resistance of the adsorption layer, experiments in a stirred two phase convection cell are conducted with transfer agents of different size. The derived mass transfer coefficients are utilized to quantify the impact of the absorption layer.
The decay of the concentration gradient is evaluated visually by Schlieren experiments. Single drop experiments are performed to observe mass transfer under process like conditions, in this setup both effects become relevant. For the evaluation of the impact of the fluid dynamics the results from chapter 3 are also taken into account. The obtained parameter from single drop experiments are used for evaluation by process simulations in chapter 6.

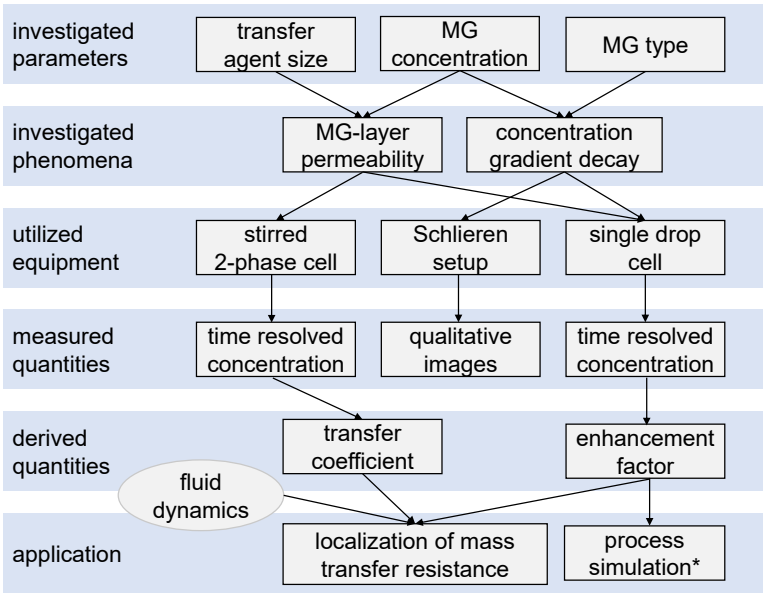

Figure 4.3.: Experimental approach for the investigation of the impact of microgels on mass transport

4

4.3.1. Experiments at Flat Interfaces

For the investigation of time-resolved mass transfer through a microgel-covered interface, a stirred two-phase cell is utilized as introduced by Nitsch et al. [87, 111] and modified by Kalem [112]. The cell and the periphery are shown in figure 4.4.

The total volume of the cell is 500 mL, the interfacial area is 44.18 cm^2. Before the experiments, toluene and water are mutually saturated by stirring for at least 60 min and subsequent phase separation in a separation funnel. The phases are filled in the reservoirs, the aqueous phase is filled in the cell from the bottom, the organic phase enters the cell from the top, as shown in figure 4.4. To ensure a defined flat interface, the stirring is adjusted to equal Reynolds numbers in both phases, e.g. for a Reynolds number of 3000, the stirrer is adjusted to 73 rpm in the aqueous phase and 102 rpm in the organic phase, due to the lower viscosity of toluene.

The microgels are introduced to the interface by free adsorption of the microgels, they are added to the aqueous phase, then the system is paused for 120 min while gentile stirring, allowing the microgels to cover the inter-

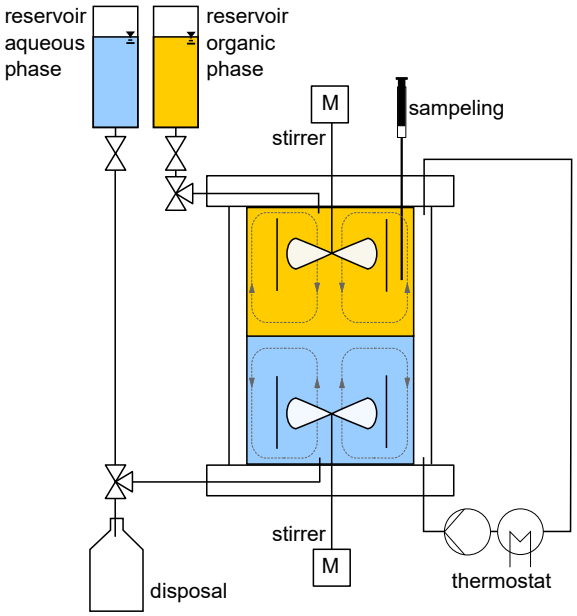

Figure 4.4.: Scheme of the experimental setup of for the quantitative investigation of mass transfer at flat interface

face. The time required to cover the interface is adjusted in preliminary experiments, described in the appendix figure A.6. The utilized amount of microgels was calculated to be more than sufficient to cover the interface.

At the beginning of the mass transfer measurement, the transfer component is injected into the cell via the sampling point (see figure 4.4). Depending on the direction of mass transfer the transfer agent is either injected to the organic or the aqueous phase using cannulas of different lengths. The experiment starts with injection of the transfer agent. When acetone is used as transfer agent, it is injected to the aqueous phase and mass transfer is tracked by sampling the organic phase and gas chromatography analysis. Per experiment 18 samples of each $0.5\,\mathrm{mL}$ are taken, the samples size and number is chosen to ensure that the annular gap on top of the organic phase remains filled throughout the experiment. Besides acetone, polyethyleneglycol (PEG) with different molecular weight is used (PEG2000, PEG4000). The PEG is melted and diluted with toluene to a stock solution with $30\,\mathrm{w\,\%}$ of PEG. Then, after the phases are filled in the cell and the interface is covered with microgels, $60\,\mathrm{mL}$ of the stock solution are filled to the cell, leading to an initial concentration of $7\,\mathrm{w\,\%}$ in the organic phase. The accumulation of the PEG in the aqueous phase is tracked by IR spectroscopy (MIR, Bruker,

Germany) using a probehead that fits through the sampling nozzle).

4.3.2. Visualization of Mass Transfer at Flat Interface

To enhance the understanding of the microgel impact on the mass transfer, experiments to visualize the mass transfer are conducted. Therefore, the mass transfer is visualized by Schlieren technique in a setup shown in 4.5. The Schlieren technique is based on changes in refractive index caused by the presence of the transfer component, the differences in refractive index are enhanced by the lenses and the slit. Details on the optical components are listed in the appendix A.6. A cuvette (QS 10 mm Hellma, Germany) is placed between the lenses. The cuvette is filled with 1.5 mL of toluene, as organic phase, and 300 µL of the aqueous phase. The phases are mutually saturated. Microgels are applied by injection of 30 µL of microgel stock solution diluted with 20 w% isopropanol. Then 1.5 mL of aqueous phase containing 15 w% acetone are injected to the bottom of the cuvette by the syringe pump (PSD6 Hammitlon, Switzerland). The hoisting speed of the pump is set to 30 allowing a slow injection without disturbance of the interface. The mass transfer process is recorded by a camera (α6000, Sony, Japan).

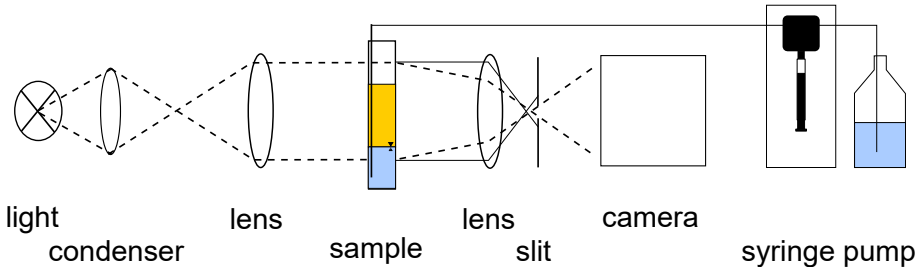

Figure 4.5.: Scheme of the experimental setup of for the qualitative vitalization of mass transfer at flat interface using the Schlieren technique

4.3.3. Single Drop Experiments

The experimental setup for the investigation of mass transfer on single drops is shown in figure 4.6. It consists of a special glass column, that has a conical shape in the middle. There the drop is kept at a roughly constant height by

a counter current flow, this setup enables an easy way to control residence time without changing the height of the column. The top left connector is the inlet for continuous phase, which is pumped in a loop by a gear pump and exits the column through the bottom left connector. Additionally, a reservoir in the loop increases the overall volume of continuous phase. The volume of the continuous phase is large compared to the disperse phase, thus it is assumed, that the concentration of the transfer agent in the continuous phase is not affected and remains at its initial value during the experiments. At the top a funnel is attached, which collects the drops into the tubing, through which they are withdrawn by a Hamilton PSD2 syringe module. The tubing connects to a Hellma OS flow through cuvette, where the spectra are recorded with the Raman-spectrometer. The device is controlled with iC Raman™software from Mettler Toledo, which is also used to record and store the spectra on the computer used. At the bottom a drop generator is attached as also used for the fluid dynamic experiments (see section 3.3.2). From the right inlet, microgel solution can be injected into the generator and from the bottom a capillary is installed, which creates the disperse phase drops. Both the disperse phase and microgel solution are pumped by a syringe module (PSD6, Hamilton, Switzerland). All the pumps are controlled from a separate computer via LabVIEW (National Instruments, USA).

In the following, the experimental procedure is described. First the mutual saturation of the solvents is explained, afterwards the determination of the partition coefficient is outlined and finally the mass transfer experiments are described.

To mutually saturate the two solvents, they are placed into a bottle and stirred for 60 min. Then they are left to rest in a separator to settle, and separate the phases.

The partition coefficient k is determined by shake-flask method in 20 mL glass flasks. The weight of each of the three components, the two mutually saturated solvents and transfer component, is measured with a precision scale (VWR, Germany), afterwards the flasks are shaken vigorously and left to rest for 24 h. Then the organic phase is extracted and Raman spectra are collected to determine y. The concentration in the aqueous phase, x, is then

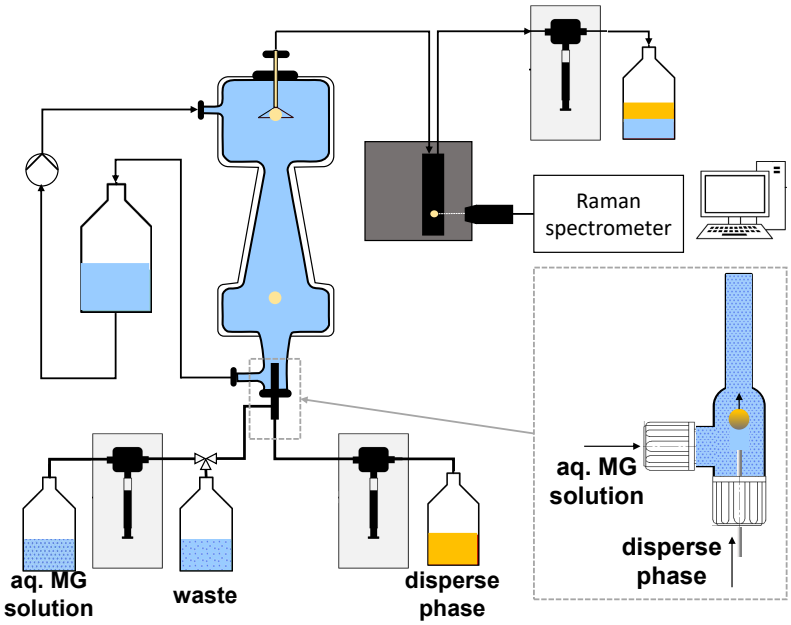

Figure 4.6.: Scheme of the experimental setup for the quantitative investigation of mass transfer at single drops

calculated by mass balance.

For the mass transfer experiments, the continuous phase is prepared by creating a 3 w% solution of acetonitrile in the aqueous phase. The continuous phase is then filled into the glass column via the reservoir and afterwards the drop generator is inserted from the bottom. When the continuous phase is exchanged between experiments, the column and reservoir are flushed with bi-distilled water. The microgel solutions are prepared and microgel covered drops are generated according to the procedure decribed in 3.3.2. The drops enter the glass column at the bottom. In the column a counter current is created by pumping the continuous phase in a loop. The flow rate is adjusted to the drop size in order to prohibit the drop passing the conical section in the middle of the column. The drop resides in the counter current flow for a specified time, afterwards the pump is turned off and the drop rises into the funnel at the top of the column. The drop is withdrawn into the tubing, leading to the flow cuvette (channelwidth 2 mm from Hellma, Germany), by the syringe pump (PSD2, Hamilton, Switzerland).
The surface area between the drop and the continuous phase is greatly reduced, once the drop enters the tubing connected to the funnel. Thus it is

assumed, that no further mass transfer occurs after the drop has entered the tubing. After the drop is withdrawn, the PSD6 syringe pump at the drop generator withdraws the microgel solution and disposes it, subsequent fresh microgel solution is injected to the drop generator for the next drop.

This procedure is repeated multiple times, and a column of drops forms in the tubing on top of the column, as illustrated in figure 4.6. The number of drops was adjusted to the drop diameter, such that a similar volume of disperse phase is used for each drop size. After the last drop is withdrawn, the droplet column is drawn to the cuvette, where the Raman measurements take place. The first Raman spectrum is recorded of the aqueous phase and afterwards the PSD2 syringe pump moves the drop column further along the tubing and another spectrum is acquired. To allow for measuring multiple samples for each drop the selected step size of the syringe pump is smaller than the volume of a single drop. This is repeated until multiple spectra show no strong presence of disperse phase. Then the tubing is flushed with continuous phase and reference spectra are collected to ensure no residual disperse phase in the tubing.

4.4. Results

4.4.1. Mass Transfer at Flat Interfaces

The experiments at a flat interface are performed according to the procedure described in section 4.3.1. The accumulation of the transfer component acetone in the organic phase is shown in figure 4.7 as dimensionless distance to equilibrium according to equation 4.9. The results compare the pure system and MG1, a large, weakly crosslinked microgel. The course of all experiments show a decrease in the dimensionless concentration difference, meaning the system approaches towards equilibrium over time. Two different microgel concentrations are tested. The microgel mass referred to the interfacial area is $3.13 \cdot 10^{-3}\,\mathrm{g\,cm^{-2}}$ and $1.65 \cdot 10^{-3}\,\mathrm{g\,cm^{-2}}$, respectively. Compared to the interfacial loads from Langmuir trough experiments (see

Appendix A.3) the amount is sufficient to fully cover the interface. The deviation between the pure system and the systems with MG1 is within the uncertainty of the measurements. Thus no impact of the microgels on the mass transfer is detectable.

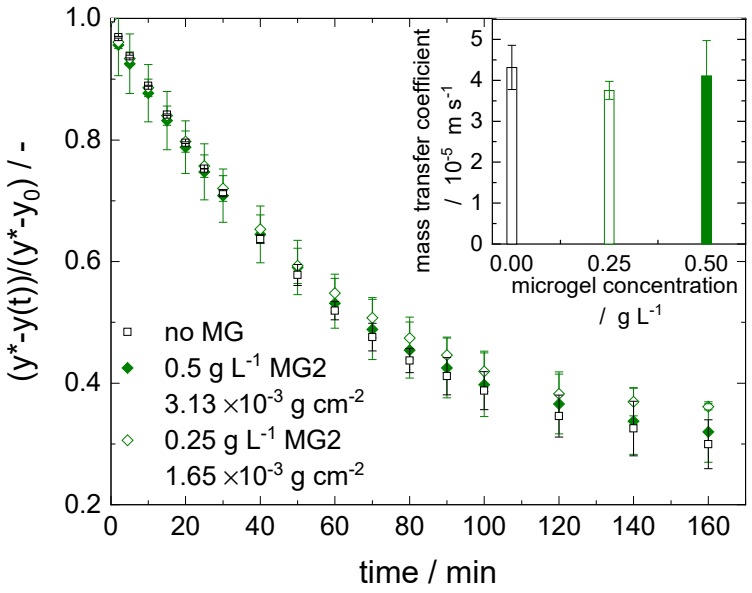

Figure 4.7.: Dimensionless concentration difference over time for the toluene/water/acetone($w \rightarrow t$) for initial concentration $x_0 = 1\,\mathrm{w}\,\%$ for the reference system and two different concentrations of the large, weakly crosslinked MG1. The inset shows the corresponding fitted mass transfer coefficients for the three depicted systems.

In order to transfer these results into a more applicable form, the mass transfer coefficient β is determined from the gradient of the time dependent concentration. For the calculation it is assumed, that the microgels are uniformly distributed, permeable, and penetrated. Consequently, the mass transfer area equals the cross-sectional area of the cell, the results are shown in the inset in 4.7. As the minor deviation in the concentration course suggests, the deviation in the mass transfer coefficient is also within the uncertainty of measurement.

However, it should be noted that the experimental setup is not sensitive enough to detect small scale effects, considering a reduction of mass transfer according to equation 4.3 area reductions smaller $20\,\%$ would not be

detectable (see A.9 for details). The mechanisms and phenomena require small scale observations as they can be realized experimentally and theoretically. An experimental approach could use super resolved fluorescent microscopy methods with very sensitive substances or tags, which allow for the localization of single molecules even within a microgel network [114]. While theoretical approaches could use elaborated analytical models [115] or molecular dynamic simulations [113] to determine potential pathways through the interfacial microgel network.

Effect of Transfer Compenent Size

For small mass transfer components such as acetone no significant impact of the microgel layer can be determined as reported above. Nevertheless, it should be noted that acetone is a small molecule with a diameter of $0.62\,\mathrm{nm}$ [116]. Therefore, the transport of polyethylenegylcol (PEG) with molecular weight of 2000 and 4000 is also tested. The resulting mass transfer coefficients are shown in figure 4.8. For better comparison the mass transfer coefficients are derived considering molar concentrations as the large difference in molecular weight would distort the comparison by weight fractions. The mass transfer coefficient decrease with increasing molecular weight of the component due to lower diffusion. Between the pure system and the microgel system no significant difference can be observed. Therefore, it can be concluded that the microgel layer is also permeable for larger components.

For enhanced assessment of the results from these experiments, the size of the PEG molecules is calculated by the approach for the Stokes radius $r = 0.33 \cdot M_W^{0.46}$ [45]. The sizes of the different molecules are listed in table 4.1.The diameter of the components are all within the range of typical microgel mesh sizes ($1\,\mathrm{nm}$ to $10\,\mathrm{nm}$ [32, 12, 45]), thus a size exclusion is not expected.

However, Fänger et al. report only neglectable uptake of dextrane molecules with similar molecular weight and size. The difference between the results

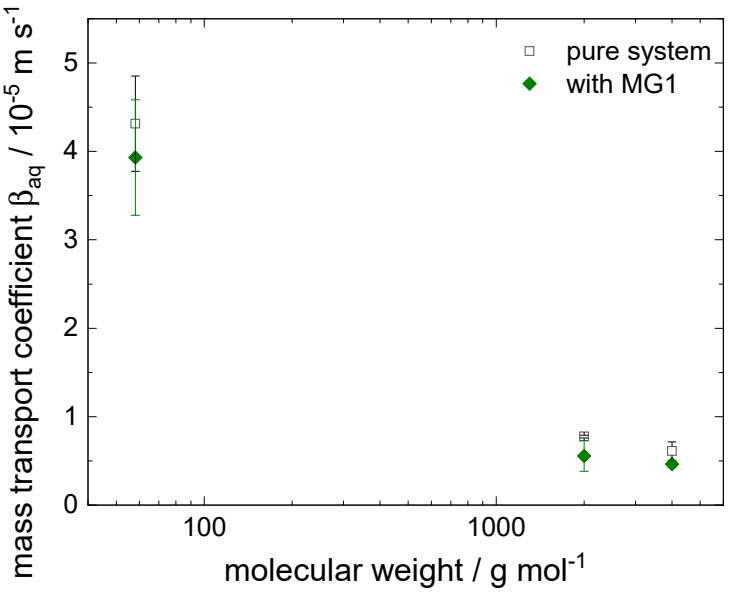

Figure 4.8.: Determined mass transfer coefficients for transfer agents of different molecular weight with and without the large, weakly crosslinked MG1. Their sizes of the transfer components are listed in table 4.1.

Table 4.1.: Tested mass transfer components and their molecular size

component	size / nm	
acetone	0.62	[116]
PEG2000	2.18	[45]
PEG4000	3.00	[45]

can be explained by the observed system, while Fänger et al. studied the permeability of single large microgel particles, the utilized experimental setup is this study regards the transport through a microgel covered liquid interface. Therefore, the pathway of the mass transport is not considered and due to the not uniform crosslinking distribution, mass transfer could be unevenly distributed and occur most likely in the weaker crosslinked periphery than the denser core. Moreover, an increase in average mesh size for adsorbed microgels is reported in literature [32].

4.4.2. Visualization of Mass Transfer

The mass transfer is observed qualitatively by Schlieren experiments as described in section 4.3.2. Figure 4.9 shows a qualitative comparison

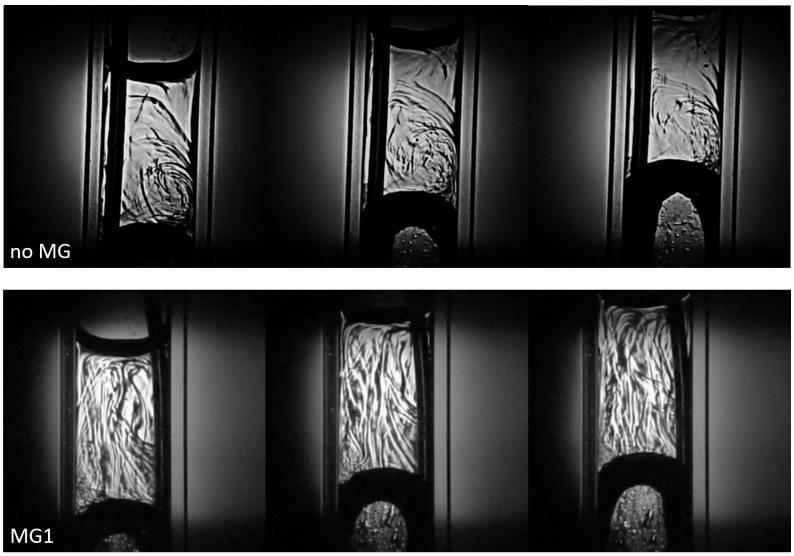

Figure 4.9.: Mass transfer of acetone from aqueous to organic phase, visualized via Schlieren, with and without microgels present at the interface. Pictures taken at $5, 30, 120\,\mathrm{s}$.

between the pure system and a system with MG1. The interface elevates over times as the acetone/water mixture is inserted. The contrast and the amount of Schlieren are not representative for the extend of mass transfer, as the dynamic of the system is not captured in the images. Nevertheless, two observations can be made.
First, mass transfer occurs in both systems. This is in good agreement with the findings from the experiments in the stirred cell from 4.4.1, that the mass transfer of small molecules, in particular acetone, is not hindered by the microgels at the interface.

The second observation concerns the flow pattern visualized by the Schlieren. In the pure system, a vortex is formed at the right just above the interface, that can be interpreted as roll cell. In the microgel system on the other hand the flow is more uniform and perpendicular to the interface. One reason for the different flow patterns, could be a stronger gradient in interfacial tension in the pure system, as acetone lowers the interfacial tension. In the microgel system the interfacial tension is already reduced by the microgels thus the gradient is less pronounced. Furthermore, the formation of roll cells requires a fully mobile interface as described in section 4.2.

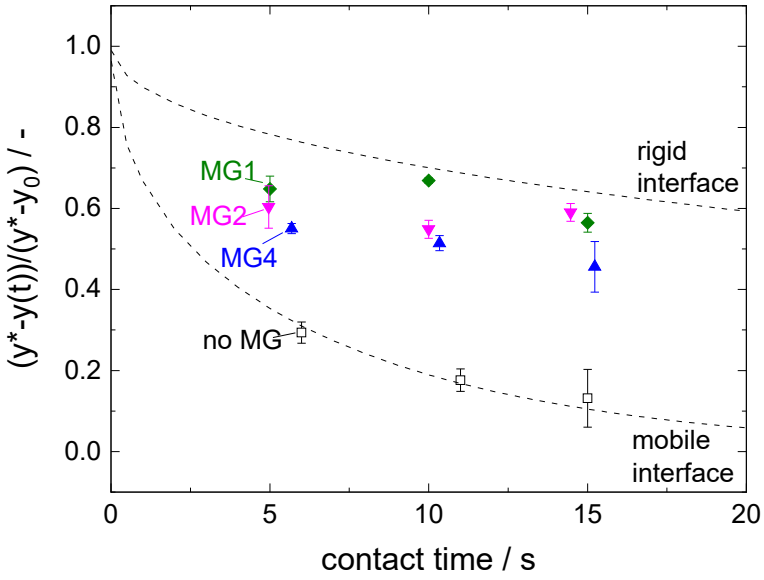

Figure 4.10.: Dimensionless concentration of acetonitiril in 3.06 mm n-butyl actetate drops for different contact times, for the reference system and different microgels. Also shown are theoretical scenarios for mobile and rigid interfacial conditions.

These two observations underlines that microgels do not impede mass transfer but at high concentrations they change the interfacial properties which can subsequently affect mass transport processes.

4.4.3. Single Drop Mass Transfer

The single drop experiments are conducted according to the procedure described in section 4.3.3. Instead of acetone, acetonitril is used as a transfer agent due its better detectability in the Raman spectrum. The pure n-butyl-acetate(d)/water(c)/acetonitril($c \rightarrow d$) is shown as reference, three microgels are utlized in the experiments to cover the drops surface, all with a concentration of $0.1\,\mathrm{g\,L^{-1}}$ in the drop generator. The results are shown as dimensionless concentration difference to equilibrium (see equation 4.9) for 3.06 mm drops in figure 4.10.

To better assess the results, figure 4.10 also displays two theoretical scenarios. First the scenario of a rigid interface, where drop-sided mass transfer is solely diffusive. The rigid interface scenario is described using the Newman model (equations 4.11 and 4.12). The diffusion coefficient

for acetonitril in n-butyl acetate estimated by the Wilke-Chang approach to $2.833 \cdot 10^{-9}\,\mathrm{m\,s^{-2}}$ (for details see Appendix A.7).
Second, a scenario with a mobile interface is displayed. The model for mobile interfacial behavior from Henschke is used which accounts for drop internal turbulence. The displayed course refers to $C_{IP} = 6448$, which is reported by Henschke [19] for a similar system utilizing acetone instead of acetonitril as transfer agent (n-butyl-acetate(d)/water(c)/aceton($c \rightarrow d$)).

The obtained data for the pure system indicates fast mass transfer. The difference to equilibrium decreases with increasing contact time as more acetonitril accumulates in the drop. The trend is in excellent agreement with the prediction of the model from Henschke for the n-butyl-acetate(d)/ water(c)/ aceton($c \rightarrow d$) system. This findings show that similar to the acetone system the mass transfer in the pure system is significantly enhanced by turbulence inside the drop.

For the microgel covered drops, results are shown for drops generated with a microgel concentration of $0.1\,\mathrm{g\,L^{-1}}$. Three different microgels are investigated, two microgels with large diameter and low and medium crosslinking, MG1 $2.5\,\mathrm{mol}\,\%$ and MG2 $5\,\mathrm{mol}\,\%$, respectively. Moreover, the size of the microgels is varied by utilizing MG4 which has a medium crosslinking but is about half the size of MG2 (see also table 1.1). For all microgel covered drops the distance to equilibrium is larger compared to the pure system for all contact times. Nevertheless, the difference to the rigid interface scenario indicates that mass transfer enhancement is still present and the mass transfer inside the drop is not solely diffusive but enhanced by internal mixing.

This observation is in contrast to the results from sedimentation experiments (without mass transfer) in section 3.4.1, which show that for the utilized microgel concentration the drops velocities are similar to rigid spheres for all utilized microgels. Wegener and Paschedag [63] report similar observations in their study with anionic surfactants. For high surfactant concentrations, the sedimentation velocity indicates rigid conditions at the interface but mass transfer is still enhanced [63]. The numerical results from Cuenot et al. [96] provide a possible explanation. They describe the extend of contamination by surfactants by using stagnant cap angles (see figure 3.2).

They found that at an angle of 65° the sedimentation velocity is comparable to rigid sphere while mass transfer is still enhanced at his angle [96]. The mass transfer enhancement in these systems is accounted to the ability of the surfactants to lower the interfacial tension and thus locally increase the Marangoni stress leading to turbulence promoting interfacial instabilities [63, 96, 84].

Transferring these considerations to microgels, they also lower the interfacial tension but the dimensions of the microgels are much larger than of surfactants. Therefore, the local gradients in interfacial tension might be less pronounced. Moreover, the comparison between surfactant and microgels on sedimentation velocity in section 3.4.1 indicates that the microgels not only lower the interfacial tension but they affect the viscoelastic properties of the interface which should be also considered.

Besides the general difference between the pure system and microgel containing system, the results in figure 4.10 show differences between the microgel types. For the less crosslinked, large microgel MG1 the mass transfer reduction is most significant, whereas, the impact of the small, medium crosslinked MG4 is less distinctive. This order of impact is similar to the observations in sedimentation velocity at lower concentrations, the more the microgel tends to spread at the interface the more the drop behaves like a rigid sphere. Therefore, the interfacial mobility is more reduced by the stronger spreading microgels (see section 3.4.1). This trend is also reflected in the mass transfer results in figure 4.10. However, additional experimental data is required to draw more distinct conclusions.

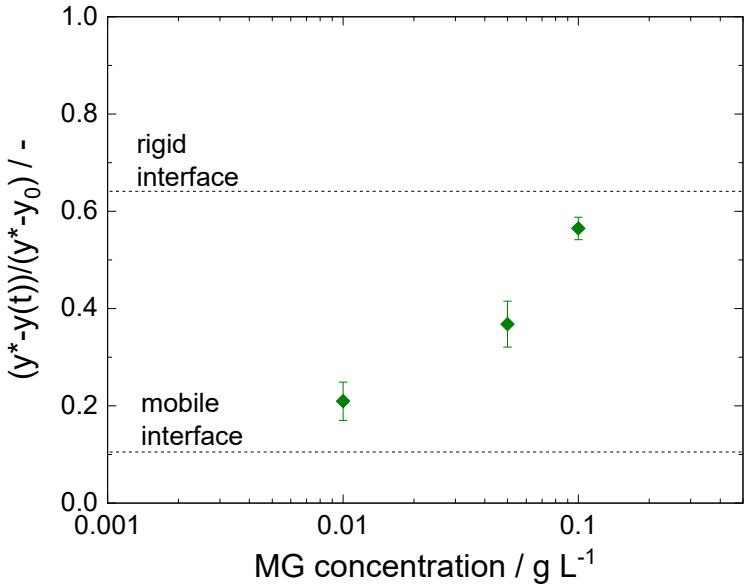

Figure 4.11.: Dimensionless concentration of acetonitiril in 3.06 mm n-butyl actetate drops with 15 s contact time for different concentrations of MG1 in the drop generator.

Figure 4.11 depicts the dimensionless distance to equilibrium for 3.06 mm drops covered with microgels for different concentrations of MG1 in the drop generator. With increasing concentration the difference to equilibrium increases towards the scenario of a rigid interface. However, as mentioned previously the results from sedimentation experiments in chapter 3 indicate rigid sphere like behavior for concentrations above $0.03\,\mathrm{g\,L^{-1}}$. Whereas, the results in figure 4.11 reveal mass transfer enhancement for concentrations above this value. Besides the considerations on stagnant cap angles from Wegener and Paschedag [63] and Cuenot et al. [96] as discussed before, the mixing and solvent conditions inside the microgels should be considered in future investigations. As Gumerov et al. [113] demonstrate in their study on amphilic microgels, they can act as mixer at the interface of two immiscible liquids. This mixing effect could also compensate for reduction of the interfacial mobility. However, these considerations require more detailed investigations and models could help understand the effect of microgels on mass transfer in disperse systems.

First attempts are made in this work to describe the mass transfer in microgels with the models introduced in section 4.2.1 to increase under-

standing on the origin of mass transfer enhancement and its reduction in microgel systems, respectively. The pure system can be described very well utilizing the Henschke approach. As can be seen from figure 4.10 the C_{IP} value of 6448 which is reported by Henschke [19] for the acetone system describes the course for the acetonitril system very good. For the acetonitril system $C_{IP} = 6171$ is determined by fitting to experimental data for drops with a diameter of $2.12\,\mathrm{mm}$ to $3.06\,\mathrm{mm}$ and contact times between 5 and $15\,\mathrm{s}$. The fitting shows good accuracy for the larger drops but for small drops mass transfer is underestimated, the mean squared error is 0.014. The modified Handles and Baron model from Wegener and Paschedag [63] is also utilized for fitting with mean squared error of 0.03 for $\alpha = 0.59$. Since both model approaches underestimate the dependency of the drop diameter, the parameters C_{IP} and α are fitted separately for different diameters for the reference system and the microgel containing system. The predicted courses of the fitted models are compared to experimental data for the reference system and different concentrations of MG1 in figure 4.12.

For the $3.06\,\mathrm{mm}$ drops at low microgel concentration no systematic difference to the reference system can be detected. With increasing microgel concentration the dimensionless concentration and thus the difference to equilibrium increases as indicated in figure 4.11 for $15\,\mathrm{s}$ contact time.

For the $2.12\,\mathrm{mm}$ drops the decrease in dimensionless concentration over time is rapid. For the pure system the difference to equilibrium is reduced below $10\,\%$ within $5\,\mathrm{s}$ contact time between the phases. For this drop size the microgel impact is less pronounced. For concentrations of 0.01 and $0.05\,\mathrm{g\,L^{-1}}$ no difference to the reference system is detected. For the high microgel concentration the distance to the rigid interface scenario is larger compared to the $3.06\,\mathrm{mm}$ drops at the same concentration. This is in contrast to the trends observed in the sedimentation experiments in section 3.4.1. For the fluid dynamic behavior the impact of the microgels at the interface increases with decreasing drop size as the surface to volume ratio increases. This trend is not observable in the mass transfer experiments, here the larger volumespecific interfacial area of the small drops diminishes the importance of mixing flows inside the drop. This holds also true for the pure system, where

mass transfer is more rapid in smaller $2.12\,\mathrm{mm}$ drops compared to the larger drops as shown in figure 4.12. This relation could cause the reduced impact of the microgels for small drop sizes. Since the mass transfer resistance of the microgel layer can be neglected as shown in the experiments at the flat interface in section 4.4.1. Thus, the microgels impact refers mainly to the flow conditions in the drop, and their impact increases with increasing drop size.

Regarding the model approaches the experimental observations of decreasing mass transfer with increasing concentration is also reflected by the increasing values of the parameter C_{IP} and decreasing values of α. It should be noted that both models use the system specific sedimentation velocity of the drops, therefore, the same parameter can lead to different results in the reference and the microgel system as can be seen in 4.12(b) for $\alpha = 0.5$ in the reference system and for the very low microgel concentration.
The model predicts increasing mass transfer with decreasing sedimentation velocity. However, it is noticeable, that the course of the models for increasing contact time does not reflect the experimental data. The decrease in dimensionless concentration in the experiments is less pronounced than the models predict. There are two plausible causes for this observation.
First, initial mass transfer effects are dominant . This hypothesis is based on the assumption that the microgels absorb rapidly to the interface but they require time to adjust before they reach their terminal conformation [54](see also chapter 2). Studies on mass transfer of fixed drops reveals that a large proportion of mass transfer occurs during the first seconds, when the concentration difference between the phases is the largest. Combining these findings, the strong initial mass transfer would not be impeded by the still adjusting microgel layer. And the contribution of mass transfer occurring at longer contact times, when the microgel layer reaches its steady form, is minor.
Second, the generation of microgel covered drops requires more time than for the pure system. During the generation of the next drop the previous drop is withdrawn in the funnel and via the small cross sectional area of

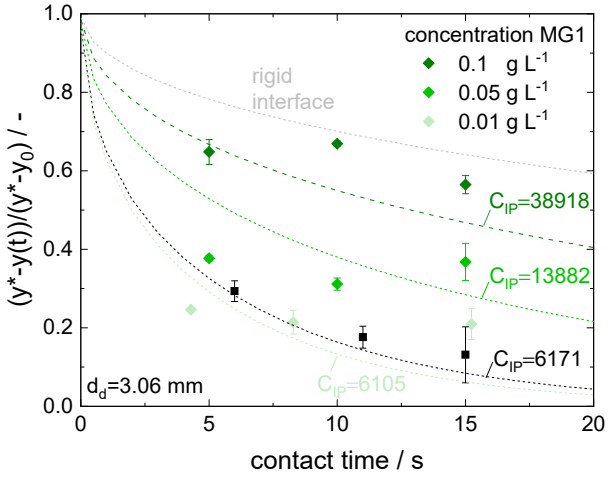

(a)

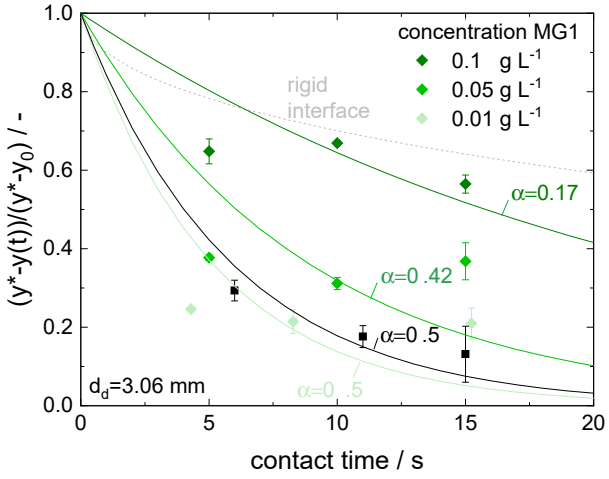

(b)

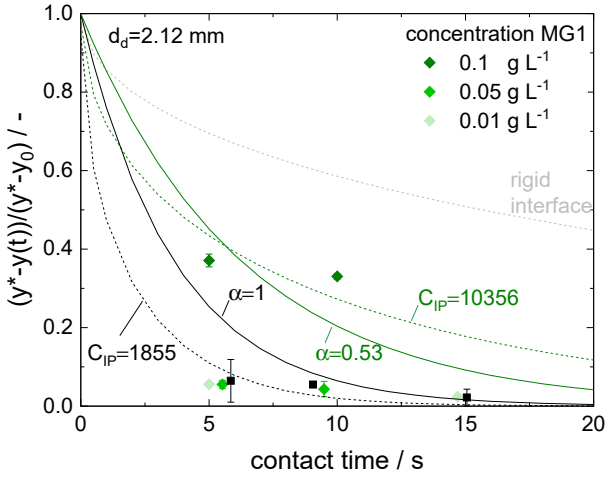

(c)

Figure 4.12.: Dimensionless concentration of acetonitiril in 3.06 mm (a)(b) and 2.12 mm (c) n-butyl actetate drops for different contact time for different concentrations of MG1 in the drop generator, experimental data and prediction by model approaches from Henschke (a)(c) and Wegener and Paschedag (b)(c), with fitting parameters C_{IP} and α, respectively.

the funnel still in contact with the continuous phase. Due to the longer generation procedure this funnel contact time is longer compared to the reference system. This effect is more relevant for short contact times and could lead to a distortion towards smaller dimensionless concentrations for short contact times as the ratio between the contact time in the cell and in the funnel is smaller.

These effects should be tested before considering the introduction of further impact parameters to the models, such as the rheological properties of the interface. A suitable originator for such considerations would be the model approach developed by Paul et al. [61], who introduce a model for external mass transfer processes in micellar surfactant systems considering the surfactant concentration and the viscous properties of the interface.
Furthermore, the investigation of different solvent systems could reveal insights on the proportion of effects, e.g. a system with dominant internal circulation during mass transfer would be very interesting to study. Whereby, the identification of suitable model solvent systems is challenging. A model system with dominant internal circulation during mass transfer presumes the absence of concentration gradient introduced turbulence. These systems are characterized by low interfacial tension which is accompanied high transversal solubility. The high transversal solubility could effect the microgels properties and performance as demonstrated for the n-octanol/water system [25, 14].
Last but not least, the continuous improvement of contactless concentration measurements as for example Raman spectroscopy or laser induced fluorescence (LIF) could help understanding the conditions inside microgel-covered drops by spatially and time resolved online measurements.

4.5. Conclusion

In this chapter the impact of microgels on mass transfer across a liquid-liquid microgel-covered interfaces is investigated. The investigations are divided in observations considering the microgel layer as physical barrier to mass

transfer and observations considering the impact of the microgel layer on the flow conditions and thus the mixing within the drop.

The experiments in a stirred biphasic cell with defined interface with different sized mass transfer components reveal no significant systematic impact of the interfacial microgel layer on the mass transfer. The tested transfer components are between 0.6 nm and 3 nm stokes diameter, within the range of typical mesh sizes of PINPAM microgels reported in literature [45, 12, 32]. This result is in good agreement with previous observations from literature for microgels in bulk [45, 107] and at interfaces [108]. Nevertheless, for the detailed understanding of mass transfer through microgel covered interfaces, more detailed insights are required that cannot be provided by the utilized experimental setup.

Moreover, the visualization of mass transfer by Schlieren technique indicated different flow patterns in case of a microgel covered interface compared to the pure system. This observation underlines the finding from chapter 3 that the microgel at high concentrations significantly affect the interfacial mobility and thus the drop internal flow conditions.

This finding is also reflected by the single drop experiments. The impact of the microgels increases with increasing concentration and increasing drops size. At small drops the large volume specific interfacial area compensates for poor mixing. As the microgel layer is fully permeable, as demonstrated in the flat interface experiments, the microgels impact is less pronounced than for larger drop sizes. At large drops and high microgel concentrations the effect of the microgels is observable. Although rigid sphere like behavior is observed for the investigated drop size in the sedimentation experiments, the mass transfer is enhanced. This is in good agreement with observations in surfactant systems [63, 84] and indicates a partial mobility of the interface [96]. The relation of the results to the interfacial mobility is underlined by the extent of impact of the different microgel types, which correlates with the tendency of the microgel to spread at the interface, similar to the observations on fluid dynamics of microgel covered drops in chapter 3.

Finally, the experimental results are compared to theoretical models. Al-

though the accuracy of the fit by means of the mean square error is below $20\,\%$, the course of the prediction does not match the experimental data and further investigations are required to determine the origin of the mismatch. Nevertheless, the results demonstrate the high impact of interfacial properties of the microgels on mass transfer, therefore these properties should be further characterized in future studies.

5. Phase Separation and Coalescence

Parts of this chapter have been published as:
Microgels for the Intensification of Liquid-Liquid Extraction Processes - Feasibility and Advantages, Chemical Engineering and Technology, 2020
Miriam Faulde, Josia Tonn, Andreas Jupke
DOI: 10.1002/ceat.201900407

5.1. Introduction

The ability of microgels to stabilize and destabilize liquid-liquid systems, such as emulsions, on demand has been demonstrated in numerous studies [1, 14, 17, 117, 108]. The switchable stabilization is a key feature for the successful application of microgels in liquid-liquid extraction, since coalescence is a mixed blessing in these processes: In the active part of an extraction column, where mass transport occurs, coalescence is countered to preserve a large interfacial area. On the other hand, on top of the column, coalescence is required to separate the phases before they proceed to subsequent process steps. To take the different conditions of these two scenarios into account, different experimental approaches are utilized.

Coalescence of single drops as it occurs in the active part of the column is investigated in a newly setup measuring cell. The coalescence probability is determined for different microgel types and microgel concentrations. Combined with the findings on fluid dynamics from chapter 3 and high speed images from the collision the observations provide first indication of relevant effects for stabilization at microgel covered drops in liquid-liquid application

such as extraction.

Considering coalescence as part of phase separation, experiments in a standardized batch settling cell are conducted. These experiments refer to the conditions at the top of the column, where a dense packed drop zone coalesces forming a coherent phase. Based on the results a prototype settler device is designed and tested, operating under continuous, technical lab scale conditions.

5.2. Fundamentals

Coalescence is the fusing of two drops or a drop with an interface. It is a dynamic process and the characteristic quantity is the coalescence time. This dynamic process can be divided in different stages which are illustrated in figure 5.1. [118, 119, 120]

When the drops are approaching, they deform. Gravity and attractive forces between the drops cause the approaching drop to displace the continuous phase between the two drops. The process of displacement of the continuous phase is referred to as film drainage. When the film of continuous phase is reduced to a critical height, interfacial and hydrostatic forces are of the same setup, causing the film to tear and the drops merge.[121] This stage is referred to as film rapture.

The critical height for film rapture depends on the solvent system and its

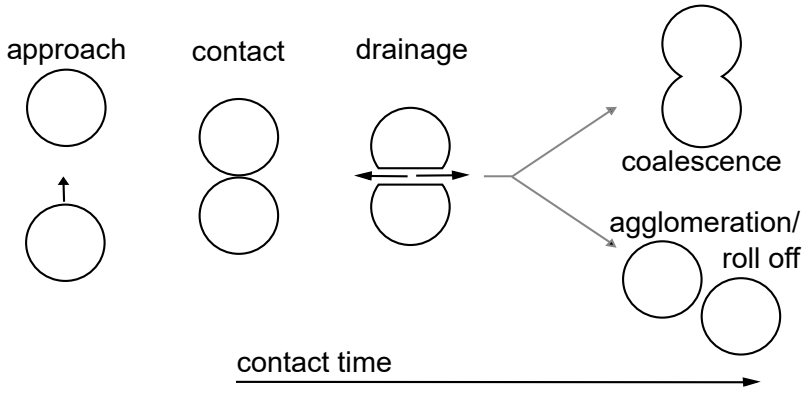

Figure 5.1.: Scheme of two approaching drops, if the contact time exceeds the drainage time the drops coalesce (adopted from [119])

conditions, e.g. pH. Experimentally obtained values reported in literature range from 10 to multiple 100 nm [122]. This process and the described stages are also transferable to coalescence between a drop with the interface of its coherent phase.

In unit operations involving disperse systems, coalescence between the free disperse drops is mostly unwanted as it decreases the volume specific interfacial area; whereas, most processes include subsequent separation of the disperse phase where coalescence is required. With regard to the different appearance of coalescence within the process different experimental setups have been introduced in literature.

For the consideration of coalescence between sedimenting drops as e.g. in the active part of an extraction column the coalescence frequency is determined by the collision frequency and the coalescence probability. In the past, the latter was commonly set to unity before the introduction of single drop experiments to determine the coalescence probability [123]. Different setups exist, which can be further divided to static and dynamic experiments. In static experiments at least on of the drops is fixed, most commonly to a needle or the tip of a canular. This fixation enables very good observablity but it also brings an additional external influence.[119, 124] In dynamic setups, the drops are brought together by manipulating the flow conditions e.g. by applying shear [125].

In contrast, coalescence in context of phase separation is observed as an integral phenomena, e.g. by the standardized batch settling experiments introduced by Henschke [121]. In these experiments, the time depending evolution of the phase separation is observed and can be used to determine the required dimensions of a settler device [121]. During experiments a dense packed drop zone builds up; hence, collision rate and energy are not relevant.

In both cases, single drops coalescence and phase separation, the coalescence depends on three major categories of impact parameters [118, 119]:

- physico-chemical properties of the solvent system

- apparatus geometry
- energy input

5.2.1. Single Drop Coalescence Model Approaches

To describe and determine coalescence probability of single drops two different physical model approaches are employed in literature. The energy model and the film drainage model.

The energy model was first introduced by Howarth [126] and extended by Sovová [127]. It relates coalescence to the energy of the system, therefore the coalescence probability increases when the drop velocity exceeds a critical value. This critical value is defined by the kinetic energy of the drops which is high enough to overcome the interfacial energy represented by the interfacial tension.[126, 119] The kinetic energy is dominated by flow conditions and hence attractive or repulsive forces between the drops are neglected. The energy model predicts increasing coalescence probability with increasing drop diameter and increasing velocity, respectively.

This is in contrast to the idea of the film drainage model. The model is based on the work from Coulaloglou and Tavlarides [128] who relate the contact time subsequent to collision of the drops to the required time for film drainage.[119] The drainage time and the force required for film rapture depends on the properties of the system and the energy input. The coalescence probability increases when the contact time exceeds the drainage time. This basic idea has been extended by different approaches accounting for the deformation of the drops which enlarge the film width, as well as the interfacial conditions which determine the flow conditions of the draining film. The mobility of the interface is commonly related to the viscosity ratio of the phases and the presence of impurities and surface active species. [119, 129] In case of a rigid interface the velocity at the interface is zero due to the adhesion condition. This condition leads to a

parabolic velocity profile for laminar flow of the draining film. While, in case of a mobile interface, no slip is present which leads to a uniform velocity profile and a quicker drainage of the film compared to the rigid conditions.[119]

Furthermore, the film drainage is affected by simultaneous mass transfer. Thereby, the direction of mass transfer is decisive; if the system is sensitive to Marangoni effects as described in 4.2. In case of mass transfer from the disperse to the continuous phase, the drainage of the film is enhanced, since the concentration of the transfer component in the center of the film interface is the highest. This local concentration difference leads to the movement of the interface in direction of the film drainage to compensate the interfacial tension gradient.

In the other mass transfer direction, from continuous to disperse phase, the concentration is the lowest in the center of the film interface and the compensation movement of the interface is opposite to film drainage, leading to longer drainage times and thus reduced coalescence probability.[19, 119, 130]

5.2.2. Effects of Surface Active Species on Coalescence

The coalescence and settling behavior is very sensitive. Simon [119] and Villwock [131] report effects even between different production lots of the utilized chemicals from the same retailer. Thus the settling behavior is affected without measurable changes in the physical properties of the system. Henschke [121] emphasizes the role of interfacial mobility, van der Waals attraction and electrostatic repulsion, which are hardly predictable and thus experimental determination of the settling behavior is indispensable [121].

The stabilizing effects of different surface active agents have been studied intensely in the past to reveal stabilization mechanisms and identify related properties. The differences and similarities of species like particles and surfactant can help to categorize the effects of microgels on coalescence. Especially, the stabilization of liquid-liquid systems by solid particles is a well studied field. These systems are commonly named Pickering emulsions referring to Spencer U. Pickering who investigated this phenomenon in the

beginning of the 20th century. By analogy, the term Mickering emulsion for microgel stabilized systems was introduced in literature [38, 1, 132]. The term emphasizes similarities and differences between the stabilization mechanisms. The two most commonly regarded stabilization mechanisms for contaminated systems are steric hindrance [30, 133] and slowed film drainage [134, 135].

In case of solid particles, most studies consider steric hindrance and regard the wettability of particles. Furthermore, the size and interactions between molecules and particles such as electrostatic repulsion are often related to the stability of the dispersion.[136, 137] A measure for the wettability of a solid particle is the contact angle of the particle at the interface as described in section 2.2.3. For efficient stabilization the particle must be partially wettable by both phases [137]. The direction of dispersion predominantly depends on the wettability. The phase with the better wettability holds the larger portion of the particle. Therefore, the interface tends to curve such that the larger portion of the particle is located on the convex side. Thus, the phase with better wettability preferably constitutes the continuous phase.[30] This is also true for surfactants, where the wettability is expressed by the hydrophilic lipophilic balance (HLB), describing the ratio between the polar and the apolar parts of the molecule.[30]

In case of surfactants the detailed numerical investigation of Chesters and Bazhlekov [134] and Cristini et al. [135] considers the film drainage between surfactant covered drops. The study demonstrates the fluid dynamic complexity of the film drainage due to the interplay between Marangoni stress, surfactant distribution, interfacial velocity, and the gap width. Thereby, the film drainage is slowed due to Marangoni stress, which is caused by flow induced changes and asymmetries in the interfacial surfactant distribution.[134, 135, 138]

Microgels are different and do not match exactly the above definitions as they deform at the interface and are not amphiphil. However, they are highly hydrophilic and thus favor the aqueous phase as continuous phase. Oil in water emulsions are obtained using organic solvents of different polarity [25].

However, both directions of dispersion can be obtained using microgels [14]. Nonetheless, water in oil emulsion with microgels are less stable than oil in water emulsions [14, 25]. The main difference between the two directions of dispersion is the appearance of the microgels at the interface. For oil in water emulsion the microgels highly deform and build a film at the interface as described in section 2.2.3. In contrast, if the aqueous phase is dispersed the microgels are less deformed and multi layers are reported [25].

As their deformability makes them different to solid particles, it is in focus of many studies on the stabilization mechanism of microgels in biphasic systems. The stability increases with the softness of the microgels [17]. Therefore, weak crosslinked and large microgels, which show more pronounced deformation at the interface, are more effective stabilizers than more crosslinked or smaller microgels, respectively. Destribats et al. [17] argue that the stability refers to the morphology and rheological properties of the microgel layer. In case of weakly crosslinked microgels, the highly interpenetrated and elastic microgel layer effectively prevents coalescence. On the other hand, the reduced interpenetration and elasticity of the layer formed by higher crosslinked microgels are insufficient to protect the drops from coalescence.[17, 34]

Besides macroscopic observations of emulsion stability few studies present a detailed view on the film between drops. Destribats et al. [139] investigated the structure of the thin film between drops by cryo-SEM for different crosslinked microgels with a bulk diameter of approximately 700 nm. In case of weakly crosslinked microgels, they observed thicker and inhomogeneous films . The films are about 700 nm thick and show dendrite like structures. The cross sectional view of these structures reveals that they originate from cavities. The authors attribute these cavities to two monolayers on top of each other. Within this non adhesive bilayer only a few microgels bridge between the drop interfaces. For the higher crosslinked microgels they observed a thinner more homogeneous bridged monolayer with no cavities and a thickness of approximately 250 nm. They relate the resulting stability to the mobility of the microgels. The formation of bridges requires the rear-

rangement of the microgels at the interface. In case of weakly crosslinked microgels their mobility is reduced due to the high interpenetration of their periphery. Moreover, the reduced mobility of the interface reduces the drainage velocity. Therefore, the weaker crosslinked microgels show less bridging.

Other studies by Cohin et al. [47] and Keal et al. [140] regard the dynamics of the film drainage. In both studies the formation of a dimple between the interfaces is observed. For low crosslinked microgels a symmetric drainage is observed, whereas in case of higher crosslinked microgels the dimple drains less symmetrically. A symmetric drainage indicates a high surface viscosity, thus the difference in drainage symmetry indicates different rheological properties of the interface. [47, 140]

Keal et al. [140] studied the film thinning in an air/ water system. Their results with different interfacial loads and crosslinking densities confirm the findings and hypotheses from Destribats et al. For low interfacial loads they observed bridging and monolayer formation, resulting in an adhesive film between the drops. Whereas, higher interfacial loads lead to the formation of a non adhesive bilayer. Moreover, for higher crosslinked microgels the bridging increases and the film drains faster, encouraging the hypothesis on the microgels mobility effect.[139]

However, the extraordinary features of microgels and their complex interfacial properties make it difficult to draw general conclusions. The complex interaction of these parameters increase difficulty to characterize an universally applicable stabilization mechanism for microgels [41]. Especially, the most exciting feature of the microgels, their switchability and the propagating switchable stabilization mechanism is still not fully resolved yet.

The temperature triggered collapse of microgels at the interface is significantly different from microgels in bulk. The collapse in bulk is rapid and uniform in radial direction [141, 142], whereas the deformed microgels at the interface change their morphology only in lateral direction [36]. Thus the distance between the microgels is not affected. Moreover, a desorption of microgels from the interface is not reported in literature [47, 7]. How-

ever, the properties of the microgel covered interface change drastically. When the temperature is raised above the VPTT the interface is less elastic [14]. Brugger et al. [14] state that the interaction between the microgels decreases due to reduced hydrophilicity of the collapsed microgels. In contrast, Monteux et al. [143] report a minimum in interfacial tension around the VPTT. They relate the minimum to an increased amount of microgels adsorbed at the interface. Furthermore, they observe coalescence in emulsions when exposed to temperature increase at the same temperature level. They conclude, that an increased number of microgels adsorbed below the VPTT and an increased tendency of the microgels to cluster formation above the VPTT could lead to a rapture of the water film between the drops enabling coalescence and ultimately phase separation [143]. The minima in interfacial tension around the VPTT was also found by Li et al. [144]. Their interfacial tension experiments with temperature ramps also demonstrate that the temperature at which the microgels adsorb is relevant. Furthermore, it shows that microgel covered drops generated above the VPTT and cooled behave different than, drops generated below the VPTT.[144]

5.3. Methods and Materials

The investigation of the microgel impact on coalescence considers two scenarios, the approach is sketched in figure 5.2. First, coalescence in a dense packed drop zones as it occurs during phase separation, therefore, the integral settling behavior is observed in a standardized settling cell. Furthermore, these experiments are the basis for the design of a continuous operating settler prototype, which was also tested. Second, single drop experiments are conducted, reflecting the conditions during the free sedimentation of the drops in the active part of the column. In combination with the results on fluid dynamics and interfacial conditions from chapter 3 these experiments reveal first indications on the stabilization of microgel-covered drops.

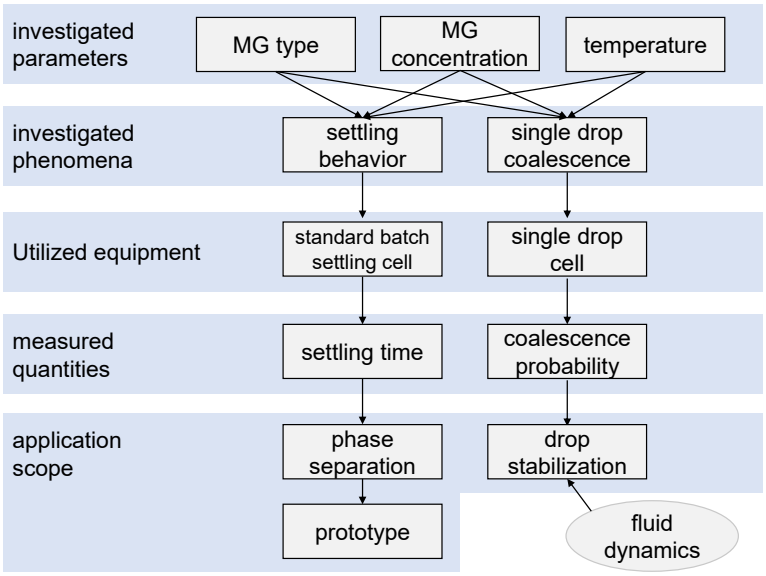

Figure 5.2.: Experimental approach for the investigation of the impact of microgels on coalescence

5.3.1. Batch Settling Experiments

Settling experiments are conducted in a standardized batch settling cell [121]. The experimental setup is shown in figure 5.3. The center piece of the setup is a glass cylinder with 80 mm diameter. In the cylinder two stirrers are placed, which are connected to a motor on top of the cell by a gear (not shown in figure 5.3). At the bottom of the cell the stirrers are fixed in a Teflon plate. The temperature can be adjusted by a thermostat which is connected to the squared plexi glas housing, surrounding the cell. Furthermore, a millimeter scale is put on the front of the housing for the determination of the height of coalescence and sedimentation line, respectively.

Prior to the experiments, the phases are mutually saturated for 2 hours to avoid mass transfer effects during phase separation or shifting of the phase ratio. The phase ratio between organic (toluene) and aqueous phase are varied between 1:2 and 3:2. The aqueous phase is modified regarding microgel concentration and ionic strength. The ionic strength is adjusted using sodium chloride. Next, the microgels are added to the aqueous phase. After the cell is filled with the solvent system the temperature is adjusted via the thermostat. When the system reaches the adjusted temperature

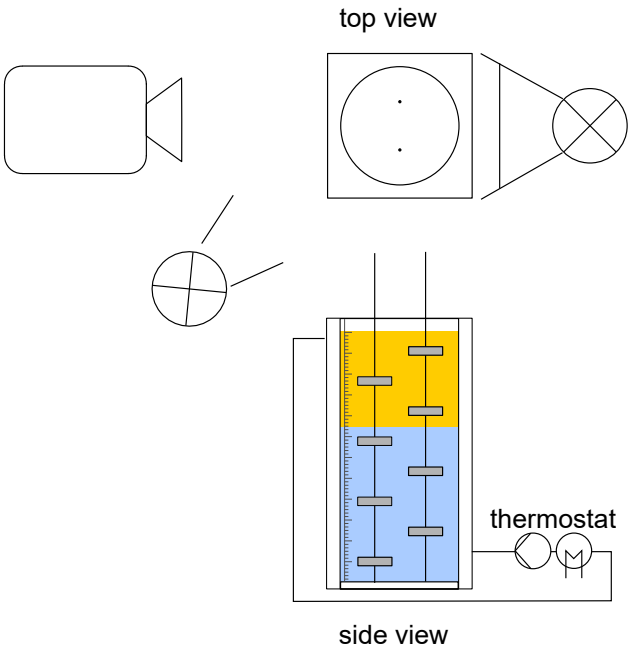

Figure 5.3.: Experimental setup of the standardized batch settling experiments proposed by Henschke [145]

the experiment starts. Both phases are stirred at 800 rpm for 120 s in the cell. After the stirrer is stopped, the phase separation is recorded by a video camera. The stop and thus the start of the settling process is indicated by hand sign on the recording. The process is declared finished when only half of the interface is covered by drops, this is also indicated on recording by hand sign. If the system does not completely separate within 20 min, the experiment is stopped. The experiments are repeated between 3 and 5 times, depending on the deviation.

5.3.2. Continuous Settler Experiments

For the experimental investigation of the feasibility of continuous operating phase separation a horizontal settler with about 80 mm length, double wall and additional coil for temperature control is used in the setup shown in figure 5.4.

The phases are mutually saturated, for better visual observation of the separation process the organic phase is died blue by addition of Cerres blue dye. The aqueous phase is pumped through the setup by a gear pump

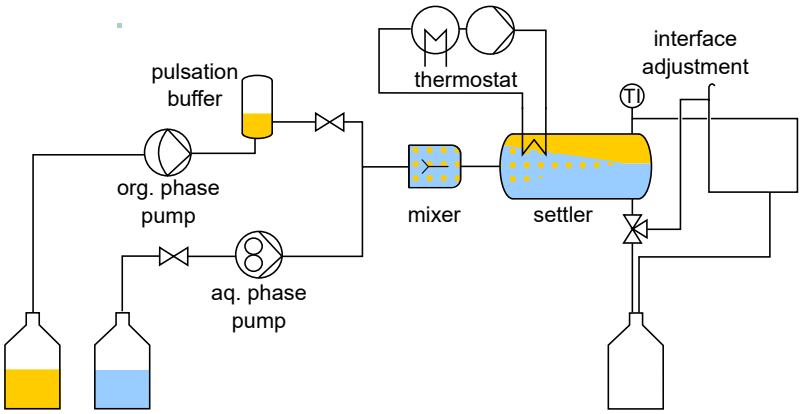

Figure 5.4.: Experimental setup for testing continuous settler operation

MPZ-standard (Ismatec, Germany), for the organic phase a membrane pump (Dulcometer Typ D4a 0308 from ProMinent GmbH, Germany) is used. Additionally, a pulsation damper is installed in the line to avoid oscillating flow. The phase ratio can be adjusted by the flow rates of the pumps. The flows are combined right before a static mixer (kenics type, $d_{mixer} = 5mm$, $l_{mixer} = 22.5mm$), which generates the dispersion. The horizontal settler is connected to a thermostat (CF31 from Julabo GmbH, Germany). The settler outlet temperature is measured in the organic phase outlet. A vertically adjustable tubing on the aqueous phase outlet allows to adjust the phase interface height in the settler. A vent is included to avoid siphon effects.

Experiments are conducted below and above the VPTT of the microgels, with temperature set point of the thermostat of 20 °C and 70 °C, respectively. The volume flows are chosen between 17.9 L h^{-1} to 40.5 L h^{-1} reflecting typical loads of laboratory scale DN50 extraction columns as they can be found in literature [146].

5.3.3. Single Drop Experiments

The single drop experiments are performed in a newly setup single drop cell, which is shown in figure 5.5. The cell consists of a double walled glass cell. The cell has a rectangular shape to reduce distortion during observation of the collision. Moreover, the cell is equipped with a double wall which is connected to a thermostat and allows for temperature adjustment. The

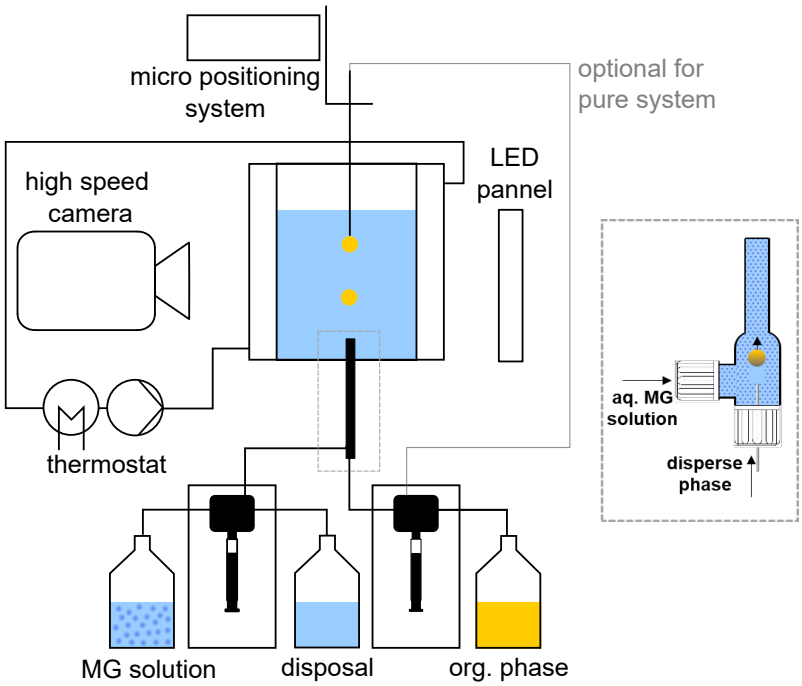

Figure 5.5.: Experimental setup of the single drop coalescence cell

microgel covered drops are generated according to the procedure described in section 3.3.2. The position of the canulla, carrying the upper drop can be adjusted in three spatial directions by a micro positioning system (MFA-PPD from Newport Spectra-Physics GmbH, Darmstadt, Germany) with 25 mm adjustment range in each direction.

The collision is recorded by high speed camera (Os4S1-C-O4 from ImagingSolutions GmbH, Eningen, Germany), with 2000 frames per second allowing for high time resolution of the recording. For sufficient illumination a LED panel is placed behind the cell opposite to the camera. The panel runs with direct current to avoid fluctuation due to power frequency.

The images from the highspeed camera are analyzed using a Matlab®script based on the work from Kamp et al. [147]. The frame-wise analysis allows to determine the velocities of the drops as a function of distance to the canula. Since the distance between the canulas is minimized in order to maximize the hit rate, the distance is too short for the drops to reach their terminal velocity. Therefore, the terminal velocity is recorded previously for all drop diameters. To enable similar collision velocities of the drops in the experiment, the distance between the canullas is adjusted

based on the image analysis results.

5.4. Results

5.4.1. Phase Separation Behavior

Coalescence of microgel covered drops is considered as integral process of phase separation by standardized settling experiments. The experiments are conducted and the data is evaluated as described in section 5.3.1.

Effect of Microgel Concentration

Figure 5.6 shows propagating phase separation over time as heights of the coalescence and sedimentation exemplary for the pure system and two different concentrations of the large, medium crosslinked microgel MG2. The phase ratio between toluene and water is 1:2. The dispersed toluene drops sediment through the water phase, form a densely packed zone, and finally coalesce forming the upper coherent phase. The sedimentation is indicated by the lower set of data points for each experiments. These data points represent the height of the lowest raising drop, thus no dispersed drops are below this height and the height increases over time. Ultimately, it reaches the height of the interface in the separated system.

On the other side, the upper set of data points represents the evolution of coalescence forming the coherent phase. Coalescence starts at the top of the mixture and the data points represent the height of the interface of the formed coherent toluene phase. Thus the height of the coalescence line decreases over time.

The disperse drops are located between the upper and lower data points, but the visual examination does not allow clear distinction between free rising drops and the dense packed zone. For the pure system the separation process takes about 80 s.The end of the separation process is indicated by the union of coalescence and sedimentation.

The sedimentation is faster than the coalescence, as can be seen by

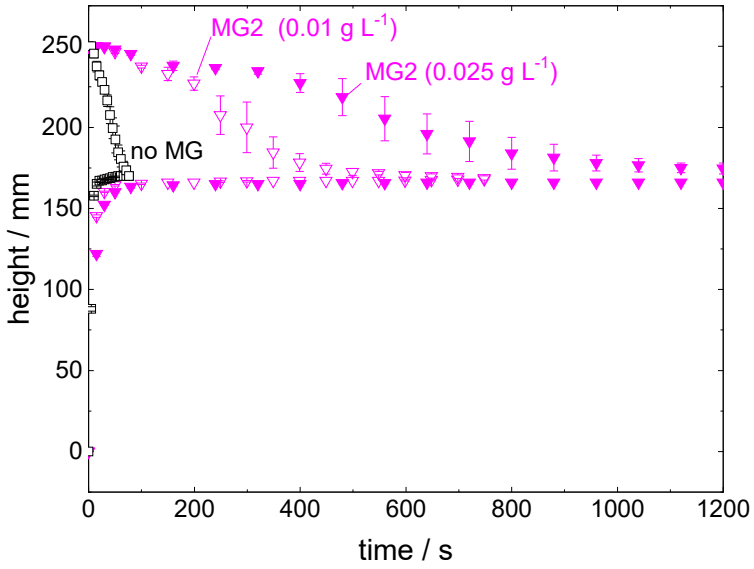

Figure 5.6.: Phase separation in standardized settling cell, for the toluene/water system, below the VPTT at 25 °C, phase ratio 1:2, ionic strength 50 mmol L^{-1} at neutral pH, coalescence and sedimentation shown for the pure system and with two different concentrations of the large, medium crosslinked microgel MG2

the slope of the data points. For the microgel system the sedimentation is not significantly affected, but the effect on coalescence is very strong. The effect increases with increasing microgel concentration. In literature it is often referred to as limited coalescence regime [137]. Due to the absence of desorption the drops coalesce until the interface is fully covered and the energy required to squeeze the interfacial microgel layer, to obtain an even denser packing, exceeds the energy gain by reducing the interfacial area through coalescence.

The interfacial area can be approximated using the Sauter mean diameter that is obtained from the slope of the sedimentation line [145]. As the slope of the sedimentation is only marginally affected by the microgels, the resulting deviation in the derived Sauter mean diameter is small. In these experiments the Sauter mean diameter is determined between 1.2 mm and 1.38 mm. For the low concentration of 0.01 g L^{-1} this leads to a ratio between the initial microgel amount and the available interfacial area of $3.88 \cdot 10^{-4}$ mg cm^{-2}. Comparing this value to the information on the surface pressure from Langmuir trough experiments in the appendix A.3, this ratio

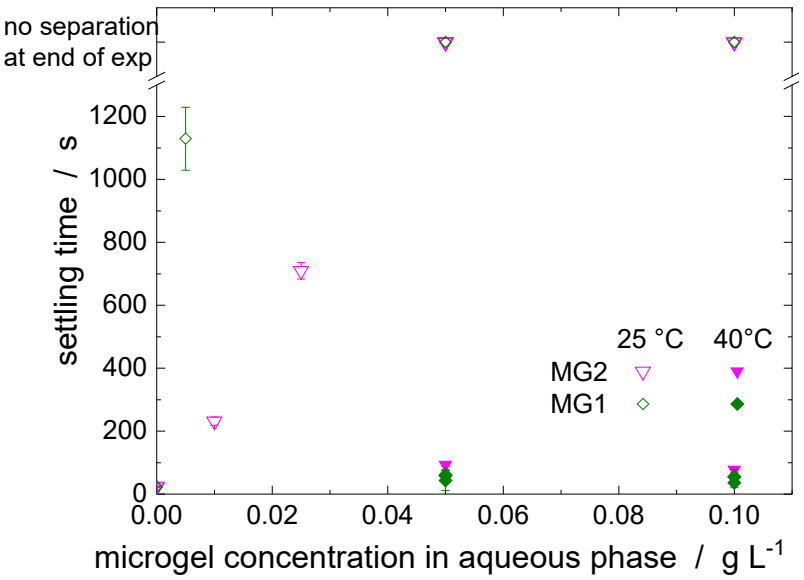

Figure 5.7.: Settling time for different concentrations of MG1 and MG2, below (25 °C) and above (40 °C) the VPTT. The end of experiment is defined at 20 min

is about three times lower than full coverage for MG2.

5

The effect of concentration on the phase separation is shown for a wider range of concentrations in figure 5.7. Furthermore, two microgels with different amount of crosslinker and thus spreading behavior at the interface are investigated. Moreover, the experiments are conducted at temperatures below and above the VPTT, thus the swollen and the collapsed state of the microgels are regarded.

As mentioned above, the sedimentation and also the initial drop size is not affected by the microgels, thus the concentrations can be easily compared. In the swollen state, below the VPTT, for both microgels the stability increases with increasing microgel concentration. For concentrations above $0.05\,\mathrm{g\,L^{-1}}$ the two phases do not separate within 20 min. This duration is defined as end of the experiment with regard to the application and the technical realization. The settling time transfers to the required apparatus size, e.g. the length of a gravity settler.

For lower concentrations the weaker crosslinked microgel MG1 stabilizes the dispersion more effective, leading to longer settling time of about 1100 s for $0.005\,\mathrm{g\,L^{-1}}$, while for the stronger crosslinked microgel MG2 only about

200 s are required for settling. This is in good agreement with the findings from other authors, that softer microgels stabilize emulsions more effectively [17].

Above the VPTT, in the collapsed state, the complete separation is observed for both microgels even at high concentrations. This behavior was demonstrated before in numerous studies in qualitative means. In the collapsed state the microgels do not stabilize the disperse system. The short settling time in the standardized experiment demonstrates the feasibility of the process concept, however, the temperature impact will be considered in more detail.

It should be mentioned, that in some cases there was absolutely no coalescence observable, however, all these experiments were conducted in the laboratories at Wüllnerstraße and were not reproduceable in the new laboratory at Forckenbeckstraße, although the demineralized, distilled water was produced by the same apparatus. Since the early results are not reproducible they are not regarded here.

Nevertheless, it can be concluded that the stabilization in general is very effective, but the ultimate extent of stabilization is sensitive.

Effect of Phase Ratio

The volumetric proportion of the phases predominantly determines whether an oil in water or water in oil dispersion is obtained. In presence of surface active species, their spatial distribution at the interface becomes an additional parameter as described in section 5.2.2. Figure 5.8 shows the time depended settling behavior of toluene and aqueous microgel solution with phase ratio 3/2 for two different concentrations of the large medium crosslinked microgel MG2. The water is dispersed in toluene, therefore the upper data points refer to sedimentation and the lower data points to coalescence.

After about 20 s the phases are completely separated. The difference

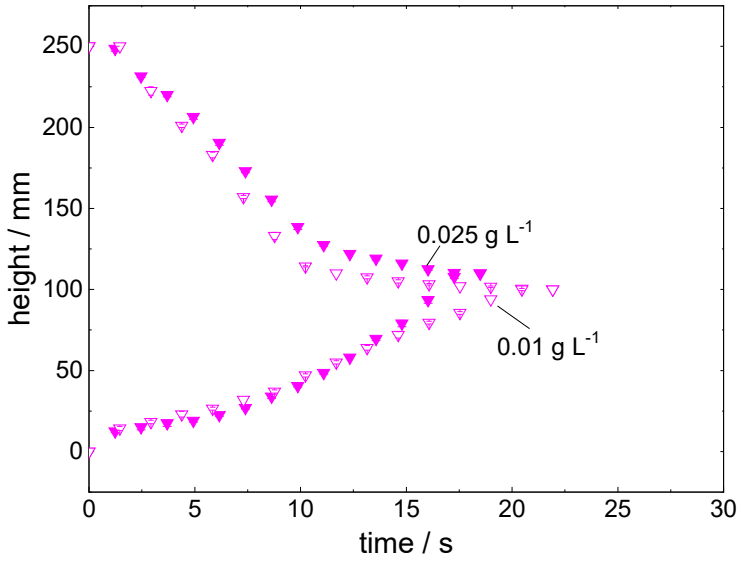

Figure 5.8.: Phase separation in standardized settling cell, for the toluene/water system, at 25 °C, phase ratio 3:2, ionic strength 50 mmol L^{-1} at neutral pH, for two different concentration of microgel MG2 in the aqueous phase

between the two tested microgel concentrations is minor. Compared to the oil in water system in figure 5.6, the settling times are significantly shorter. In case of the lower microgel concentration of 0.01 g L^{-1} the separation is about ten times faster. The faster separation, and thus less effective stabilization, can not be attributed to the reduced total amount of microgel in the reduced volume of the aqueous phase, since the difference for the different microgel concentrations is minor.

The dependency of the stabilization on the direction of dispersion has also been demonstrated qualitatively in literature [14, 25]. The difference in stabilization is referred to the curvature of the interface towards the microgel containing aqueous phase. In case of on oil in water dispersion, the convex interface allows the microgels to spread and the larger portion of the deformed microgel is located at the aqueous site of the interface (see figure 3.14). Whereas, if water is the dispersed phase the concave curved interface does not allow for spreading as the volume decreases in radial direction from the interface in direction of the aqueous phase. Therefore, Destribats et al. [25] propose the presence of undeformed microgel multilayers for water in oil systems. Thus the microgel spreading is essential for the properties of

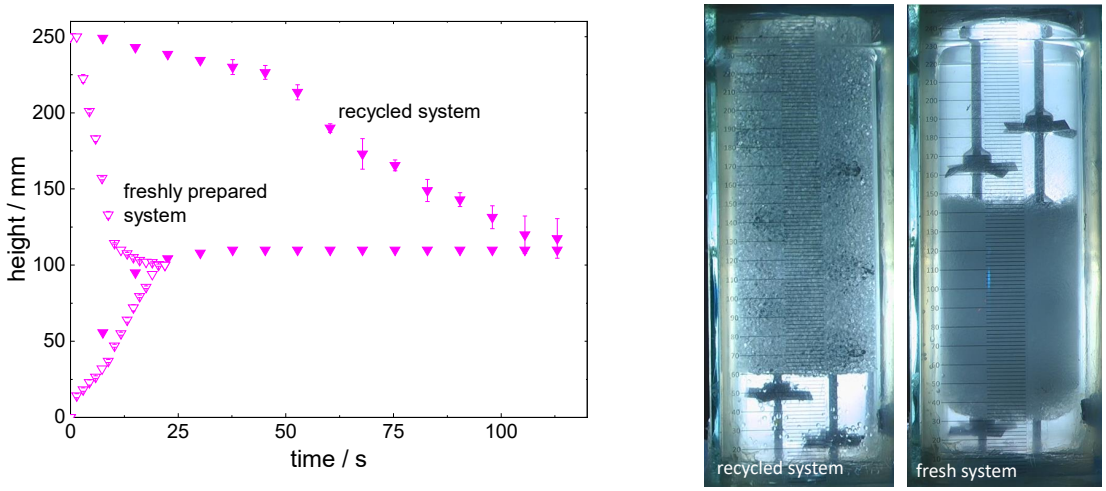

Figure 5.9.: Phase separation in stadardized settling cell, for the toluene/water system, at 25 °C, phase ratio 1:2, ionic strenght 50 mmol L^{-1} at neutral pH, for a recycled solvent system that was utilized previously at phase ratio 1:2, and a freshly prepared system

microgel stabilized systems.

Considering the application of PNIPAM microgels as switchable stabilizer in disperse liquid-liquid systems, PNIPAM microgels are not suitable for water in oil systems with apolar solvents such as toluene. Qualitative stable water in oil emulsions using fatty alcohols such as octanol are reported in literature, but octanol also causes the loss of the thermo-responsiveness of the microgels [14].

Moreover, experiments are conducted with a low concentration of microgel MG2 with microgel solutions of different ages. In the first run of the experiment a recycled system is used, which was previously utilized in experiments with phase ratio (o/w) 1/2. In case of the reused microgel solution, in all repetitions, the organic phase is the dispersed phase and the system is stabilized by the microgels. Whereas, in case of a freshly prepared microgel solution water is dispersed and the settling time is significantly less. This "memory" effect of the system could hint that the microgels are borrowed or do not fully recover their spherical shape in bulk. Potential structural changes and subsequent altered properties are interesting aspects considering perspective long term utilization of the microgels. Although the

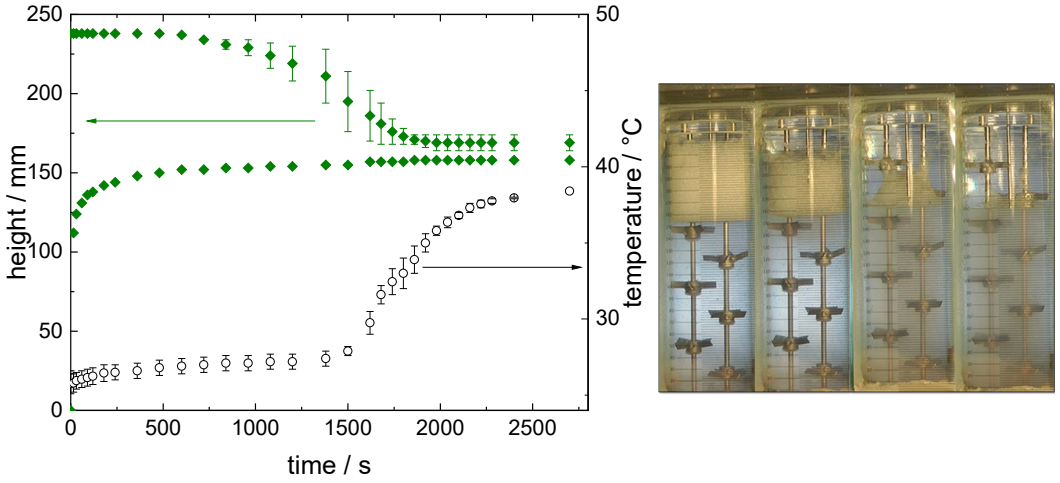

Figure 5.10.: Settling experiment with temperature ramp. At the start the temperature is set to 25 °C after 20 min the setpoint is increased to set to 40 °C. The photographs show the progress of phase separation during the heating

experiment has been performed in replica, more experiments with different initial dispersion directions and microgels with different size and softness need to be performed to draw reliable conclusions on this hypothesis.

5

Switchable Stabilization by Temperature Shift

Batch settling experiments are a versatile tool to screen effects of various parameters on the settling behavior and the stabilization by the microgels, respectively. For the sake of screening efficiency the temperature in these experiments is constant, and states below and above the VPTT are tested. For the process concept the temperature shift is crucial. Therefore, discontinuous experiments with temperature ramp are performed and based on the findings from batch settling experiments a continuous settler is designed and tested.

Figure 5.10 depicts the results from a settling experiment with temperature ramp. The first part of the experiment is unchanged only after 20 min (1200 s) the thermostat temperature is set to 40 °C. The graph in figure 5.10 shows the sedimentation and coalescence lines as well as the temperature measured in the dense packed zone, whereby the temperature measurement refers to the center of the cell due to thermometer position. When

the heating is started, the coalescence propagates quickly with increasing temperature and the coherent oil phase becomes larger. The coalescence process is nonuniform in radial and axial direction (see photos in figure 5.10). The coalescence propagates from outer radius to the center and from top downwards with different speed. A plausible cause is the slow non convective heat transport from the wall. Since the microgels kinetics are rapid [142, 148, 141], the time-determining factor for the phase separation efficiency is heat transfer.

The other finding from this experiment is the observation of increasing turbidity in the aqueous phase with propagating coalescence, which can be seen from left to right in the photos in figure 5.10. The turbidity is caused by the microgels. After the initial mixing the aqueous bulk phase appears clear as the microgels are located at the interfaces in the dense packed zone. As the phases separate, the microgels are back in the aqueous bulk phase.

This macroscopic observation is in contrast to the reported findings from microscopic observations at planar interfaces. The studies report collapse of interfacial microgels only perpendicular to the interface and no desorption of microgels is observed when increasing the temperature above the VPTT [36, 38]. However, it should be noted that the microscopic experiments are performed at flat interfaces and even in compression experiments the area is decreases by factor 10 (from 402 cm^2 to 44 cm^2 [36]). Whereas, in the utilized batch settling cell the interfacial area of the dispersed to the separated system is reduced by factor 500 (from 25000 cm^2 to 50 cm^2, for o/w ratio 1/2 and d_{drop} = 1 mm determined from sedimentation velocity). Therefore, the large difference in interfacial area reduction leads to non-comparable energetic boundary conditions between the experiments. The larger area reduction increases the energy gain by coalescence and thus the potential energy available for desorption. Therefore, microscopic findings of desorption can not be transferred directly to macroscale. The consolidation of micro- and macroscopic findings is in the focus of ongoing research. With regard to the application the migration of the microgels back to the bulk allows the recycling and reuse of the microgels by filtration from aqueous phase.

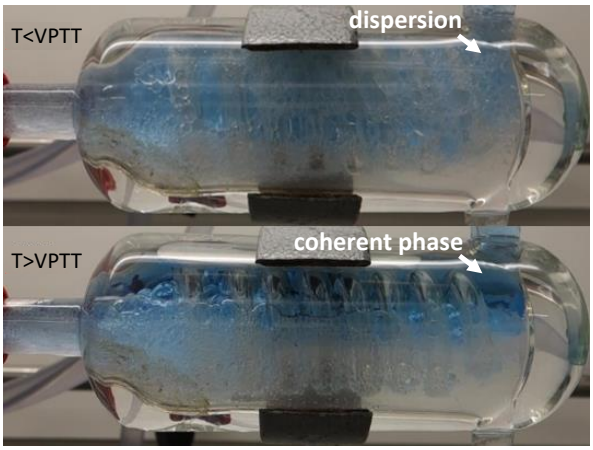

Figure 5.11.: Operation of the settler device at $40.5\,\mathrm{L\,h^{-1}}$ at $25\,°\mathrm{C}$ (top) and $40\,°\mathrm{C}$ (bottom)

Ultimately, the findings from batch settling experiments provide the basis for the design of a continuously operating settler which is tested in the experimental setup as described in section 5.3.2. As the heat transfer is identified as crucial for the apparatus efficiency the heat transfer area is enlarged by a coil. The coil also acts as baffle, increasing the mixing and thus enhancing convective heat transport. Different volume flows are tested, reflecting the volume flows of a typical technical lab scale (DN50) extraction column. It should be noted that the results for different volume flows are not exactly comparable to each other, since the energy input and thus the Sauter mean diameter obtained from the static mixer depend on the flow rate. However, for a total volume flow of $40.5\,\mathrm{L\,h^{-1}}$ the approximated Sauter mean diameter at the settler inlet of $1\,\mathrm{mm}$ is in the same range as in the batch settling experiments.

Figure 5.11 shows the settler device operating at $40.5\,\mathrm{L\,h^{-1}}$ below and above the VPTT. Below the VPTT the settler is filled with dispersion, no coalescence is observed. The phase separation is not completed within the settler length and biphasic flow is observed in the organic phase on top of the device (figure 5.11 top).

On the other hand, in the experiment with temperature above the VPTT (Set point of the thermostat $70\,°\mathrm{C}$ and measured outlet temperature $39.5\,°\mathrm{C}$ for $40.5\,\mathrm{L\,h^{-1}}$) the dispersion is fully separated. A dispersion wedge forms

along the apparatus length leading to a clear interface and no entrainment of water can be seen in the organic outlet.

Different operating points have been tested, the picture in figure 5.11 shows the operation at $40.5\,\mathrm{L\,h^{-1}}$. The outlet temperature of $39\,°\mathrm{C}$ is well above the VPTT and indicates that the capacity of the device is not fully exploited at this volume flow.

With these experiments the feasibility of continuous phase separation of the microgel stabilized liquid-liquid system by temperature shift as part of the implementation of microgels in extraction processes is successfully demonstrated.

5.4.2. Single Drop Coalescence

Besides the settling behavior as integral phenomenon, including coalescence in dense droplet packing as part of phase separation, the coalescence of single drops is regarded, reflecting the coalescence during free sedimentation of drops. Therefore, experiments with colliding single drops are performed according to the procedure described in section 5.3.3.

In order to maximize the comparability of the pure system and the microgel covered drops the drop velocity is kept constant in the experiments by variation of the distance between the drops. Therefore, the drop diameter in the experiments is fixed to $2.3\,\mathrm{mm}$. For smaller drops the impact of the canula increases and for larger drops the difference between the microgel covered drops and the pure system is too large (see section 3.4.1), exceeding the alignment length of $25\,\mathrm{mm}$ of the positioning system.

Effect of Microgel Type and Concentration

In the experiments the effects of the different crosslinked microgels MG1 and MG3 are tested at different concentrations. The obtained coalescence probability is shown in figure 5.12. It should be noted, that due to the stochastic nature of the experiment, the shown error bars refer to the width of the confidence interval with $95\,\%$ certainty. It depends on the probability

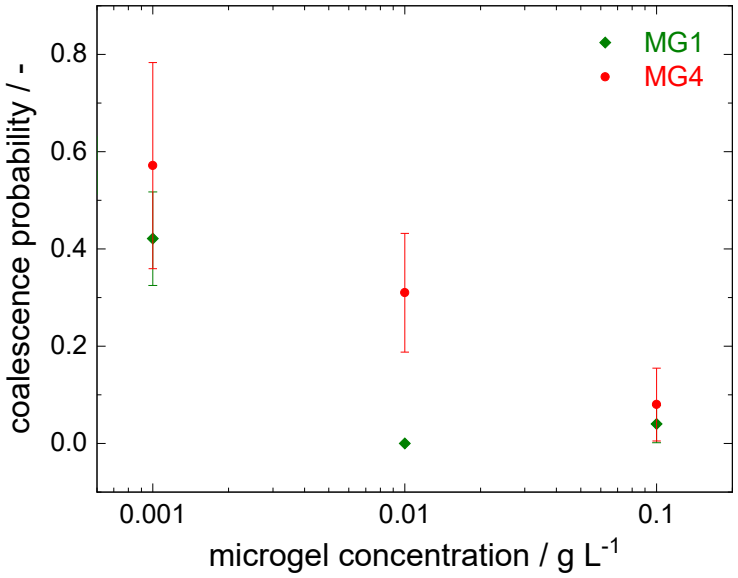

Figure 5.12.: Coalescence probability for different concentration of weakly crosslinked microgel MG1 and strongly crosslinked microgel MG3 for 2.3 mm drops at 22 °C

and the number of samples. The sample number in this experiment varies between 25 and 129 drop collisions per data point.

The coalescence probability of the n-butyl-acetate system for 2.3 mm drops is determined to 62 % for this experimental setup. The comparison of absolute probability to literature from other authors is difficult as utilized methods and solvent systems are different [149]. Nevertheless, the determined coalescence probabilities are mutually comparable and the impact of microgels and the concentration can be seen from figure 5.12.

Two observations on the impact of microgels can be made. First, the coalescence probability decreases with increasing microgel concentrations. For a low microgel concentration of 0.001 g L^{-1} the coalescence probability is only slightly reduced and the confidence interval is large. Whereas, for high concentration of 0.1 g L^{-1} the coalescence probability is below 10 % for both microgels. The width of the confidence interval decreases with increasing microgel concentration, due to the fact that the confidence interval narrows with decreasing probability for constant amount of samples.

Second, the drops covered with the weakly crosslinked microgel MG1 show lower coalescence probabilities than the drops covered with highly

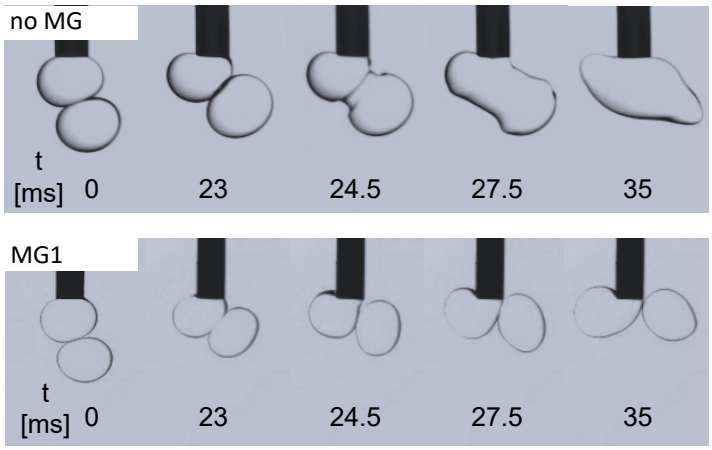

Figure 5.13.: Time resolved collision of drops without microgels (top) and covered with microgel MG1

crosslinked microgel MG3, although the confidence intervals partially overlap a trend is observable.

From these observations first conclusions on the stabilization of colliding microgel covered drops can be sketched. One possible cause is the immobilization of the interface. Comparing the effect on the coalescence probability to the extend of sedimentation velocity reduction in figure 3.11 as an indication for the interfacial mobility, it can be seen that for microgel MG1 the sedimentation velocity is slightly reduced at $0.001\,\mathrm{g\,L^{-1}}$, while drops covered with microgel MG3 at the same concentration rise with the velocity comparable to a mobile interface. The impact on the velocity increases with increasing concentration and for concentration of $0.1\,\mathrm{g\,L^{-1}}$ the velocity is similar to a rigid interface for both microgels. Therefore, the immobilization of the interface is a likely cause for the reduced coalescence probability. For an immobile interface the film drainage is decelerated due to the adhesion condition at the interface, leading to a laminar profile of the out-flowing continuous phase. Thus, the contact time is shorter than the time required for the drainage to reach the critical film thickness to cause film rapture and ultimately merging of the drops.

The time resolved collision process captured by the high speed camera is depicted in figure 5.13 exemplary for the pure system and drops covered

with microgel MG1 at $0.1\,\mathrm{g\,L^{-1}}$. In the pure system the film raptures between $23\,\mathrm{ms}$ to $24.5\,\mathrm{ms}$ after first contact. Whereas, in the system with microgel MG1 the drop rolls off within $35\,\mathrm{ms}$. Thus the contact time is not sufficient to allow for drainage of the film for coalescence or the film is too thick to drain within the contact time, respectively. The reported critical film thickness for standard solvent systems varies from 10 to multiple $100\,\mathrm{nm}$, while theoretical studies predict significantly thinner film thicknesses in the range of $1\,\mathrm{nm}$ [122]. For microgel covered interfaces, the study from Keal et al. [140] investigates film drainage dynamics in foams using a thin-film pressure balance, they report steady film thicknesses between $450\,\mathrm{nm}$ to $5000\,\mathrm{nm}$ for microgels with a crosslinker content between $1.5\,\mathrm{mol\,\%}$ to $5\,\mathrm{mol\,\%}$ and concentrations between $0.1\,\mathrm{w\,\%}$ to $1\,\mathrm{w\,\%}$. The films in their study were stable for several minutes up to hours. Although, their findings are not directly transferable to the utilized setup, they emphasize the different setup in time scale for drainage in highly concentrated microgel systems.

Moreover, the images in figure 5.13 show that the microgel covered drops also deform. Between the pure system and the microgel covered drops no difference in deformation can be observed qualitatively from the obtained images. In section 3.4.2 the resistance of microgel covered drops towards deformation during free sedimentation is shown, but the forces during the collision are significantly larger and cause the microgel covered drops to deform. Therefore, the hypothesis of interfacial mobility as possible cause for coalescence prevention is most plausible. However, these qualitative observations provide a first indication but viscoelastic effects should also be considered in future investigations.

Effect of Temperature

Furthermore, the temperature responsive switchability of the stabilization is tested in the single drop setup. Therefore, the temperature of the cell is raised to $40\,^{\circ}\mathrm{C}$ though the double wall, while the drop generation underneath the cell remains at room temperature as it is not included in the thermostat

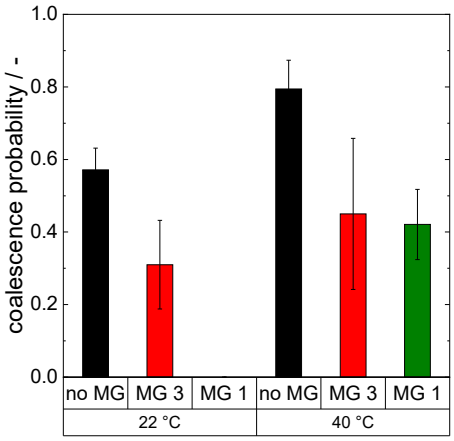

Figure 5.14.: Coalescence probability of single drops below (25 ℃) and above the VPPT(40 ℃), for single drops without microgels and covered with weakly crosslinked MG1 and highly crosslinked MG3, microgel covered drops generated at $0.01\,\mathrm{g\,L^{-1}}$

cycle and fresh microgel solution is used for every drop. The results for the two microgels at $0.01\,\mathrm{g\,L^{-1}}$ and the reference system are displayed in figure 5.14.

With the increase in temperature to 40 ℃ the coalescence probability in the pure system increases, this can be caused by the change in physical properties e.g. reduced viscosity. For the strongly crosslinked microgel MG3 the effect is in the same order of setup as for the pure system. However, for the weakly crosslinked microgel MG1 the effect is severe from no observed coalescence at 25 ℃ to about 40 % coalescence probability at 40 ℃. For the elevated temperature the coalescence probability of both microgels is comparable. The collapse of interfacial microgels is in focus of ongoing research. These results are needed to draw solid conclusions on the impact of structural changes of the microgels on coalescence. Sedimentation experiments at elevated temperature could lead first insights on the interfacial conditions and mobility and thus reveal valuable information concerning the effect of microgels interfacial mobility on coalescence probability.

5.5. Conclusion

The switchable stabilization of disperse liquid liquid systems by microgels is a key enabler for their intensification potential in extraction processes. With regard to this application two scenarios are regarded. The coalescence in dense packed droplets layers as it occurs at the top of the column where phase separation is required and the coalescence of rising single drops as in the active part of the extraction column.

Considering phase separation, the results from standardized batch settling experiments at high microgel concentrations below and above the VPTT demonstrate the feasibility of switchable phase separation in technical lab scale. The microgel concentration required for sufficient stabilization increases with increasing crosslinker content of the microgels, which is related to the ability to spread and thus the coverage of the interface.

The increasing turbidity in the temperature ramp experiment indicates that the microgels migrate back to the aqueous bulk phase with progressing phase separation. For the apparatus design the heat transfer is identified as crucial factor and the continuous operation of a settler with integrated heating is successfully demonstrated in technical lab scale.

Regarding the coalescence of single drops a newly setup measuring cell is utilized. The coalescence probability decreases with increasing microgel concentration. The observation that the coalescence probability decreases with decreasing crosslinker content and thus increasing spreading supports the hypothesis that the immobilization of the interface by the microgels prolongs the film drainage time and thus prevent coalescence. However, further investigation is required to test this hypothesis. Besides the mobility, other rheological effects of the microgels on the interface such as the viscoelasticity, which was demonstrated in chapter 3, should be considered.

Finally, the switchability of the microgels allows for temperature controlled stabilization and phase separation in technical scale. The results presented

in this chapter show that the stabilization can be tuned by microgel type and amount. Since these parameters also affect mass transfer a propitious combination between stabilization and mass transfer has to be determined.

6. Process Evaluation

Parts of this chapter have been published as:
Microgels for the Intensification of Liquid-Liquid Extraction Processes - Feasibility and Advantages, Chemical Engineering and Technology, 2020
Miriam Faulde, Josia Tonn, Andreas Jupke
DOI: 10.1002/ceat.201900407

6.1. Introduction

The experimental results from the previous chapters demonstrate the feasibility of the proposed process concept, this chapters aims to evaluate and quantify the arising potential. Thus the propagation of findings on single drop scale to apparatus scale is evaluated by a simulation study.

For the evaluation ReDrop [19, 150, 151, 152] is used as a simulation tool for extraction columns that accounts for the single effects studied in the previous chapters.

To quantify the intensification, potential experimental data from column experiments provided by Garthe [146] is used as a reference scenario. For the microgel covered drops the parameters are adjusted based on the results from previous chapters. The evaluation considers the fluid dynamic feasible operating range as well as the separation performance. Besides the comparison to the polydisperse reference, different cases are considered for monodisperse microgel covered drops. Since the microgels impact on interfacial mobility is determined as an essential factor in the previous chapters it is also focused in the evaluation.

6.2. Simulation Set-up

For the evaluation of the process performance, ReDrop is used, which is a population balance simulation tool based on representative drops. The tool calculates drop velocity, coalescence, breakage, and mass transfer for each drop class [19].

As a reference scenario, data from experiments in a DN80 pulsed sieve tray extraction column without microgels is used [146]. The data contains four stationary operating points with different loads and one flooding point. The process model is fitted to the experimental data of the four operating points, whereby only the parameters for coalescence and axial dispersion are fitted. The model parameters for mass transfer and sedimentation solely depend on the solvent system and are taken from literature [19]. The parameter set, column geometry and physical properties are summarized in table 6.1. The fluid dynamic and concentration profile obtained from simulation are in good agreement with the experimental data (parity plots are shown in appendix A.8).

For the evaluation of the microgel-stabilized system, the simulation parameters are modified. To account for the stabilizing effect of the microgels, the probability of coalescence and breakage of the drops is set to zero, by setting $Ccoal$ to 20000. Since ReDrop considers breakage as statistical phenomenon with no adjustable parameters, the breakage terms are eliminated for the simulation of microgel covered drops. The potential impact on mass transfer is regarded by a parameter study by variation of the instability parameter C_{IP} accounting for turbulent mixing inside the drops (see chapter 4).

For the evaluation of the fluid dynamic operating window, the load and the phase ratio are varied, starting at a volume flow of $4\,\mathrm{L\,h^{-1}}$ for the continuous phase the volume flow is increased until flooding occurs. This is repeated for 12 phase ratios $\dot{V}_d : \dot{V}_c$ between $1:8$ and $8:1$. For the evaluation of fluid dynamics, the flow though the column is simulated for 900 s, for mass transfer 3600 s are simulated to ensure steady state conditions.

Table 6.1.: Parameters used in simulation and utilized values for reference case

Parameter	Value	Unit	Reference
Column Geometry			
h_{col}	2.95	m	[146]
d_{col}	0.08	m	[146]
ϕ	20	%	[146]
d_{hole}	2	mm	[146]
h_{tray}	0.1	m	[146]
Model Parameter			
C_{IP}	5527		[19]
c_{coal}	13		
D_{ax}	0.001	$m^2\,s^{-1}$	
d_{um}	7.1	mm	[19]
a_{15}	1.52		[19]
a_{16}	4.5		[19]
a_{20}	0.734		[19]
Energy Input			
a	16	mm	[146]
f	1.25	s^{-1}	[146]
Physico-chemical Properties			
ρ_c	988.8	$kg\,m^{-3}$	[19]
ρ_d	8767.5	$kg\,m^{-3}$	[19]
η_c	1.029	mPa s	[19]
η_d	0.596	mPa s	[19]
γ	34.31	mN m	[19]
D_c	1.153	$m\,s^{-2}$	[19]
D_d	2.788	$m\,s^{-2}$	[19]

Furthermore, the effects of the interfacial mobility are studied with higher spacial resolution for different monodisperse drops sizes. Since the use of monodisperse drop sizes eliminates the need for population balances, the calculations are carried out in Matlab®with a simplified model. The model utilizing the same set of equations for sedimentation, hold-up and mass transfer calculation but it only considers a single drop size and no energy input by pulsation and thus no changes in drop size due to the absence of coalescence and breakage.

With this reduced model the propagating differences between mobile and rigid interfaces can be regarded in more detail. The distinction to the rigid interface is made at three positions in the model:

- sedimentation velocity of rigid sphere (see section 3.4.1)
- hold-up calculation using $c_d = \frac{24}{Re} + \frac{4}{Re^{0.5}} + 0.4$ [66]
- mass transfer with $D_{eff} = D_d$ (see section 4.2.1)

To test the quality of the results obtained from the simplified model, the four monodisperse operating points are tested and compared to the results obtained by ReDrop. For the comparison the minimal feasible drop diameter is used. For small loads of $\dot{V}_c$ =40 L h^{-1} the deviation is $8.67\,\%$, but the deviation increases with increasing load. Moreover, the smallest load allows for comparison of a wider range of monodisperse drop sizes. Therefore, the study uses the smallest load.

6.3. Results

6.3.1. Fluid Dynamic Operation Window

The fluid dynamic operating window is evaluated by simulating operating points with different volume flows and phase ratios. Figure 6.1 shows the resulting operating window as area of feasible operating points for the polydisperse reference (a) and the monodisperse microgel stabilized system (b). The operating window is limited by the hold-up, with increasing load

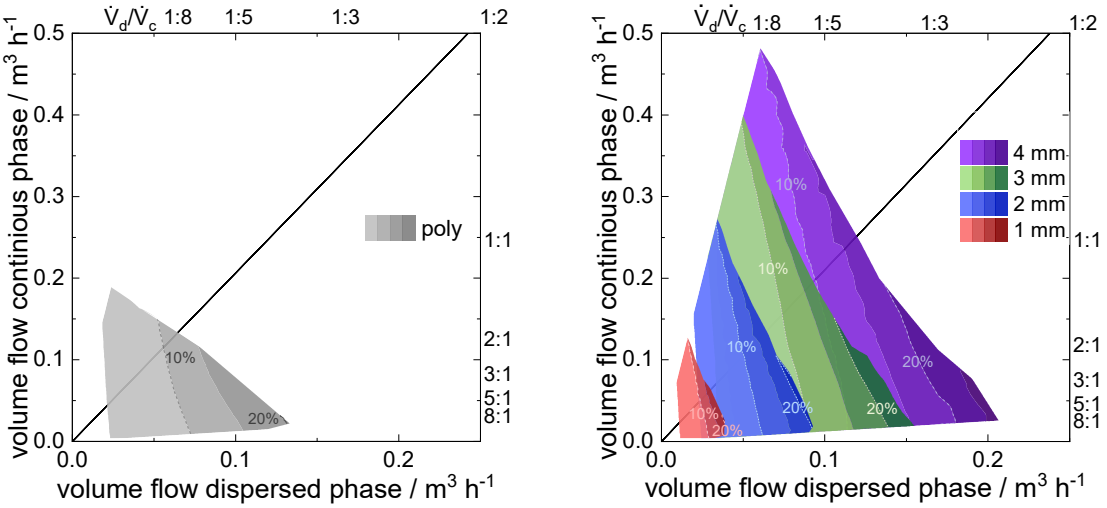

Figure 6.1.: Fluid dynamic operating window determined by simulation, for polydisperse reference (d_{32} ≈2.3 mm) and monodisperse drops with different diameter, color shading and dashed lines indicate hold-up with an increment of 5 %

the drop velocity in the counter current flow decreases, leading to local accumulation of drops and thus an increasing hold-up [19]. The flooding point, which is the upper limit of the operating window is typically defined by a local hold-up of 50 %, since for larger hold-ups phase invasion could occur. The lower limit was set to a hold-up of 3 %. Typically, a hold-up below 30 % is targeted for operation [153].

Comparing the operating windows for different monodisperse drops in figure 6.1, the flooding limit is shifted to higher loads with increasing drop diameter. Furthermore, the operating window of the different monodisperse cases is larger compared to the polydisperse reference case. Especially for phase ratios smaller than one, the advantages of the monodisperse drops are particularly strong. For example, in the polydisperse reference at a phase ratio of $1:8$ the maximum load is 44.76 $m^3\,m^{-2}\,h^{-1}$, while for 2 mm monodisperse drops the maximum load is 58.19 $m^3\,m^{-2}\,h^{-1}$, for 4 mm the maximum load at this phase ratio is approximately doubled to 107.43 $m^3\,m^{-2}\,h^{-1}$. This operating range at small phase ratios is dominated by the velocity of the continuous phase. Thus, monodisperse drops are especially advantageous due to the absence of entrainment of small drops as it occurs in

polydisperse scenarios. Due to the low hold-up the continuous flow is not significantly affected by the disperse phase and the flooding condition by $50\,\%$ local hold-up is very sharp when the velocity of the drops equals the continuous flow and the counter current flow ceases.

At the other end of the operating window, at high phase ratios, the hold-up and thus the interaction between the phases increases with increasing volume flow. The color shading in figure 6.1 indicates the hold-up. The shading refers to increments of $5\,\%$. The steep slope of the gradient lines in figure 6.1(a) and (b) indicates that the hold-up is predominantly determined by the disperse phase (it should be noted, that scales for disperse and continuous phase flow are different in figure 6.1). A large hold-up is often desirable as it is associated better contact between the phases and makes the apparatus more efficient [154, 18]. The maximum hold-up is reached for large phase ratios and high loads. In the polydisperse reference case the hold-up in the operating range is below $20\,\%$. For the monodisperse drops the maximum hold-up increases with increasing drop size. Therefore, the fluid dynamic operation conditions could compensate the smaller volume specific mass transfer area with increasing drop size. The mass transfer is regarded in more detail in the following section.

Nevertheless, the fluid dynamic feasible operating range highly depends on the drop diameter and can be enlarged by microgel covered monodisperse drops significantly.

6.3.2. Process Performance

Besides the fluid dynamic operating range of the apparatus, the separation performance depending on the monodisperse drop diameter is evaluated. First, the overall separation performance of the microgel intensified monodisperse scenario is compared to the polydisperse reference. As the previous chapters demonstrated the interfacial mobility plays a major role for the successful implementation of microgels. Therefore, the effects of the interfacial mobility on the separation performance will be regarded in more detail.

Evaluation of Overall Process Performance

As a first indication the overall separation performance of different monodisperse drops is regarded. The interfacial mobility reduction is accounted for by variation of the instability parameter C_{IP}, it affects the effective diffusion coefficient D_{eff} in equation 4.17, which is used in the simulation. To account for a reduced mixing due to the repulsion of interfacial mobility by the microgels, the parameter C_{IP} is varied in multiples of the references value, up to the ten fold value, which is the range of impact. Since the utilized solvent system in the single drop experiments and the simulations based on the column experiments from Garthe [146] differ, the experimentally derived C_{IP} values can not be directly applied. The C_{IP} value for the reference system is 5527 [19].

The results are shown in figure 6.2 as multiples of the initial parameter value of the polydisperse reference system. The results are displayed as obtained HETS (height equivalent of theoretical stage) for different loads. The lower the HETS, the more theoretical equilibrium stages can be realized in the given column geometry, which means separation performance and efficiency are increased.

For the polydisperse reference and all monodisperse scenarios, the HETS decreases with increasing load. With increasing load the hold-up increases, thus the contact between the phases is improved, which is reflected in the separation performance. Moreover, the impact of the variation of C_{IP} value increases with increasing drop diameter in the monodisperse scenarios. This is in good agreement with the findings from single drop experiments in section 4.4.3. With decreasing drop sizes the large, volume specific interfacial area diminishes the effect of internal turbulence. Therefore, the effect of the instability parameter on the HETS is less pronounces for small drops.

Comparing the separation performance of the monodisperse scenarios and the polydisperse reference with regard to application two cases can be identified. First, the separation efficiency at constant load is regarded. Comparing the polydisperse and $1.5\,\mathrm{mm}$ drop scenarios, an increase in separation efficiency and hence a reduction of HETS of about $20\,\%$ can be

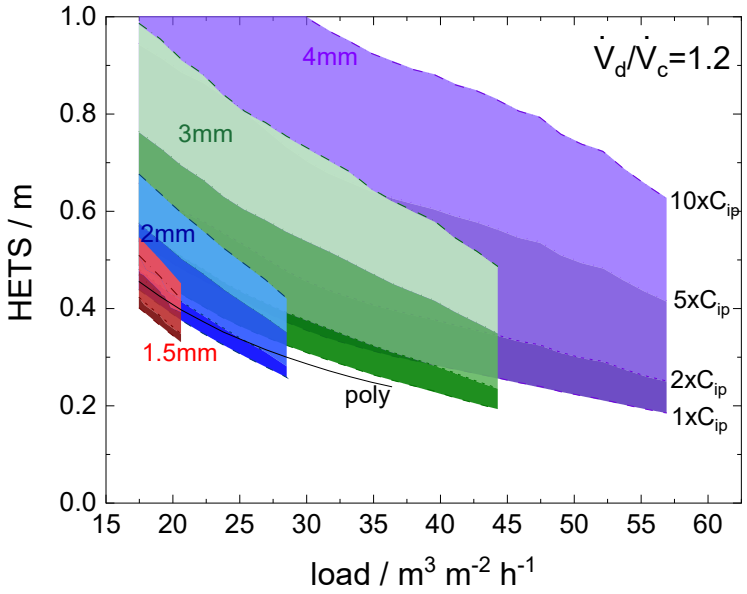

Figure 6.2.: Separation performance for different capacities, for the polydisperse reference case with a Sauter mean diameter of $2.3\,\mathrm{mm}$ and different monodisperse drop size scenarios accounting for reduction of interfacial mobility by increased C_{IP}

achieved. For lower loads, the provided interfacial area is the dominant effect for mass transfer. In this case, the smaller monodisperse drops are favorable since for larger drops the resulting hold-up is insufficient to provide the separation performance.

Second, the capacity is regarded as maximum load at constant HETS. Thus, the HETS referring to the maximum load of the polydisperse reference is compared to the monodisperse scenarios. For bigger drops the capacity of the apparatus can be increased by up to $55\,\%$ for $4\,\mathrm{mm}$ drops at equal separation performance, presupposing that the effect of the microgels on mass transfer is minor ($2 \cdot C_{IP}$). Thus, the advantages of the broader fluid dynamic operation window discussed above can be utilized to exploit the apparatus capacity.

Evaluation of Space Time Yield

For a more detailed investigation of the propagation of the observed effects from single drop to apparatus scale, mass transfer along the column is

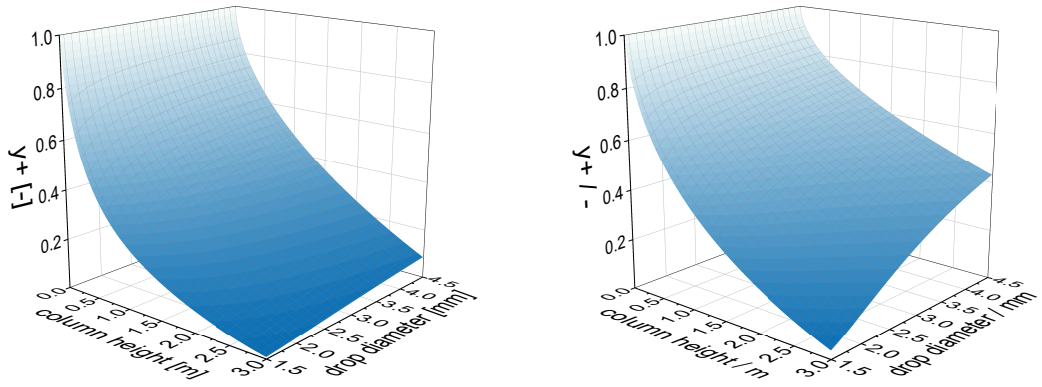

(a) mobile interface (b) rigid interface

Figure 6.3.: Dimensionless concentration difference (see equation 4.9) along the active part of the column for different monodisperse drop sizes with rigid and mobile interface

regarded by the simplified model. The two limiting cases of an mobile and an rigid interface are regarded. The interfacial mobility is considered in the model by means of mass transfer, sedimentation velocity and also hold-up (see section 6.2). For both cases of interfacial mobility the obtained concentrations along the column height are in figure 6.3 as dimensionless concentration (equation 4.9) for different monodisperse drop diameters. The results are shown for the operating point of $\dot{V}_c$ =40 L h^{-1}, to allow the comparison for a wider range of drop diameters.

In case of a mobile interface, at the lower part of the column the concentration difference is rapidly reduced. Especially in the first meter of the column and with small drops of 1.5 mm the gradient is high. For larger drop diameter the gradient is less pronounced in the lower part and more constant along the complete height. The dimensionless concentration difference is very low (0.006 for 1.5 mm drops). However, at the top of the column in the disperse phase outlet is only marginally affected by the drop diameter by a total difference of 0.078. Thus, the overall impact of the drop diameter for the separation efficiency is minor in case of a mobile interface.

On the other hand in case of a rigid interface the effect of the drop diameter is more pronounced. The slope of the gradient along the column height as well as the concentration at the disperse outlet at the column top strongly

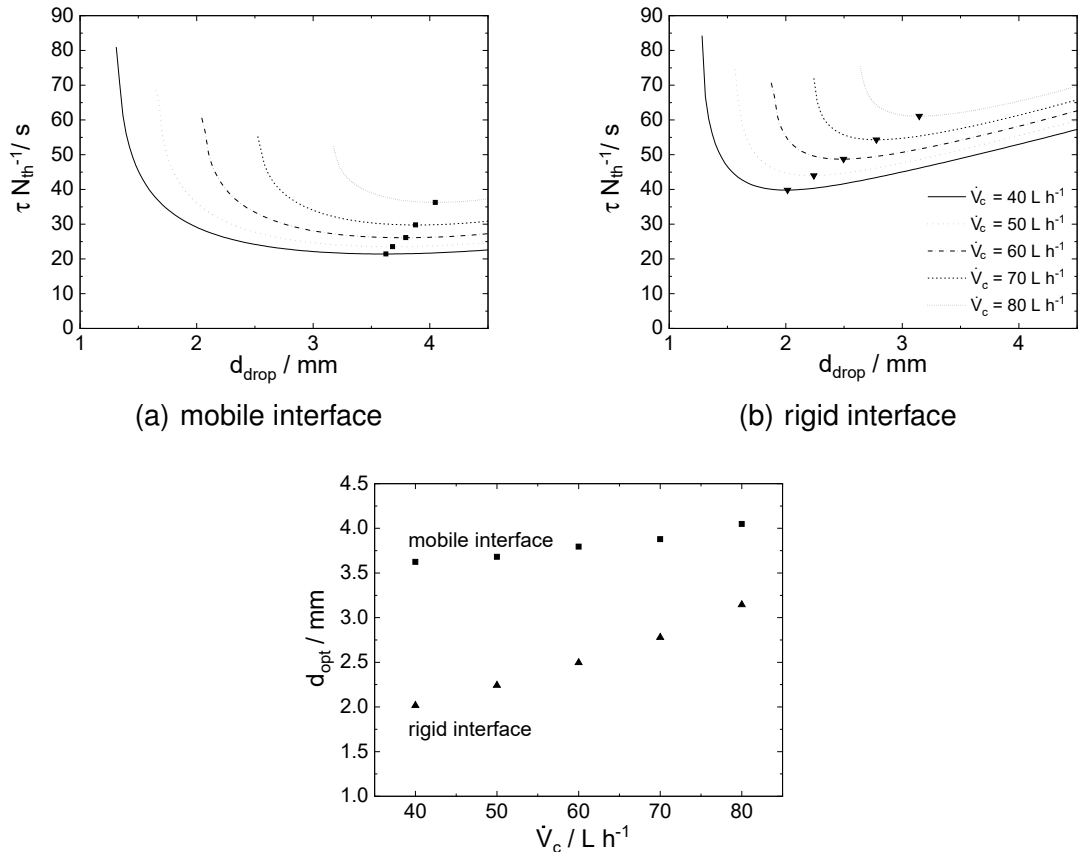

(a) mobile interface

(b) rigid interface

(c) summery both cases

Figure 6.4.: Separation efficiency of the column for different monodsierpse drop sizes at different loads, for mondisperse drops with mobil and rigid interface respectivele. As well as the summarized most efficient drop diameters depending on the load.

depend on the drop diameter. For small drops the outlet concentration is close to equilibrium with 0.032, whereas for larger drops the difference is significantly larger at 0.430.

Moreover, the contact time varies in the scenarios due to different sedimentation velocities and hold-up, respectively. Therefore, the residence time of the drops in the column should be also considered for the efficiency evaluation regarding space time yield.

To compare the space time yield of the two cases for different drop diameters and loads the residence time of a drop is related to the number of theoretical stages in figure 6.4. Thus the required contact time for equal sep-

aration performance can be compared for the different interfacial conditions and drop diameters. The smallest drop diameter for each load is determined by flooding criterion. As already discussed in figure 6.1 the flooding limit is shifted with increasing drop diameter and vice versa. For small loads the difference between the mobile and the rigid interface is minor, but with increasing load the difference in minimal feasible drop diameter increases. The steep slope indicates the increasing hold-up and thus the rapid increase in residence time close to the flooding point. In both cases a minimum can be found before the increase, which is more pronounced in case of rigid interface. For both interfacial conditions the most efficient drop diameter increases with increasing load. The increase is more significant for rigid interface. The range of the most efficient diameters is in good agreement with other proposals from literature ranging from 2 mm to 3 mm [19, 155].

These theoretical findings suggests that the results from the single drop experiments propagate to apparatus scale and the knowledge on fluid dynamic conditions is essential for application.

6.4. Conclusion

In this chapter the intensification potential of introducing microgels to extraction columns is shown by a theoretical case study. ReDrop is utilized as a simulation tool and a reduced version for the special comparison of the interfacial conditions and their impact on apparatus scale. The investigation covers the fluid dynamic feasible operating range as well as separation performance.

With regard to the feasible operating range, the stabilized monodisperse drops allow for a broader operating range. Especially, at lower phase ratios where the continuous phase velocity dominates the monodisperse drops entrainment. On the other hand, for small phase ratios, especially large monodisperse drops show the potential to enable larger hold-ups at higher capacities.

This is also reflected by the observed potentials on separation performance. Two cases can be distinguished, for small loads the HETS can be

significantly reduced by small monodisperse drops, providing a large transfer area. On the other hand, at high loads the capacity can be increased for constant separation performance utilizing larger monodisperse drops.

The more detailed investigation on the interfacial mobility, demonstrates the propagating importance to apparatus level. The separation performance is decisively dependent on the interfacial mobility. The results from chapters 5 and 4 show that the stabilization is increased by the reduction of the mobility while the mass transfer is reduced. Thus the balance of these effects becomes a Pareto problem with no distinct optimum. The extent of mobility depends on the individual application, the properties of the solvent system and the boundary conditions of the separation task. The understanding of structure property relations and their effects on interfacial mobility gives rise to future application of tailored microgels.

7. Summery, Conclusion and Outlook

Processes in liquid-liquid extraction columns are affected by many parameters and variables with complex interactions. However, holistic intensification of this unit operation quickly focus on drop size and drop size distribution. For optimal separation performance the drop size should be as small as possible and as large as necessary, withstanding the counter current flow. Thus a narrow drop size distribution is targeted to enable operation close to the flooding point. Drop size is commonly controlled by design and energy input, trying to balance coalescence and breakage of the drops, a new atypical approach is the introduction of microgels. These smart polymers cover the interface and stabilize the drops in the active part of the column. They prevent coalescence and thus preserve a monodisperse drop size distribution. At the top of the column, a temperature shift switches the microgels properties to allow coalescence and enable phase separation.

The aim of this work was to investigate the applicability of microgels to extraction columns, by elucidating the influence of the microgels on the underlying phenomena. Therefore, the impact of the interfacial microgel layer on sedimentation, mass transfer, and coalescence, is considered individually by single drop experiments.

In all experimental series at single drops their impact on interfacial mobility was present. The individual results from single drop experiments can be summarized as follows:

- The sedimentation velocity of microgel covered drops is slower and at high microgel concentration their velocity equals a volume equivalent rigid sphere. The reduced interfacial mobility hinders momentum transfer across the interface and thus prevent the formation of internal circulation. The effect correlates with the ability of the microgels to spread at the interface. It is more pronounced for weakly crosslinked large microgels, which spread more at the interface. Furthermore, the microgel covered drops are more resistant to deformation, although, the microgels reduce the interfacial tension. This strongly indicates that rheological properties of the interfacial microgel layer such as viscoelasticity are affected and should be considered in future investigations.

- The mass transfer at microgel covered drops is hindered. Since no significant inhibition was observed at flat interfaces the reduction is accounted to the reduced interfacial mobility, which reduces laminar circulation and random turbulent like flow inside the drop. This reduces drop internal mixing and thus slower decay of the radial concentration gradient which reduces the driving force for mass transfer due to higher concentration close to the interface.

- The coalescence probability of microgel covered drops is reduced. For low crosslinked microgels the probability is reduced to zero below the VPTT. The images from high speed camera suggest that the film drainage is decelerated, which can be attributed to a reduced interfacial mobility.

All theses effects increases with increasing microgel concentration and increasing softness of the microgels, which is related to the crosslinker content and size of the microgels. This finding empowers the hypothesis of the interfacial mobility reduction. The cyro-SEM images from this study and literature show that the spreading of the softer microgels is more pronounced and they interpenetrate more, thus their interfacial layer is more like a smooth film while the more crosslinked microgels form a bumpy layer

with more discrete particles.

Furthermore, the findings from this work allows for a first evaluation of potential advantages of the application of microgels on the process performance in liquid liquid extraction processes. The simulative case study indicates that the monodisperse drop size, which is enabled by the microgel stabilization, can broaden the fluid dynamic feasible operating window. Regarding the separation performance two cases can be distinguished. First, small monodsiperse drops can increase the separation efficiency at low loads. And second, large monodisperse drops can increase the capacity of the apparatus at equal separation performance. Both cases require that the extend of mass transfer hindrance by the interfacial microgel layer is not at the rigid interface level.

This also reveals the dilemma of the microgels effect on coalescence and mass transfer regarding the process. If the microgel concentration is increased or softer microgels are chosen, the stabilization is more effective but at the price of reduced mass transfer, since both effects originate from the reduction of interfacial mobility.

More sophisticated theoretical models could help to find suitable operating options. These models would need to predict mass transfer and coalescence probability as a function of microgel concentration and microgel structure. Since current model approaches only account for interfacial tension as interfacial properties more detailed investigation is required to find new approaches suitable for microgels. Therefore, the viscoelasticity should be considered as an experimentally accessible measure to characterize the interfacial microgel layer for different microgel types and concentration.

An other important factor is the exact determination of the interfacial microgel concentration and coverage, respectively. The device for the generation of microgel covered drop from this work is a practical and allows the generation of different interfacial loads, but it lacks the quantitative adjusting of the interfacial load. The interfacial coverage could be determined from dynamic interfacial tension measurements during free adsorption. The model

approach presented in this work can not reflect the experiment due to a lack of information on adsorption kinetics. This could be overcome by the combination of interfacial tension measurements and imaging methods which could reveal the at high loads whether rearrangement or further adsorption cause the dynamic trend of interfacial tension.

With regard to the successful realization of the proposed process concept, two factors are decisive: First, the switchable stabilization of the disperse system, and second, the interfacial microgel layer must be permeable for mass transport. Both criteria were tested experimentally.

Switchable stabilization was successfully upscale and transferred to continuous operation. Since with increasing apparatus dimensions the heat transfer becomes limiting, the implementation of the continuous operating prototype at $40\,\mathrm{L\,h^{-1}}$ was realized with a special settler design including temperature control by double wall and internal coil.

Permeability of interfacial microgel layer was successfully demonstrated for molecules ranging from $58\,\mathrm{g\,mol^{-1}}$ to $4000\,\mathrm{g\,mol^{-1}}$. Although the exact mass transport path through the microgel covered interface is unclear, the range of the tested molecules is within the average mesh size of the polymer network. The size range of the tested component allows for the transfer of the results to future application systems.

In summery, it can be stated that the application of microgels in liquid liquid extraction processes can lead to operational advantages. However, countervailing effects on mass transfer and coalescence make it difficult to fully exploit the advantages of the switchable stabilization. Thus, the arising potential for simple PNIPAM microgels is not sufficiently large to be widely established in extraction processes. Nevertheless, the findings from this work are a basis for further application of microgels in disperse systems. Since microgels can easily be functionalized, further functionalities could be incorporated to introduce e.g. additional selectivity. Microgels can carry loads which could be utilized to selectively separate ions, as it is already shown for membranes [13], the transfer to liquid liquid interfaces could be

utilized in metal recovery. Furthermore, microgels can be used to immobilize catalysts, this combination allows for in-situ product removal. This aspect will be focused in the project C5 in the third funding period of the SFB985.

A. Appendix

A.1. Microgel Synthesis

component	unit	MG1	MG2	MG3	MG4
NIPAM	g	5.4008			4.5443
BIS	g	0.18303	0.3677	1.4708	0.3329
water	mL	450			172
AMPA	g	0.1503			
APMH	g				0.1228
V50	g				0.0468
CTAB	g				0.0058
reaction conditions					
stirring speed	rpm	200			500
reaction time	h	2			3.5
Temperature	℃	70			67
purification			cellulose dialysis		ultracentrifugation

Table A.1.: Microgel synthesis parameters

A.2. Cryo-SEM Image Analysis

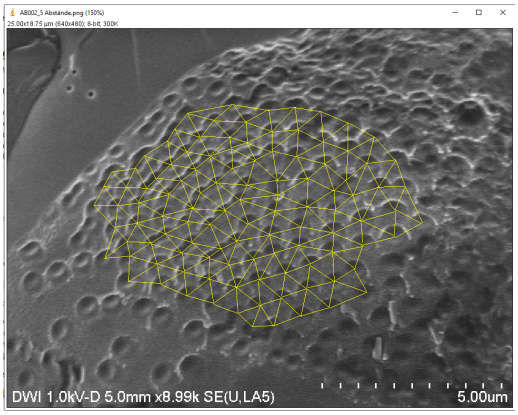

(a) MG1 2.5 mol %

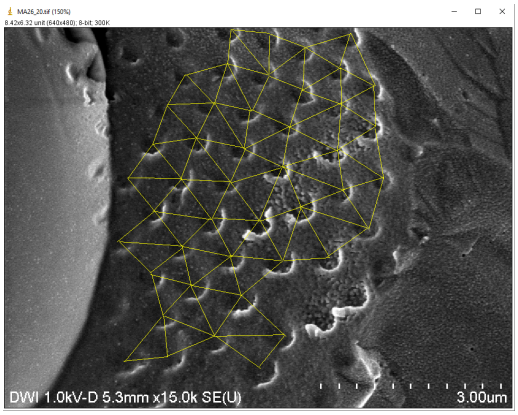

(b) MG2 5 mol %

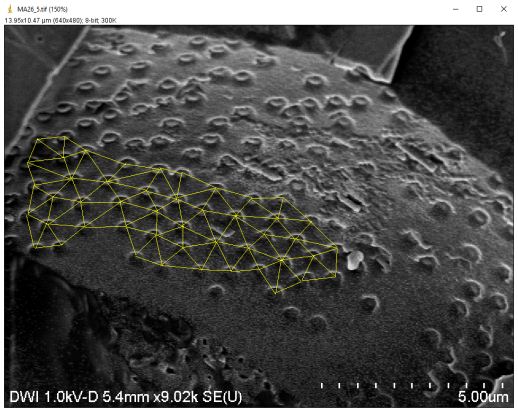

(c) MG2 5 mol %

Figure A.1.: Measurement of the center to center distance of mcirogels at the interface using the software ‘imageJ´

A.3. Compression Isotherms

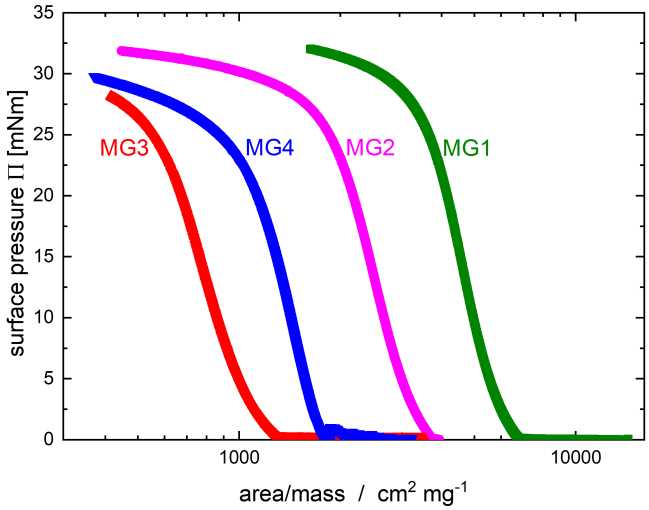

Figure A.2.: Surface pressure evolution over microgel amount at the interface (Data from Steffen Bochenek)

A.4. Interfacial Tension Measurement Methods

The liquid-liquid interface is a thin separation plane between two phases. At this boundary the intermolecular forces are out of equilibrium and interfacial tension appears to keep the equilibrium. The pressure inside the drop is increased due to interfacial tension. The forces are shown in figure A.3.[156]

The internal force (F_i) is compensated by the external (F_0) and the interfacial force (F_γ). A force balance for spherical drops results in:

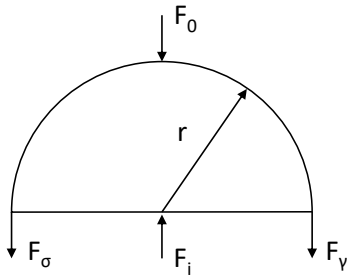

Figure A.3.: Representation of the forces that cause interfacial tension at a spherical drop [156]

$$F_0 + F_\gamma = F_i \tag{A.1}$$

$$\pi r^2 p_0 + 2\pi r\gamma = \pi r^2 p_i \tag{A.2}$$

$$p_i - p_0 = \frac{2\gamma}{r} \tag{A.3}$$

The interfacial tension gives information on the state of the interface. In this thesis, the interfacial tension of toluene drops in a microgel solution is measured in order to determine the time it takes for the microgels to completely cover the interface. As microgels are surface active, their presence at the interface will reduce the interfacial tension. In chapter further details about microgels and their influence on the interface will be explained.

Two principles to determine the interfacial tension are presented. On the one hand, the interfacial tension can be determined with the drop volume method, on the other hand the drop deformation can be examined.

In a drop volume tensiometer toluene drops are produced in a vertical capillary filled with water. The measurement principle of the drop volume tensiometer is shown in figure A.4.

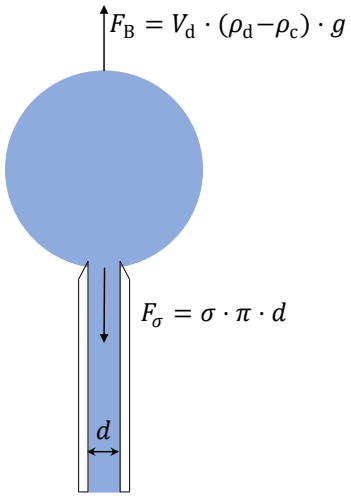

Figure A.4.: Measurement principle of the drop volume tensiometer

Applying a force balance at the drop, the following equation results:

$$\gamma = \frac{V_{\mathrm{d}} \cdot (\rho_{\mathrm{d}} - \rho_{\mathrm{c}}) \cdot g}{\pi \cdot d} \tag{A.4}$$

For the specification of the interfacial age, the volume at which the drops detach from the capillary is measured, as well as the time between two detaching drops. Hence, the interfacial tension is measured as a function of the interfacial age.

Disadvantages of this method are that the measurements take a long time because of the small dosing velocity for high interfacial ages. In addition to that, the dosing velocity is limited to a minimum velocity because of the used syringe. Therefore, the maximum interfacial age is limited as well. Due to adsorbing surface active particles the interfacial tension decreases and the drop diameter is not constant during the measurements.

Using the pendent drop method the measurements are faster, higher interfacial ages can be reached and the drop diameter is constant during the measurements. The profile of a drop of one liquid in another is determined. Due to a changing interfacial tension, the drop deforms over time. Hence, the radii r_1 and r_2 change. The interfacial tension is calculated from the Young-Laplace-equation:

$$\Delta p = \gamma \left(\frac{1}{r_1} + \frac{1}{r_2} \right) \tag{A.5}$$

The pressure difference can be rewritten as:

$$\Delta p(z) = \Delta p_0 + \Delta \rho g z \tag{A.6}$$

With $r_2 = \frac{x}{\sin(\Phi)}$ equation A.5 becomes:

$$\underbrace{\frac{\Delta p_0}{\gamma}}_{2/r} + \frac{\Delta \rho g z}{\gamma} = \frac{1}{r_1} + \frac{\sin(\Phi)}{x} \tag{A.7}$$

A parametrisation over the arc length, the following equation results:

$$\frac{\mathrm{d}\Phi}{\mathrm{d}s} = -\frac{\sin(\Phi)}{x} + \frac{2}{r} + \frac{\Delta\rho g z}{\sigma} \tag{A.8}$$

The boundary and initial conditions are

$$\frac{\mathrm{d}x}{\mathrm{d}s} = \cos(\Phi) \tag{A.9}$$

$$\frac{\mathrm{d}z}{\mathrm{d}s} = \sin(\Phi) \tag{A.10}$$

$$0 = x(s=0) = z(s=0) = \Phi(s=0) \tag{A.11}$$

A.5. Adsorption Model Zhang

Several authors already described the influence of surfactants on the interfacial tension of drops in a continuous polymer solution: The general idea of van Eijk and Cohen Stuart[157] is a three step adsorption process. The protein molecule is brought to the drop interface by diffusion and/or convection and adsorbs. Then it spreads and occupies a certain area according to the available space.Miller et al.[48] generalized the diffusion model of adsorption kinetics [48]. They assume that protein molecules in the surface layer can exist in states of different molar area. A diffusion controlled adsorption model is developed by [158]. The surfactants are initially inside the drop. They adsorb at the inner side of the drop and diffuse through the interface into the surrounding phase.

Zhang and Pelton[51] investigated the influence of PNIPAM microgels on the surface tension of aqueous microgel dispersions. Applying a variation of this model on the generated interfacial tension measurement values gives good results. Moreover this model is simple and easy to handle. Assumptions are the following:

- the microgels which adsorb at the air/water interface are rigid spheres
- the adsorption of microgels at the interface is irreversible

- the adsorption of microgels does not dilute the solution
- the microgels are not aware of the sphere's curvature
- the saturated surface consists of spheres in cubic close packing

A model based on the Langmuir kinetics model is developed by [51]:

$$\frac{\mathrm{d}\Theta}{\mathrm{d}t} = k_1 \cdot (n_0 - \Theta)\,(1 - \Theta) \tag{A.12}$$

where Θ describes the ratio of adsorbed to maximum number of adsorbed microgels and

$$k_1 = \alpha \cdot k_{\mathrm{sm}} \cdot c \tag{A.13}$$

with

$$m_{\mathrm{total}} = n_{\mathrm{total}} \cdot m_{\mathrm{gel}} \tag{A.14}$$

A.6. Schlieren Set up

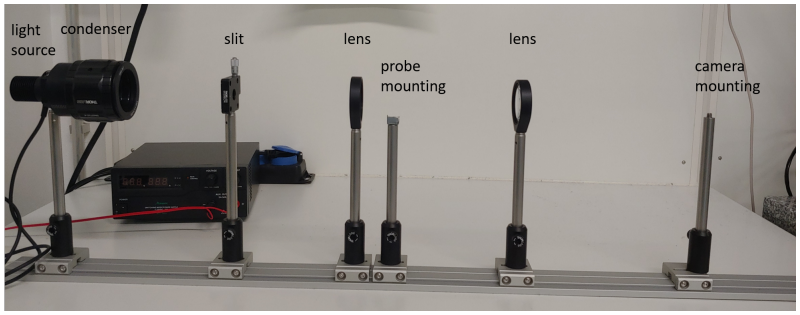

Figure A.5.: Set up for experiments for the Schlieren technique

Table A.2.: Specification of the components of the schlieren set up shown in schematic drawing in figure 4.5 and photograph in figure A.5. All components except the camera are purchased from ThorLabs, Germany

component	specification
light source	70 mW nominal wavelength 470 – 850 nm
condenser	collimation adapter with aspheric condenser lens (∅ = 50.8 mm , F= 32 mm)
lens	biconvex lens (∅ = 50.8 mm , F= 150 mm)
slit	max. width 6 mm
camera	Sony α600 with macro objectiv

Table A.3.: Physical properties of the mutually saturated phases at T = 22 °C

Phase	Density $\rho\,[\mathrm{kg \cdot m^{-3}}]$	Dynamic viscosity $\eta\,[\mathrm{mPa\,s}]$	Surface tension $\sigma\,[\mathrm{N \cdot m^{-1}}]$
Aqueous	996.2	0.988	14.1
Organic	879.7	0.723	

A.7. Estimation of Diffusion Coefficient

Since no values of the diffusion coefficient of acetonitrile are reported in literature, it is approximated by the correlation A.16 from Wilke and Chang, with the value of parameter $\alpha_b u = 1$ acquired from Miyabe and Isogai. Here $T = 295.15\,\mathrm{K}$ is the temperature, $M_{bu} = 116.158\,\mathrm{g\,mol^{-1}}$[161] is the molecular weight of pure n-butyl acetate, $\eta_{bu} = 0.730\,\mathrm{mPa\,s}$[24] is the dynamic viscosity for pure n-butyl acetate at 20 °C and $V_a = 57.584\,\mathrm{cm^3\,mol^{-1}}$ is the molecular volume for acetonitrile at the standard boiling point. V_a is calculated according to equation A.15, where $M_a = 41.052\,\mathrm{g\,mol^{-1}}$[162] is the molecular weight of acetonitrile and $\rho_a = 0.713\,\mathrm{g\,cm^{-3}}$[163] is the density of acetonitrile at the standard boiling point.
With all these parameters known, D_d calculates to $2.833\mathrm{e}-9\,\mathrm{m^2\,s^{-1}}$.

$$V_a = \frac{M_a}{\rho_a} \tag{A.15}$$

$$D_d = \frac{7.4 \cdot 10^{-8} T \sqrt{\alpha_{bu} M_{bu}}}{\eta_{bu} V_a^{0.6}} \tag{A.16}$$

A.8. Contact Time in Nitsch Cell

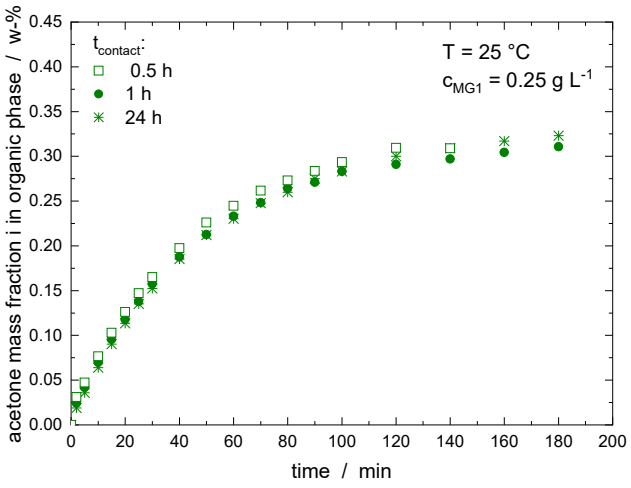

Figure A.6.: Accumulation of the transfer agent in the organic phase. MG1 supplied in the aquous phase, with different contact times of gentil stirring for the microgels to adsorb to the interface prior to the injection of the acetone.

A.9. Sensitivity of Mass Transfer Experiments at Flat Interface

To rationalize the result the sensitivity of the experiment is studied theoretically. Therefore, a hindrance of the mass transport by the microgels is considered in two ways. First, a reduction of the interfacial area by the microgels is considered as shown in (a). For a detectable difference in the concentration profile an area reduction of 20 % is required. In contrast, the porous structure of the microgels is assumed in literature with 10 V% polymer under bulk conditions [1]. At the interface, an increased polymer density is found in molecular simulations due energetically more favorable adsorption of the polymer chains to the interface [113]. However, an area reduction of 20 % would require a very compressed microgel layer. Furthermore, microgels are no static network and their dynamic can compensate steric effects [44, 113, 106].

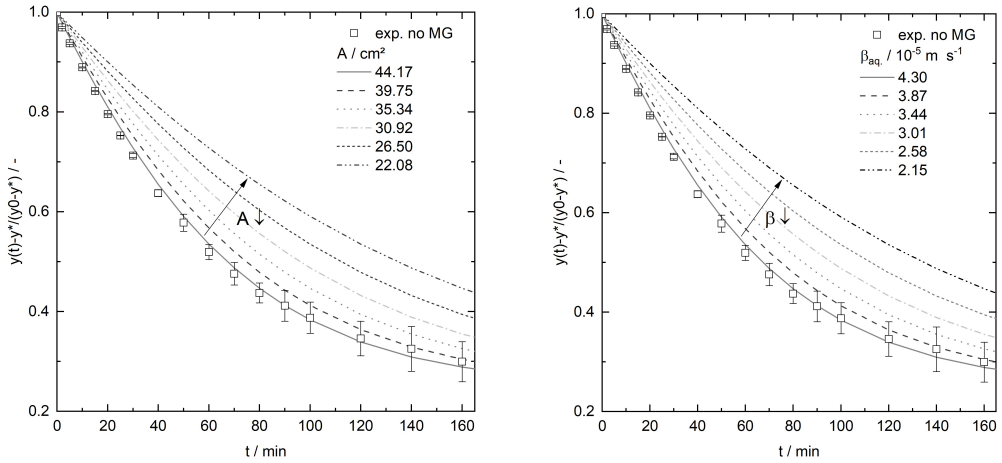

Figure A.7.: Sensitivity of mass transfer in the investigated system to provided interfacial area and mass transfer coefficient.

Secondly, the microgels are regarded as a viscous film at the interface. Consequently the mass transfer area is not affected but the mass transfer through the layer is, due to the viscosity or tortuosity of the gels, which is reflected by an decreased mass transfer coefficient as shown in A.7(b). The course for decreasing mass transfer coefficient shows that a decrease in the mass transfer coefficient of $20\,\%$ can be clearly detected in the experimental setup considering the standard deviation. A simple approach to exemplify the mass transfer coefficient in more vivid values is the film theory by Lewis and Withman [87]. This theory postulates thin films on both sides of the interface according to Prandtls boundary layer theory. Within this layer the flow is sufficiently slow to describe the transport in these films by stationary diffusion according to Fick‘s 1. law [87]. Therefore, the mass transfer coefficient can be determined by the ratio of the diffusion coefficient D and the film thickness δ as $\beta = D/\delta$.

For the pure system the film thickness derived from the experimental results is $2.65\,\mu\mathrm{m}$. A thickening of the layer by the bulk diameter of the microgels would result in a decrease of the mass transfer coefficient by $20\,\%$, which would be in the detectable range of the experiment. As the microgels deform at the interface their lateral dimension at the interface is smaller and the resulting difference would not be detectable.

The other parameter affecting the mass transfer coefficient according to this theory is the diffusion coefficient D.The diffusion coefficient is very sensitive to viscosity as described in the Stokes Einstein equation. Regarding the microgel as a homogeneous viscous film, an increase in viscosity by $1\,\mathrm{mPa\,s}$ would halfen the diffusion coefficients and subsequently also the mass transfer coefficient which would be clearly detectable in the experiment as shown in A.7(b)).
However, it should be emphasized that the film model is a very vivid but also very simple approach and falls short on the complex physical phenomena, which complexity increases by the addition of microgels.

A.10. Parity Plots for Process Evaluation Simulation

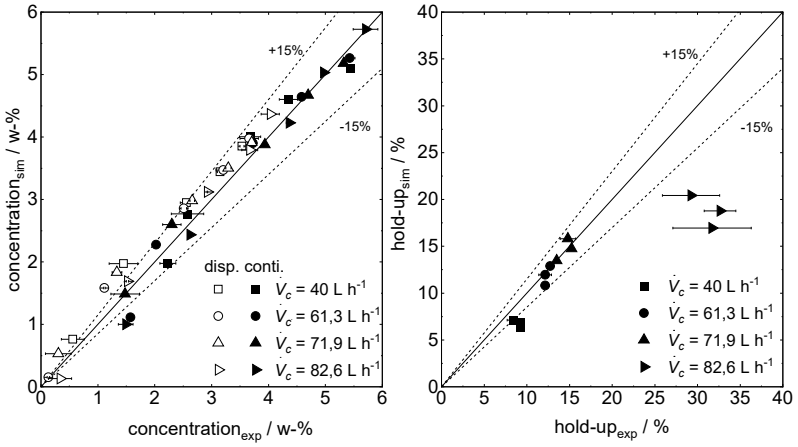

Figure A.8.: Parity plots for concentration and hold-up predicted by the simulation and experimental data from [146]

Bibliography

[1] Walter Richtering. “Responsive emulsions stabilized by stimuli-sensitive microgels: emulsions with special non-Pickering properties”. *Langmuir* 28.50 (2012).

[2] B. Saunders. “Microgel particles as model colloids: theory, properties and applications”. *Advances in Colloid and Interface Science* 80.1 (1999).

[3] R. H. Pelton and P. Chibante. “Preparation of aqueous latices with N-isopropylacrylamide”. *Colloids and Surfaces* 20.3 (1986).

[4] Felix A. Plamper and Walter Richtering. “Functional Microgels and Microgel Systems”. *Accounts of chemical research* 50.2 (2017).

[5] Gillian B. Kaggwa, Michelle J. Carey, Chris Such, and Brian R. Saunders. “A new family of water-swellable microgel particles”. *Journal of colloid and interface science* 257.2 (2003).

[6] Alexey A. Polotsky, Felix A. Plamper, and Oleg V. Borisov. “Collapse-to-Swelling Transitions in pH- and Thermoresponsive Microgels in Aqueous Dispersions: The Thermodynamic Theory”. *Macromolecules* 46.21 (2013).

[7] Bastian Brugger and Walter Richtering. “Emulsions stabilized by stimuli-sensitive poly(N-isopropylacrylamide)-co-methacrylic acid polymers: microgels versus low molecular weight polymers”. *Langmuir* 24.15 (2008).

[8] Brian R. Saunders, Nadiah Laajam, Emma Daly, Stephanie Teow, Xinhua Hu, and Robert Stepto. “Microgels: From responsive polymer colloids to biomaterials”. *Advances in Colloid and Interface Science* 147-148 (2009).

[9] Garima Agrawal and Rahul Agrawal. “Stimuli-Responsive Microgels and Microgel-Based Systems. Advances in the Exploitation of Microgel Colloidal Properties and Their Interfacial Activity”. *Polymers* 10.4 (2018).

[10] He Cheng and Guangzhao Zhang. “Thermally Sensitive Microgels: From Basic Science to Applications”. In*Hydrogel Micro and Nanoparticles*. Ed. by L. Andrew Lyon and Michael Joseph Serpe. Weinheim, Germany: Wiley-VCH Verlag GmbH & Co. KGaA, 2012. Pp. 1–32.

[11] Huan Peng, Xiaobin Huang, Andrea Melle, Marcel Karperien, and Andrij Pich. “Redox-responsive degradable prodrug nanogels for intracellular drug delivery by crosslinking of amine-functionalized poly(N-vinylpyrrolidone) copolymers”. *Journal of colloid and interface science* 540 (2019).

[12] M. Barth, M. Wiese, W. Ogieglo, D. Go, A.J.C. Kuehne, and M. Wessling. “Monolayer microgel composite membranes with tunable permeability”. *Journal of Membrane Science* 555 (2018).

[13] F. Roghmans, E. Evdochenko, M. C. Martí-Calatayud, M. Garthe, R. Tiwari, A. Walther, and M. Wessling. “On the permselectivity of cation-exchange membranes bearing an ion selective coating”. *Journal of Membrane Science* 600 (2020).

[14] Bastian Brugger, Brian A. Rosen, and Walter Richtering. “Microgels as Stimuli-Responsive Stabilizers for Emulsions”. *Langmuir* 24.21 (2008).

[15] Garima Agrawal, Andreas Ülpenich, Xiaomin Zhu, Martin Möller, and Andrij Pich. “Microgel-Based Adaptive Hybrid Capsules with Tunable Shell Permeability”. *Chemistry of Materials* 26.20 (2014).

[16] Karen Geisel, Katja Henzler, Peter Guttmann, and Walter Richtering. “New insight into microgel-stabilized emulsions using transmission X-ray microscopy: nonuniform deformation and arrangement of microgels at liquid interfaces”. *Langmuir* 31.1 (2015).

[17] Mathieu Destribats, Véronique Lapeyre, Mélanie Wolfs, Elisabeth Sellier, Fernando Leal-Calderon, Valérie Ravaine, and Véronique Schmitt. “Soft microgels as Pickering emulsion stabilisers. Role of particle deformability”. *Soft Matter* 7.17 (2011).

[18] Ralf Goedecke, ed. *Fluidverfahrenstechnik*. Wiley-VCH, 2008. 1 online resource.

[19] Martin Henschke. *Auslegung pulsierter Siebboden-Extraktionskolonnen*. Berichte aus der Verfahrenstechnik. Aachen: Shaker, 2004. XIV, 214 S.

[20] Oded Nir, Tony Trieu, Sebastian Bannwarth, and Matthias Wessling. “Microfiltration of deformable microgels”. *Soft Matter* 12.31 (2016).

[21] Andrij Pich and Walter Richtering. *Chemical Design of Responsive Microgels*. Vol. 234. Berlin, Heidelberg: Springer Berlin Heidelberg, 2011.

[22] Florent Pinaud, Karen Geisel, Pascal Massé, Bogdan Catargi, Lucio Isa, Walter Richtering, Valérie Ravaine, and Véronique Schmitt. “Adsorption of microgels at an oil-water interface: correlation between packing and 2D elasticity”. *Soft Matter* 10.36 (2014).

[23] Robert W. Style, Lucio Isa, and Eric R. Dufresne. “Adsorption of soft particles at fluid interfaces”. *Soft Matter* 11.37 (2015).

[24] T. Misek, R. Berger, and J. Schröter. *Standard test systems for liquid extraction*. 2nd ed. Rugby: Published on behalf of the European Federation of Chemical Engineering by Institution of Chemical Engineers, 1985. 62 pp.

[25] Mathieu Destribats, Véronique Lapeyre, Elisabeth Sellier, Fernando Leal-Calderon, Véronique Schmitt, and Valérie Ravaine. “Water-in-oil emulsions stabilized by water-dispersible poly(N-isopropylacrylamide) microgels: understanding anti-Finkle behavior”. *Langmuir* 27.23 (2011).

[26] Susana Zeppieri, Jhosgre Rodríguez, and A. L. López de Ramos. “Interfacial Tension of Alkane + Water Systems †”. *Journal of Chemical & Engineering Data* 46.5 (2001).

[27] Hans-Dieter Dörfler. *Grenzflachen und kolloid-disperse systeme. Physik und chemie*. Berlin: Springer, 2002. XVII; 989.

[28] Josiah Willard Gibbs. “On the Equilibrium of Heterogeneous Substances”. *Transactions of the Connecticut Academy of Arts and Sciences* 3 (1879).

[29] Andreas Pfennig. *Thermodynamik der Gemische*. Berlin, Heidelberg: Springer Berlin Heidelberg, 2004. Online-Ressource.

[30] Bernard P. Binks. “Particles as surfactants—similarities and differences”. *Current Opinion in Colloid & Interface Science* 7.1-2 (2002).

[31] Nicholas Ballard, Adam D. Law, and Stefan A. F. Bon. “Colloidal particles at fluid interfaces: behaviour of isolated particles”. *Soft Matter* 15.6 (2019).

[32] A. Scotti, S. Bochenek, M. Brugnoni, M. A. Fernandez-Rodriguez, M. F. Schulte, J. E. Houston, A. P. H. Gelissen, I. I. Potemkin, L. Isa, and W. Richtering. “Exploring the colloid-to-polymer transition for ultra-low crosslinked microgels from three to two dimensions”. *Nature communications* 10.1 (2019).

[33] Bastian Brugger, Jan Vermant, and Walter Richtering. “Interfacial layers of stimuli-responsive poly-(N-isopropylacrylamide-co-methacrylicacid) (PNIPAM-co-MAA) microgels characterized by interfacial rheology and compression isotherms”. *Physical chemistry chemical physics : PCCP* 12.43 (2010).

[34] Mathieu Destribats, Mayalen Eyharts, Véronique Lapeyre, Elisabeth Sellier, Imre Varga, Valérie Ravaine, and Véronique Schmitt. “Impact of pNIPAM microgel size on its ability to stabilize Pickering emulsions”. *Langmuir* 30.7 (2014).

[35] Pascal Massé, Elisabeth Sellier, Véronique Schmitt, and Valérie Ravaine. “Impact of electrostatics on the adsorption of microgels at the interface of Pickering emulsions”. *Langmuir* 30.49 (2014).

[36] Steffen Bochenek et al. “Effect of the 3D Swelling of Microgels on Their 2D Phase Behavior at the Liquid-Liquid Interface”. *Langmuir : the ACS journal of surfaces and colloids* 35.51 (2019).

[37] Karen Geisel, Walter Richtering, and Lucio Isa. “Highly ordered 2D microgel arrays: compression versus self-assembly”. *Soft Matter* 10.40 (2014).

[38] Karen Geisel, Lucio Isa, and Walter Richtering. “Unraveling the 3D localization and deformation of responsive microgels at oil/water interfaces: a step forward in understanding soft emulsion stabilizers”. *Langmuir* 28.45 (2012).

[39] Haruka Minato, Masaki Murai, Takumi Watanabe, Shusuke Matsui, Masaya Takizawa, Takuma Kureha, and Daisuke Suzuki. “The deformation of hydrogel microspheres at the air/water interface”. *Chemical communications (Cambridge, England)* 54.8 (2018).

[40] Eric Siemes, Oleksii Nevskyi, Dmytro Sysoiev, Sarah K. Turnhoff, Alex Oppermann, Thomas Huhn, Walter Richtering, and Dominik Wöll. “Nanoscopic Visualization of Cross-Linking Density in Polymer Networks with Diarylethene Photoswitches”. *Angewandte Chemie (International ed. in English)* 57.38 (2018).

[41] Omkar S. Deshmukh, van den Ende, Dirk, Martien Cohen Stuart, Frieder Mugele, and Duits, Michel H G. “Hard and soft colloids at fluid interfaces: Adsorption, interactions, assembly & rheology”. *Advances in Colloid and Interface Science* (2014).

[42] Zifu Li, Karen Geisel, Walter Richtering, and To Ngai. “Poly(N-isopropylacrylamide) microgels at the oil–water interface. Adsorption kinetics”. *Soft Matter* 9.41 (2013).

[43] Omkar S. Deshmukh, Armando Maestro, Michel H. G. Duits, van den Ende, Dirk, Martien Cohen Stuart, and Frieder Mugele. “Equation of state and adsorption dynamics of soft microgel particles at an air-water interface”. *Soft Matter* 10.36 (2014).

[44] Tetyana Kyrey, Judith Witte, Vitaliy Pipich, Artem Feoktystov, Alexandros Koutsioubas, Egor Vezhlev, Henrich Frielinghaus, Regine von Klitzing, Stefan Wellert, and Olaf Holderer. “Influence of the cross-linker content on adsorbed functionalised microgel coatings”. *Polymer* 169 (2019).

[45] Christian Fänger, Holger Wack, and Mathias Ulbricht. “Macroporous Poly(N-isopropylacrylamide) hydrogels with adjustable size "cut-off" for the efficient and reversible immobilization of biomacromolecules”. *Macromolecular bioscience* 6.6 (2006).

[46] Nikita V. Bushuev, Rustam A. Gumerov, Steffen Bochenek, Andrij Pich, Walter Richtering, and Igor I. Potemkin. “Compression and Ordering of Microgels in Monolayers Formed at Liquid-Liquid Interfaces: Computer Simulation Studies”. *ACS Applied Materials & Interfaces* (2020).

[47] Yann Cohin, Maelle Fisson, Kévin Jourde, Gerald G. Fuller, Nicolas Sanson, Laurence Talini, and Cécile Monteux. “Tracking the interfacial dynamics of PNiPAM soft microgels particles adsorbed at the air–water interface and in thin liquid films”. *Rheologica Acta* 52.5 (2013).

[48] R. Miller, V. B. Fainerman, A. V. Makievski, J. Krägel, D. O. Grigoriev, V. N. Kazakov, and O. V. Sinyachenko. “Dynamics of protein and mixed protein/surfactant adsorption layers at the water/fluid interface”. *Advances in Colloid and Interface Science* 86.1-2 (2000).

[49] Christine Picard, Patrick Garrigue, Marie-Charlotte Tatry, Véronique Lapeyre, Serge Ravaine, Véronique Schmitt, and Valérie Ravaine. “Organization of Microgels at the Air. . .Water Interface under Compression: Role of Electrostatics and Cross-Linking Density”. *Langmuir* 33 (2017).

[50] Robert Aveyard, Bernard P. Binks, and John H. Clint. “Emulsions stabilised solely by colloidal particles”. *Advances in Colloid and Interface Science* 100-102 (2003).

[51] Ju Zhang and Robert Pelton. “Poly(N -isopropylacrylamide) Microgels at the Air−Water Interface”. *Langmuir* 15.23 (1999).

[52] Robert D. Groot and Simeon D. Stoyanov. “Equation of state of surface-adsorbing colloids”. *Soft Matter* 6.8 (2010).

[53] Alma J. Mendoza, Eduardo Guzman, Fernando Martinez-Pedrero, Hernan Ritacco, Ramon G. Rubio, Francisco Ortega, Victor M. Starov, and Reinhard Miller. “Particle laden fluid interfaces: dynamics and interfacial rheology”. *Advances in Colloid and Interface Science* 206 (2014).

[54] Van De Ven, Theo G.M. “Kinetic aspects of polymer and polyelectrolyte adsorption on surfaces”. *Advances in Colloid and Interface Science* 48 (1994).

[55] Matthias Kraume. *Transportvorgänge in der Verfahrenstechnik*. Berlin, Heidelberg: Springer Berlin Heidelberg, 2012.

[56] K. Bäumler, M. Wegener, A. R. Paschedag, and E. Bänsch. “Drop rise velocities and fluid dynamic behavior in standard test systems for liquid/liquid extraction—experimental and numerical investigations”. *Chemical Engineering Science* 66.3 (2011).

[57] M. Wegener. “A numerical parameter study on the impact of Marangoni convection on the mass transfer at buoyancy-driven single droplets”. *International Journal of Heat and Mass Transfer* 71 (2014).

[58] M. Wegener, N. Paul, and M. Kraume. “Fluid dynamics and mass transfer at single droplets in liquid/liquid systems”. *International Journal of Heat and Mass Transfer* 71 (2014).

[59] Roland Clift, John R. Grace, and Martin E. Weber. *Bubbles, drops, and particles*. eng. New York, NY: Acad. Press, 1978. 380 pp.

[60] D. Agble and M. A. Mendes-Tatsis. “The effect of surfactants on interfacual mass transfer in binary liquid-liquid systems”. *International Journal of Heat and Mass Transfer* 43 (2000).

[61] Niklas Paul, Matthias Kraume, Sebastian Schön, and Regine von Klitzing. “Transport processes at single droplets in micellar liquid/liquid systems”. *AIChE Journal* 61.3 (2015).

[62] Niklas Paul. “Theoretische und experimentelle Untersuchungen von Transport- und Grenzflächenphänomenen in mizellaren Flüssig/flüssig-Systemen”. Berlin: TU Berlin, 2014. 156 pp.

[63] M. Wegener and A. R. Paschedag. “The effect of soluble anionic surfactants on rise velocity and mass transfer at single droplets in systems with Marangoni instabilities”. *International Journal of Heat and Mass Transfer* 55.5-6 (2012).

[64] M. Wegener, J. Grünig, J. Stüber, A. R. Paschedag, and M. Kraume. “Transient rise velocity and mass transfer of a single drop with interfacial instabilities – experimental investigations”. *Chemical Engineering Science* 62.11 (2007).

[65] Matthias Kraume. “Integrierte chemische Prozesse in flüssigen Mehrphasensystemen”. *Chemie Ingenieur Technik* (2013).

[66] H. Brauer and D. Mewes. “Strömungswiderstand sowie stationärer Stoff- und Wärmeübergang an Blasen und Tropfen”. *Chemie Ingenieur Technik* 44.15 (1972).

[67] R. Clift and W. H. Gauvin. “Motion of entrained particles in gas streams”. *The Canadian Journal of Chemical Engineering* 49.4 (1971).

[68] Heinz Brauer. “Impuls-, Stoff- und Wärmetransport durch die Grenzfläche kugelförmiger Partikeln”. *Chemie Ingenieur Technik* 45.18 (1973).

[69] Holger Martin. “Wärme- und Stoffübertragung in der Wirbelschicht”. *Chemie Ingenieur Technik* 52.3 (1980).

[70] Martin Henschke, Adekojo Waheed, and Andreas Pfennig. “Wandeinfluss auf die Sedimentationsgeschwindigkeit von Kugeln”. *Chemie Ingenieur Technik* 72.11 (2000).

[71] Zhi-Gang Feng and Efstathios E. Michaelides. “Drag Coefficients of Viscous Spheres at Intermediate and High Reynolds Numbers”. *Journal of Fluids Engineering* 123.4 (2001).

[72] P. M. Krishna, D. Venkateswarlu, and G. S. R. Narasimhamurty. “Fall of Liquid Drops in Water. Terminal Velocities”. *Journal of Chemical & Engineering Data* 4.4 (1959).

[73] Shegen Hu and R. C. Kinter. “The fall of single liquid drops through water”. *AIChE Journal* 1.1 (1955).

[74] S. Winnikow. “Droplet Motion in Purified Systems”. *Physics of Fluids* 9.1 (1966).

[75] John R. Grace, WAIREGI T, and NGUYEN TH. “Shapes and velocities of single drops and bubbles moving freely through immiscible liquids”. *Transactions of the Institution of Chemical Engineers* 54.3 (1976).

[76] Evangelos Bertakis, Sven Groß, Jörg Grande, Oliver Fortmeier, Arnold Reusken, and Andreas Pfennig. “Validated simulation of droplet sedimentation with finite-element and level-set methods”. *Chemical Engineering Science* 65.6 (2010).

[77] J. F. Harper. “The Motion of Bubbles and Drops Through Liquids”. In*Advances in Applied Mechanics Volume 12*. Vol. 12. Advances in Applied Mechanics. Elsevier, 1972. Pp. 59–129.

[78] G. Thorsen, R. M. Stordalen, and S. G. Terjesen. “On the terminal velocity of circulating and oscillating liquid drops”. *Chemical Engineering Science* 23.5 (1968).

[79] Bin Xu, Ning Huang, Wei He, and Youxing Chen. “Investigation on terminal velocity and drag coefficient of particles with different shapes”. *Journal of Physics: Conference Series* 822 (2017).

[80] Sabine Tran-Cong, Michael Gay, and Efstathios E. Michaelides. “Drag coefficients of irregularly shaped particles”. *Powder Technology* 139.1 (2004).

[81] A. Haider and O. Levenspiel. “Drag coefficient and terminal velocity of spherical and nonspherical particles”. *Powder Technology* 58.1 (1989).

[82] Gary H. Ganser. “A rational approach to drag prediction of spherical and nonspherical particles”. *Powder Technology* 77.2 (1993).

[83] Sze-Foo Chien. “Settling Velocity of Irregularly Shaped Particles”. *SPE Drilling & Completion* 9.04 (1994).

[84] Niklas Paul, Philipp Schrader, Sabine Enders, and Matthias Kraume. “Effects of phase behaviour on mass transfer in micellar liquid/liquid systems”. *Chemical Engineering Science* 115 (2014).

[85] M. Wegener, T. Eppinger, K. Bäumler, M. Kraume, A. R. Paschedag, and E. Bänsch. “Transient rise velocity and mass transfer of a single drop with interfacial instabilities—Numerical investigations”. *Chemical Engineering Science* 64.23 (2009).

[86] Ross Taylor and R. Krishna. *Multicomponent mass transfer*. New York etc.!: John Wiley, 1993. 579 pp.

[87] W. Nitsch, M. Raab, and R. Wiedholz. “Zum Transportmechanismus der Wärme- und Stoffübertragung zwischen turbulent bewegten flüssigen Phasen”. *Chemie Ingenieur Technik* 45.16 (1973).

[88] W. H. Piarah, A. Paschedag, and M. Kraume. “Numerical simulation of mass transfer between a single drop and an ambient flow”. *AIChE Journal* 47.7 (2001).

[89] Martin Henschke and Andreas Pfennig. “Mass-transfer enhancement in single-drop extraction experiments”. *AIChE Journal* 45.10 (1999).

[90] M. Wegener and A. R. Paschedag. “Mass transfer enhancement at deformable droplets due to Marangoni convection”. *International Journal of Multiphase Flow* 37.1 (2011).

[91] Robin Schott. *Stofftransportinduzierte Nanotropfen und ihr Einfluss auf ungeordnete Instabilitäten an Flüssig-Flüssig-Phasengrenzen*. Berichte aus der Verfahrenstechnik. Aachen: Shaker, 2005. 140 pp.

[92] H. Sawistowski. “Interfacial Phenomena”. In*Recent Advances in Liquid-Liquid Extraction*. Ed. by C. Hanson. Kent: Elsevier Science, 1971. Pp. 293–365.

[93] Stefan Wolf. *Phasengrenzkonvektionen beim Stoffubergang in Flussig-Flussig-Systemen*. Vol. Nr. 584. Fortschritt-Berichte VDI. Reihe 3, Verfahrenstechnik. Dusseldorf: VDI Verlag, 1999. 178 pp.

[94] John C. Berg and Carl R. Morig. “Density effects in interfacial convection”. *Chemical Engineering Science* 24.6 (1969).

[95] D. Agble. “Interfacial Mass Transfer in Binary Liquid-Liquid Systems With Added Surfactants”. Imperial College of Science, Technology and Medicine. Ph.D. Thesis. London: University of London, 1998. 313 pp.

[96] B. Cuenot, J. Magnaudet, and B. Spennato. “The effects of slightly soluble surfactants on the flow around a spherical bubble”. *Journal of Fluid Mechanics* 339 (1997).

[97] H. Brauer. “Unsteady state mass transfer through the interface of spherical particles—II”. *International Journal of Heat and Mass Transfer* 21.4 (1978).

[98] Albert B. Newman. “The drying of porous solids: Diffusion calculation”. *Trans. AIChE* 27 (1931).

[99] R. Kronig and J. C. Brink. “On the theory of extraction from falling droplets”. *Applied Scientific Research* 2.1 (1951).

[100] J. S. Hadamard. “Mouvement permanent lent d’une sphère liquide et visqueuse dansun liquide visqueux”. *Comptes Rendus Hebdomadaires des Seances de V Academie des Sciences (París)* 152 (1911).

[101] P. M. Heertjes, W. A. Holve, and H. Talsma. “Mass transfer between isobutanol and water in a spray-column”. *Chemical Engineering Science* 3.3 (1954).

[102] A. E. Handlos and T. Baron. “Mass and heat transfer from drops in liquid-liquid extraction”. *AIChE Journal* 3.1 (1957).

[103] P. H. Calderbank and I.J.O. Korchinski. “Circulation in liquid drops”. *Chemical Engineering Science* 6.2 (1956).

[104] Daniel Menne, Fee Pitsch, John E. Wong, Andrij Pich, and Matthias Wessling. “Temperature-modulated water filtration using microgel-functionalized hollow-fiber membranes”. *Angewandte Chemie (International ed. in English)* 53.22 (2014).

[105] Wenkai Wang, Amir H. Milani, Zhengxing Cui, Mingning Zhu, and Brian R. Saunders. “Pickering Emulsions Stabilized by pH-Responsive Microgels and Their Scalable Transformation to Robust Submicrometer Colloidoisomes with Selective Permeability”. *Langmuir* 33.33 (2017).

[106] Swen Lehmann, Sebastian Seiffert, and Walter Richtering. “Diffusion of guest molecules within sensitive core-shell microgel carriers”. *Journal of colloid and interface science* 431 (2014).

[107] Natasha Kamerlin and Christer Elvingson. “Tracer diffusion in a polymer gel: simulations of static and dynamic 3D networks using spherical boundary conditions”. *Journal of physics: Condensed matter : an Institute of Physics journal* 28.47 (2016).

[108] Hélène Monteillet, Marcel Workamp, Xiaohua Li, Boelo Schuur, J. Mieke Kleijn, Leermakers, Frans A. M., and Joris Sprakel. “Multi-responsive ionic liquid emulsions stabilized by microgels”. *Chem. Commun.* 50.81 (2014).

[109] Yi Gong, Mao Wang, and Jianying He. “The behavior of hydrophobic-core/hydrophilic-shell structured microgels at an interface: from Mickering emulsion to colloidosomes with dual-level controlled permeability”. *RSC Advances* 6.97 (2016).

[110] Marissa E. Wechsler, Regan E. Stephenson, Andrew C. Murphy, Heidi F. Oldenkamp, Ankur Singh, and Nicholas A. Peppas. “Engineered microscale hydrogels for drug delivery, cell therapy, and sequencing”. *Biomedical microdevices* 21.2 (2019).

[111] W. Nitsch. “Zur hydrodynamischen Stoffübergangshemmung durch Adsorptionsschichten an flüssig/flüssig-Phasengrenzen”. ().

[112] Murat Kalem. *Einzeltropfenbasierte Simulation von pulsierten Siebbodenkolonnen für die Reaktivextraktion*. Berichte aus der Verfahrenstechnik. Aachen: Shaker, 2015. 147 pp.

[113] Rustam A. Gumerov, Sergei A. Filippov, Walter Richtering, Andrij Pich, and Igor I. Potemkin. “Amphiphilic microgels adsorbed at oil-water interfaces as mixers of two immiscible liquids”. *Soft Matter* 15.19 (2019).

[114] Ashvini Purohit, Silvia P. Centeno, Sarah K. Wypysek, Walter Richtering, and Dominik Wöll. “Microgel PAINT – nanoscopic polarity imaging of adaptive microgels without covalent labelling”. *Chemical Science* 10.44 (2019).

[115] Jonas Riest, Thomas Eckert, Walter Richtering, and Gerhard Nägele. “Dynamics of suspensions of hydrodynamically structured particles: analytic theory and applications to experiments”. *Soft Matter* 11.14 (2015).

[116] Alexey B. Nadykto and Fangqun Yu. “Uptake of neutral polar vapor molecules by charged clusters/particles: Enhancement due to dipole‐charge interaction”. *JOURNAL OF GEOPHYSICAL RESEARCH* 108.D23 (2003).

[117] To Ngai, Helmut Auweter, and Sven Holger Behrens. “Environmental Responsiveness of Microgel Particles and Particle-Stabilized Emulsions”. *Macromolecules* 39.23 (2006).

[118] G.W Stevens, H.R.C Pratt, and D.R Tai. “Droplet coalescence in aqueous electrolyte solutions”. *Journal of colloid and interface science* 136.2 (1990).

[119] Martin Simon. “Koaleszenz von Tropfen und Tropfenschwärmen”. Dissertation. Kaiserslautern: TU Kaiserslautern, 2004. 127 pp.

[120] Dirk G. A. L. Aarts and Henk N. W. Lekkerkerker. “Droplet coalescence. Drainage, film rupture and neck growth in ultralow interfacial tension systems”. *Journal of Fluid Mechanics* 606 (2008).

[121] M. Henschke. “Determination of a coalescence parameter from batch-settling experiments”. *Chemical Engineering Journal* 85.2-3 (2002).

[122] Johannes Kamp and Matthias Kraume. “Influence of drop size and superimposed mass transfer on coalescence in liquid/liquid dispersions – Test cell design for single drop investigations”. *Chemical Engineering Research and Design* 92.4 (2014).

[123] G. F. Scheele and D. E. Leng. “An experimental study of factors which promote coalescence of two colliding drops suspended in water-I”. *Chemical Engineering Science* 26.11 (1971).

[124] Johannes Kamp. “Systematic coalescence investigations in liquid/liquid systems : from single drops to technical applications”. Doctoral Thesis. Berlin: Technische Universität Berlin, 2017.

[125] S. Guido and M. Simeone. “Binary collision of drops in simple shear flow by computer-assisted video optical microscopy”. *Journal of Fluid Mechanics* 357 (1998).

[126] W. J. Howarth. “Measurement of coalescence frequency in an agitated tank”. *AIChE Journal* 13.5 (1967).

[127] H. Sovová. “Breakage and coalescence of drops in a batch stirred vessel—II comparison of model and experiments”. *Chemical Engineering Science* 36.9 (1981).

[128] C. A. Coulaloglou and L. L. Tavlarides. “Description of interaction processes in agitated liquid-liquid dispersions”. *Chemical Engineering Science* 32.11 (1977).

[129] Jörn Villwock, Felix Gebauer, Johannes Kamp, Hans-Jörg Bart, and Matthias Kraume. “Systematic Analysis of Single Droplet Coalescence”. *Chemical Engineering & Technology* 37.7 (2014).

[130] J. Kamp and M. Kraume. “Einfluss des Stofftransports auf die Koaleszenz in Flüssig/Flüssig-Dispersionen”. *Chemie Ingenieur Technik* 85.9 (2013).

[131] J. Villwock. “Systematische Analyse des Koaleszenzverhaltens von zweiphasigen Flüssigsystemen bei Ionenzugabe”. Dissertation. Berlin: TU Berlin, 2019. 222 pp.

[132] Yaodong Wu, Susanne Wiese, Andreea Balaceanu, Walter Richtering, and Andrij Pich. “Behavior of Temperature-Responsive Copolymer Microgels at the Oil/Water Interface”. *Langmuir* 30.26 (2014).

[133] Seher Ata. “Coalescence of bubbles covered by particles”. *Langmuir* 24.12 (2008).

[134] Chesters and I. Bazhlekov. “Effect of Insoluble Surfactants on Drainage and Rupture of a Film between Drops Interacting under a Constant Force”. *Journal of colloid and interface science* 230.2 (2000).

[135] Vittorio Cristini, J. Blawzdziewicz, and Michael Loewenberg. “Near-contact motion of surfactant-covered spherical drops”. *Journal of Fluid Mechanics* 366 (1998).

[136] Robert Aveyard, Bernard P. Binks, and John H. Clint. “Emulsions stabilised solely by colloidal particles”. *Advances in Colloid and Interface Science* 100-102 (2003).

[137] S. Arditty, C. P. Whitby, B. P. Binks, V. Schmitt, and F. Leal-Calderon. “Some general features of limited coalescence in solid-stabilized emulsions”. *The European physical journal. E, Soft matter* 11.3 (2003).

[138] Bing Dai and L. Gary Leal. “The mechanism of surfactant effects on drop coalescence”. *Physics of Fluids* 20.4 (2008).

[139] Mathieu Destribats, Véronique Lapeyre, Elisabeth Sellier, Fernando Leal-Calderon, Valérie Ravaine, and Véronique Schmitt. “Origin and control of adhesion between emulsion drops stabilized by thermally sensitive soft colloidal particles”. *Langmuir* 28.8 (2012).

[140] L. Keal, V. Lapeyre, V. Ravaine, V. Schmitt, and C. Monteux. “Drainage dynamics of thin liquid foam films containing soft PNiPAM microgels: influence of the cross-linking density and concentration”. *Soft Matter* 13.1 (2016).

[141] Rico Keidel, Ali Ghavami, Dersy M. Lugo, Gudrun Lotze, Otto Virtanen, Peter Beumers, Jan Skov Pedersen, Andre Bardow, Roland G. Winkler, and Walter Richtering. “Time-resolved structural evolution during the collapse of responsive hydrogels: The microgel-to-particle transition”. *Science advances* 4.4 (2018).

[142] Jianping Wang, Daoji Gan, L. Andrew Lyon, and Mostafa A. El-Sayed. “Temperature-Jump Investigations of the Kinetics of Hydrogel Nanoparticle Volume Phase Transitions”. *Journal of the American Chemical Society* 123.45 (2001).

[143] Cécile Monteux, Claire Marlière, Pauline Paris, Nadège Pantoustier, Nicolas Sanson, and Patrick Perrin. “Poly(N-isopropylacrylamide) microgels at the oil-water interface: interfacial properties as a function of temperature”. *Langmuir : the ACS journal of surfaces and colloids* 26.17 (2010).

[144] Zifu Li, Walter Richtering, and To Ngai. “Poly(N-isopropylacrylamide) microgels at the oil-water interface: temperature effect”. *Soft Matter* 10.33 (2014).

[145] Martin Henschke. *Dimensionierung liegender Flüssig-flüssig-Abscheider anhand diskontinuierlicher Absetzversuche*. Düsseldorf: VDI, 1995. [1 volume].

[146] Daniel Garthe. *Fluiddynamics and mass transfer of single particles and swarms of particles in extraction columns*. 1. Aufl. Verfahrenstechnik. Garthe, Daniel (Verfasser). München: Verl. Dr. Hut, 2006. 260 pp.

[147] J. Kamp, R. Hänsch, G. Kendzierski, O. Hellwich, and M. Kraume. “Automatisierte Bilddatenanalyse zeitlich hochaufgelo¨ ster Tropfenkollisions- und Koaleszenzereignisse”. *Chemie Ingenieur Technik* 87.8 (2015).

[148] Hang Zhang, Ahmed Mourran, and Martin Möller. “Dynamic Switching of Helical Microgel Ribbons”. *Nano letters* 17.3 (2017).

[149] C. A. Coulaloglou and L. L. Tavlarides. “Drop size distributions and coalescence frequencies of liquid-liquid dispersions in flow vessels”. *AIChE Journal* 22.2 (1976).

[150] Florian Buchbender, Markus Schmidt, Tilmann Steinmetz, and Andreas Pfennig. “Simulation von Extraktionskolonnen in der industriellen Praxis”. *Chemie Ingenieur Technik* 84.4 (2012).

[151] Donni Adinata, José Ayesterán, Florian Buchbender, Murat Kalem, Nicole Kopriwa, and Andreas Pfennig. “Tropfenpopulationsbilanzen zur Auslegung von Extraktionskolonnen”. *Chemie Ingenieur Technik* 83.7 (2011).

[152] José Ayesterán, Nicole Kopriwa, Florian Buchbender, Murat Kalem, and Andreas Pfennig. “ReDrop - A Simulation Tool for the Design of Extraction Columns Based on Single-Drop Experiments”. *Chemical Engineering & Technology* 38.10 (2015).

[153] Andreas Pfennig, Theo Pilhofer, and Jürgen Schröter. “10 Flüssig-Flüssig-Extraktion”. In*Fluidverfahrenstechnik*. Ed. by Ralf Goedecke. Wiley-VCH, 2008. Pp. 907–992.

[154] Benedikt Weber, Christian Meyer, and Andreas Jupke. “Performance Map for the Design of Liquid–Liquid Extraction Columns”. *Chemie Ingenieur Technik* 54.3 (2019).

[155] N. Kopriwa and A. Pfennig. “Charakterisierung des Koaleszenzverhaltens in Extraktionskolonnen basierend auf einfachen Laborversuchen”. *Chemie Ingenieur Technik* 85.9 (2013).

[156] A. Pfennig, Florian Buchbender, P. Chuttrakul, and N. Kopriwa. “Koaleszenz in Extraktionskolonnen und Abscheidern”. *Chemie Ingenieur Technik* 85.9 (2013).

[157] M. van Eijk and M. Cohen Stuart. “Polymer Adsorption Kinetics: Effects of Supply Rate”. *Langmuir* 13.20 (1997).

[158] Liggieri, Ravera, Ferrari, Passerone, and Miller. “Adsorption Kinetics of Alkylphosphine Oxides at Water/Hexane Interface”. *Journal of colloid and interface science* 186.1 (1997).

[159] C. R. Wilke and Pin Chang. “Correlation of diffusion coefficients in dilute solutions”. *AIChE Journal* 1.2 (1955).

[160] Kanji Miyabe and Ryo Isogai. “Estimation of molecular diffusivity in liquid phase systems by the Wilke-Chang equation”. *Journal of chromatography. A* 1218.38 (2011).

[161] National Institute of Standards and Technology. *Molecular weight n-butyl acetate*.

[162] National Institute of Standards and Technology. *Molecular weight acetonitrile*.

[163] H. Kratzke and S. Müller. “Thermodynamic properties of acetonitrile 2. (p, rho, T) of saturated and compressed liquid acetonitrile”. *The Journal of Chemical Thermodynamics* 17.2 (1985).